STEREOISOMERIC SELECTIVITY OF 2,3-DIMERCAPTOSUCCINIC ACID IN CHELATION THERAPY FOR HEAVY METAL POISONING

by

Xiaojun Fang

A Dissertation Submitted to the Faculty of the

DEPARTMENT OF CHEMISTRY

In partial Fulfillment of the Requirements
For the Degree of

DOCTOR OF PHILOSOPHY

In the Graduate College

THE UNIVERSITY OF ARIZONA

1995

THE UNIVERSITY OF ARIZONA
GRADUATE COLLEGE

As members of the Final Examination Committee, we certify that we have read the dissertation prepared by Xiaojun Fang

entitled Stereoisomeric Selectivity of 2,3-Dimercaptosuccinic Acid in Chelation Therapy for Heavy Metal Poisoning

and recommend that it be accepted as fulfilling the dissertation requirement for the Degree of Doctor of Philosophy

Quintus Fernando	1/10/95 Date
Jeanne E. Pemberton	10 Jan 95 Date
Michael F. Burke	10 Jan 95 Date
Walter B. Miller	10 Jan 95 Date
Robert B. Bates	10 JAN 95 Date

Final approval and acceptance of this dissertation is contingent upon the candidate's submission of the final copy of the dissertation to the Graduate College.

I hereby certify that I have read this dissertation prepared under my direction and recommend that it be accepted as fulfilling the dissertation requirement.

Dissertation Director	1/10/95 Date

STATEMENT BY AUTHOR

This dissertation has been submitted in partial fulfillment of requirements for an advanced degree at The University of Arizona and is deposited in the University Library to be made available to borrowers under rules of the Library.

Brief quotations from this dissertation are allowable without special permission, provided that accurate acknowledgement of source is made. Requests for permission for extended quotation from or reproduction of this manuscript in whole or in part may be granted by the head of the major department or the Dean of the Graduate College when in his or her judgment the proposed use of the material is in the interests of scholarship. In all other instances, however, permission must be obtained from the author.

SIGNED: 

ACKNOWLEDGMENTS

I wish to express my sincere appreciation to the following people for their help through my graduate career:

to Dr. Quintus Fernando, my research director, for his exquisite guidance, insightful discussions, persistent encouragement, intrinsic understanding and precious friendship;

to Dr. Jeanne Pemberton for her invaluable advice and discussions;

to Dr. Michael Burke for his understanding and discussions;

to Dr. Roger Sperline for his remarkably constructive insights;

to Dr. Michael Bruck for his assistance with my research in many ways;

to Timothy Lowe, Paul Oram, Rosy Muftikian, Carina Grittini and Veronica Rodriguez-Ibarra for their assistance and friendship, for sharing their thoughts and ideas, and for making an environment exemplifying the spirit of scientific investigation;

to my family for all of their support, and especially to my parents-in-law, who spent most of their time in caring for my son;

and above all, to my wife Fengmei for her patience, understanding, encouragement and love throughout my years of schooling. This is truly **our** degree.

Finally, I want to acknowledge my indebtedness to my teacher in middle school, Mr. Qitai Zhou, who motivated me since I was a kid and I wouldn't have even thought about this degree without his encouragement 18 years ago.

DEDICATION

To my son, George, who brought joy when life was tough, to my wife, Fengmei, for her support, and to my mother, Jinlin, who has been devoted to her children.

TABLE OF CONTENTS

Pages

TABLE OF CONTENTS--Continued Pages

TABLE OF CONTENTS--Continued Pages

TABLE OF CONTENTS--Continued Pages

LIST OF ILLUSTRATIONS

Pages

LIST OF ILLUSTRATIONS--Continued Pages

LIST OF ILLUSTRATIONS--Continued Pages

LIST OF ILLUSTRATIONS--Continued Pages

LIST OF ILLUSTRATIONS--Continued Pages

LIST OF TABLES

Pages

LIST OF TABLES--Continued Pages

ABBREVIATIONS

Rac-DMSA, *racemic*-2,3-dimercaptosuccinic acid; *meso*-DMSA, *meso*-2,3-dimercaptosuccinic acid; BAL or British Anti-lewisite, 2,3-dimercaptopropanol; EDTA, ethylenediaminetetraacetate; FDA, the Food and Drug Administration; D-Penicillamine, 3-mercapto-D-valine; DMPS, Unithiol, or Dimaval, sodium 2,3-dimercapto-1-propane-sulfonate; NHNES, National Health and Nutrition Examination Survey; CDC, Center for Disease Control; ALA-D, aminolevulinic acid dehydrase; C_{max}, the maximum concentration of a drug achieved in the blood; t_{max}, the time elapsed to reach maximum concentration of a drug in the blood; $t_{½}$, the elimination half-life of a drug; CL_R, the renal clearance; PDH, pyruvate dehydrogenase; EA, ethyl acetate; PE, petroleum ether; *rac*-BATSA, *rac*-2,3-bis-(acetylthio)succinic acid; TBA, tert-butyl alcohol; DSS, sodium 2,2-dimethyl-2-silapentane-5-sulfonate; IR, infrared; R,R-DMSA, R,R-2,3-dimercaptosuccinic acid; S,S-DMSA, S,S-2,3-dimercaptosuccinic acid; TMA, tetramethylammonium; i.p., intraperitoneally; DMSA, 2,3-dimercaptosuccinic acid or 2,3-dimercaptosuccinate ion (L^{+}).

ABSTRACT

Racemic-2,3-dimercaptosuccinic acid (*rac*-DMSA)[1] was synthesized and its structure in the solid state was studied by single crystal X-ray analysis. The three-dimensional structure of *rac*-DMSA solid is stabilized by van der Waals forces, whereas the *meso*-DMSA solid is stabilized by hydrogen bonding. This accounts for the drastic difference in the solubilities of DMSA stereoisomers. The behavior of DMSA stereoisomers in aqueous solution were studied by potentiometric titration, IR and ^{1}H NMR. Rac-DMSA irreversibly converts to the *meso* form at an elevated temperature under acidic conditions. Two mechanisms were proposed to explain the conversion. At high pH, *rac*-DMSA tends to form ion-paired complexes with alkaline counter ions via two carboxylate groups. At physiological pH, DMSA stereoisomers form two intramolecular six-membered rings.

The formation constants and the structures of lead and zinc chelates of DMSA stereoisomers formed in aqueous solution were determined by potentiometric titration, IR and ^{1}H NMR. Lead and zinc complex with *rac*-DMSA to a greater extent than with *meso*-DMSA. DMSA stereoisomers tend to form dimeric chelates with Zn^{2+}, but monomeric chelates with Pb^{2+}. In the zinc chelates of *rac*-DMSA two bulky carboxylate groups of the ligand have a staggered anti-relation, whereas in the zinc chelates of *meso*-DMSA two carboxylate groups

assume a staggered gauche-relation. This accounts for that the formation constants of zinc chelates of *rac*-DMSA are invariably larger than those of the corresponding chelates of *meso*-DMSA. The binding sites in PbL of DMSA stereoisomers are two thiolate groups and one carboxylate group of the ligands. In the lead chelates of DMSA stereoisomers, *rac*-DMSA exists in a staggered anti-conformation, but *meso*-DMSA favors a staggered gauche-conformation with respect to the bulky carboxylate groups. This accounts for that the formation constants of the lead chelates of *rac*-DMSA are invariably larger than those of the corresponding chelates of *meso*-DMSA. On the basis of our studies ZnL_2 chelate of *rac*-DMSA has been proposed to be a more effective lead chelator than *meso*-DMSA for therapeutical use.

INTRODUCTION

Brief History of Chelation Therapy.

Chelation for heavy metal intoxication has been practiced in various forms for more than 40 years. The history of chelation therapy began with investigation of a dithio chelating agent, 2,3-dimercaptopropanol (British Anti-lewisite or BAL[1]), in World War II in a British laboratory in which Stockton and Thompson were concerned over the possible use of dichlorovinyl arsine, known as lewisite, as a toxic agent in warfare. BAL was initially prepared as a topical agent in oil to avert the toxicity of lewisite. BAL improved survival of animals topically exposed to lewisite and prevented the decline in oxygen uptake linked with inhibition of pyruvate dehydrogenase by lewisite (*1*). The first clinical use of BAL in humans occurred in individuals suffering from a side effect known as arsenical dermatitis (*2*), since Lewisite was never used during World War II. In 1948, pediatricians in New Orleans reported the first case of children treated with BAL for arsenic ingestion (*3*). In 1949, BAL was reported to be used to treat a series of patients who attempted suicide by ingestion of mercuric chloride. Longcope and Luetscher reported zero death among the 41 patients who were treated with BAL within four hours of ingestion of greater than 1 g of mercuric chloride, whereas, 86 patients from the preceding decade who had not been treated with BAL showed a 31.4% mortality rate (*4*). Publication of this paper

promoted adoption of BAL for use in cases of mercury intoxication. With the enthusiasm and interest created by the use of BAL in the treatment of arsenic and mercury poisoning, early investigators turned to its use in lead poisoning. The results of early studies with animals showed that BAL increased the urinary as well as the fecal excretion of lead; however, it also increased the toxicity of lead as indicated by a significant decrease in the number of survival days (*5*). Because of this, BAL did not gain wide use as a single antidote in the treatment of lead poisoning in humans. Prior to the October 1991 recommendation of the Centers for Disease Control (CDC)[1] concerning treatment of lead poisoning, 29 of 30 major lead poison treatment clinics employed chelation therapy for children with blood lead ≥25 μg/dL (*6*). Calcium disodium EDTA was the mainstay of chelation therapy for lead poisoning for more than 40 years, since its first-time use in 1952, because of the two findings that it produced an increase in the urinary excretion of lead and tended to reverse inhibition of erythrocyte aminolevulinic acid dehydrase (ALA-D[1], porphobilinogen synthetase). The primary source of lead that is chelated by EDTA is bone (*7,8*). Many clinicians have noted an adverse effect of EDTA on lead encephalopathy since $CaNa_2EDTA$ increases the brain lead level by a factor of 2 after the first injection (*9*). The acute increase in brain lead evoked by $CaNa_2EDTA$ is paralleled, in humans, by an acute increase in plasma lead at 1.5 h after injection (*10,11*). Chisolm

(*12*) found that $CaNa_2EDTA$ alone, compared with BAL, did not decrease the mortality caused by acute lead encephalopathy. The most consistent side effect of using $CaNa_2EDTA$ is the massive diuresis of zinc. In children receiving a 5-day course of 1000 mg $CaNa_2EDTA/m^2/d$, there was an approximately 24-fold increase in the daily urinary loss of lead and about a 17-fold increase in the daily loss of zinc (*13*). Despite all the adverse effects, $CaNa_2EDTA$ in combination with BAL continues to be a standard treatment for children with acute lead encephalopathy (blood Pb ≥70 μg/dL) (*30*). The efficacy of the combination of EDTA and BAL in the treatment of acute lead encephalopathy is attributed to diffusion of neutral BAL molecules, but not EDTA, into spinal fluid with the presumptive chelation of brain lead. Another reason supporting the use of combination of EDTA and BAL in acute lead encephalopathy lies in the fact that there is twice as much lead excretion by BAL-EDTA (*14*). *Meso*-DMSA was approved by the Food and Drug Administration (FDA)[1] in 1991 (*15*) for the treatment of children with blood Pb ≥45 μg/dL, and since then there has been an increasing use of oral DMSA for the pharmacological treatment of children with blood Pb ≥ 25 μg/dL. Other important chelating agents include 3-mercapto-D-valine (D-penicillamine)[1] and sodium 2,3-dimercapto-1-propane-sulfonate (DMPS, Unithiol, or Dimaval)[1]. D-Penicillamine is approved by the FDA for the treatment of Wilson's disease, cystinuria, and severe active rheumatoid arthritis. Before the

approval of DMSA it is the only available oral chelator and has been used for the long-term treatment of children with blood lead levels of 20-40 μg/dL (*16,17*). DMPS is effective in mobilizing mercury and has been used extensively in Europe in the diagnosis and the treatment of mercury poisoning, but Chisolm (*18*) believes that: "one can forget about DMPS as far as lead is concerned." Finally, quoting from Aaseth (*19*): "Enhanced excretion induced by a drug is meaningless from a therapeutic point of view if it is not paralleled by a decrease of the metal concentration in the critical organ." A major drawback of most chelating agents concerning lead detoxification is their negligible or adverse effect on brain lead. *Meso*-DMSA, at least in the rats, is quite effective compared to the other chelating agents for removal of lead from the brain (*20*), although the exact mechanism of removal of brain lead by *meso*-DMSA remains unknown.

Management of Childhood Lead Poisoning.

Effect of Low-Level Lead on Children.

The suggested management of childhood lead poisoning has changed over the past 20 years. This change was promoted by the evidence, reported by Schwartz et al. in the analysis of the second National Health and Nutrition Examination Survey (NHNES)[1] data from 2695 children 6 months through 7 years of age, that there was an unequivocal inverse correlation of blood level with

height, weight and chest circumference (*21*). It has been shown in most (*22-25*) cross sectional studies of the correlation of low-level blood lead and the cognitive performance of preschool and school-age children that a significant decrease in the cognitive and behavior score of children is associated with an elevation of average blood lead in the range 10-30 μg/dL. Topics concerning childhood lead poisoning have been reviewed by Davis and Svendsgaard (*26*) and Angle (*27*). The Clean Air Scientific Advisory Committee to the U.S. Environmental Protection Agency considers a blood lead of 10-15 μg/dL and below as a nontoxic level (*28*). Prior to October 1991 the CDC of the Department of Health and Human Services considered 25 μg/dL, obtained from a fingerstick sample, a safe lead level in blood of children (*29*), but the current recommendation (*30*) of CDC concerning lead-screening is to use an uncontaminated venous blood sample and that the children with the blood lead level ≤ 9 μg/dL will be rescreened in 1 year. The current consensus (*30*) is that a childhood blood lead of 10 μg/dL is not only the threshold for inhibition of erythrocyte ALA-D but also appears to be the threshold for association with noticeable effects on fetal maturation, mental development and hearing in preschool children and on behavioral and cognitive performance of school-age children.

Source of Childhood Lead Poisoning.

Deteriorated paint and plaster, construction and heavily contaminated soil are the primary causes. Shannon and Graef (*31*) pointed out that remodeling is the leading cause of lead poisoning in children under age of 1. The current recommendations by CDC (*30*) are that surface paint contain ≤ 0.06% lead, household soil and dust lead < 1000 ppm, tap water lead < 15 ppm, with the following maximum loading of lead in household dust: floors 200 $\mu g/f^2$; window sills 500 $\mu g/f^2$; window wells 800 $\mu g/f^2$. Individual households may also be contaminated by other sources such as folk remedies (Alarcon, Alkohol, Azarcon, Bali Goli, Coral, Ghasard, Greta, Liga, Pay-loo-ah, Rueda); cosmetics; household casting of ammunition, fish weights and toys; making stained glass, pottery; refinishing furniture; burning lead-painted wood; soldered tea kettles and water heaters; ceramic containers and glasses, and lead crystal (*30*).

Role of *Meso*-2,3-dimercaptosuccinic Acid.

Meso-DMSA is an orally active, heavy metal chelating agent that forms stable water-soluble complexes with lead *in vitro*. *Meso*-DMSA was identified as a potential agent for the treatment of heavy metal poisoning by researchers in the former Soviet Union (*32*) in 1958 and China (*33,34*) in 1965. Clinical studies of *meso*-DMSA (*35-40*) show DMSA to be specific for lead and orally effective without clinically important increases in the depletion of calcium, zinc,

or iron, although zinc excretion is found to have been increased by 1.8 times during the treatment but copper excretion varies. Side effects associated with *meso*-DMSA are relatively minor, compared with $CaNa_2EDTA$ or BAL, and include transient elevations in aminotransferase and alkaline phosphatase activities, increased trace metal excretion, rashes, nausea, vomiting, reversible leukopenia, and febrile reactions (*41*,*42*). "A careful monitoring for potential side effects" was recommended by Grandjean et al. (*41*) for *meso*-DMSA doses of 10 mg/kg and above. The role of *meso*-DMSA concerning its efficacy and tolerability in the treatment of childhood lead poisoning has been reviewed by Deborah (*43*).

Summary of Complexing Properties of *Meso*-DMSA with Metals.

The various properties of DMSA have been reviewed by Aposhian and Aposhian (*44*), Mann and Travers (*42*), Ding and Liang (*45*), Jones (*46*) (in 1991) and Angle (*47*) (in 1993). *Meso*-DMSA is a white crystalline powder with a M.P. 210°C. It is soluble in alkaline solution, very slightly soluble in water and virtually insoluble in organic solvents such as acetone, ethanol and ethyl ether. The stability of the metal chelates of *meso*-DMSA appeared to be in the order Cd(II) > Pb(II) > Fe(II) > Hg(II) > Zn(II) > Ni(II) (*48*). The formation constant of the lead chelate of *meso*-DMSA has been reported (*49*) and the structure of the chelate in the solid state has been characterized by Rivera et al.

(*50*). The speciation models of nickel, zinc, cadmium, and lead with *meso*-DMSA have been summarized by Rivera in his dissertation (*51*) on the basis of four references.

Pharmacokinetical Properties of *Meso*-DMSA.

After oral administration of *meso*-DMSA, only 20.6% of the administered DMSA was found in the urine as total *meso*-DMSA after 14 h (*52,53*). 2.5% of the administered *meso*-DMSA was found in the urine as an unaltered drug and about 18% was found in a form of a disulfide of *meso*-DMSA with two molecules of cysteine. 95% of blood DMSA in health humans, after oral administration, was found to bind to plasma protein, mainly albumin and only 5% of it was present in non-protein-bound form (*52*). Unaltered DMSA was detected in the blood of all lead poisoned patients but in only one of five healthy humans (*54*). Studies of oral administration of *meso*-DMSA to healthy human males (*52*) showed that the maximum concentration achieved in the blood $(C_{max})^1$ was about 26.2 μM, the time to achieve this maximum concentration $(t_{max})^1$ was about 3 h and the elimination half-life $(t_{1/2})^1$ was 3.2 h. The differences in the pharmacokinetical parameters between lead-poisoned and healthy humans were reported by Dart et al. (*54*). The $t_{1/2}$ of total drug, after oral administration of *meso*-DMSA, was longer in children with lead poisoning (about 3.0 h) than in adults with lead poisoning (about 1.9 h) and the renal clearance $(CL_R)^1$ of the metabolites of *meso*-

DMSA was also greater in healthy adults (64.6 mL/min/m^2) than in either adults (35.4 mL/min/m^2) or children (19.5 mL/min/m^2) with lead poisoning (*54*).

***Racemic*-DMSA as a Potentially More Effective Lead Antidote.**

DMSA exists in two diastereoisomeric forms, *meso* and *racemo*. In spite of the increasing use of *meso*-DMSA in the U.S.A. as a chelating agent for lead poisoning, the disadvantage of using it in humans is that it is virtually insoluble in acidic solution and very slightly soluble in water. From a pharmacokinetical perspective, this detracts from the gastrointestinal absorption of the drug after *meso*-DMSA is given orally, and results in an increase in the t_{max} and decrease in C_{max} of the drug in the blood. From a clinical perspective, prescription of a comparatively high dose of *meso*-DMSA, when the drug is given orally, is necessary to maintain an effective blood *meso*-DMSA level for the chelation therapy and the potential dose-related side effects occur (*41*). On the other hand, *rac*-DMSA is very soluble in strongly acidic solution, in water, and in ethyl ether (*55*). The possession of this unique characteristic of hydrophilicity and lipophilicity by this stereoisomer of *meso*-DMSA suggests that *rac*-DMSA may be a superior and more promising chelating agent than *meso*-DMSA for lead poisoning, especially in targeting brain lead. After a literature search, it was found that investigation of *rac*-DMSA is still in its infancy. In the past 27 years, only 6% of the publication related to DMSA dealt with *rac*-DMSA, probably because

it is difficult to synthesize and unavailable from commercial sources. *Rac*-DMSA has never been studied with either human subjects or animals for its efficacy in the treatment of lead poisoning. An animal study of the efficacy of *rac*-DMSA for the elimination of lead should be conducted. *Rac*-DMSA was found to be superior, at least in rats, to *meso*-DMSA in the treatment of mercury poisoning in regard to the following findings by Okonishnikova (*56*): 1) one therapeutic dose of *rac*-DMSA, administered 15 min before poisoning, ensured the survival of 2 rats out of 6 which were injected with a fatal dose (20 mg/kg) of $HgCl_2$, whereas the same dose of *meso*-DMSA did not save the animals; when the doses were doubled, *meso*-DMSA prevented 2 rats out of 6 from dying, but *rac*-DMSA saved all 6 rats from death; (2) on the very first day after one dose of *rac*-DMSA and *meso*-DMSA the excretion of Hg from the bodies of rats, relative to the rats in the control group, were 10 and 4 times higher, respectively; (3) *rac*-DMSA, in contrast to *meso*-DMSA, reduced the Hg accumulation in liver by 6 times, relative to the rats in the control group, when the drug was given orally; (4) a 3-day course of treatment with *rac*-DMSA reduced the kidney Hg level in rats by 27-29 times, while *meso*-DMSA caused a reduction of only 5-6 times. Other experimental evidence (*57*) infers that rac-DMSA is also superior to *meso*-DMSA in the treatment of acute cadmium poisoning because *rac*-DMSA increased cadmium excretion 26-fold while *meso*-DMSA increased cadmium

excretion by only 10-fold, on the first day, if the compounds were administered immediately after the rats were injected with Cd^{2+}. The increase in the accumulated cadmium excretion by *rac*- and *meso*-DMSA in the entire 3-day course of drug administrations were 8.8-fold and 3.5-fold, respectively, compared with the control. *Rac*-DMSA is almost as safe as *meso*-DMSA, although it has never been used with humans. The results of a study (*57*) with 160 white male rats show that, similar to *meso*-DMSA, *rac*-DMSA does not influence the excretion of copper, iron, and manganese. Zinc excretion was enhanced by a factor of 1.8 by *rac*-DMSA and cobalt excretion was enhanced by a factor of 1.5 by *meso*-DMSA on the first day, but no statistically significant difference between the two isomers in excretion of the two metals was observed on the following two days during the 3-day treatment course. *Rac*-DMSA is reported to be as effective as *meso*-DMSA in the mobilization and depletion of tissue arsenic (*58*), but it is superior to *meso*-DMSA for the *in vivo* reversal of the activity of pyruvate dehydrogenase (PDH)[1]. The reported toxicity of *rac*-DMSA (LD_{50}=10.84 mmol/kg, i.p.) is a little higher than that of *meso*-DMSA (LD_{50}=13.73 or 10.9 mmol/kg, i.p., depending on the source of the drug) (*58*). This may be attributed to the 2-fold increase in the depletion of endogenous zinc by *rac*-DMSA. Pharmacokinetic data for *rac*-DMSA either in animals or in humans do not exist. The stoichiometry of cadmium and lead complexes of *rac*-DMSA were postulated

by Egorova et al. (*59,60*). The stabilities of various metal complexes of *rac*-DMSA seem to be in the order zinc(II), cadmium(II), mercury(II) > cobalt(II), nickel(II) > manganese(II) (*61,62*). this conclusion was drawn only on a qualitative basis, because the metal ion complexations of *rac*-DMSA were much more complicated than those of *meso*-DMSA. Two types of 1:1 lead chelates of *rac*-DMSA (PbL) were synthesized and characterized in the solid state by Rivera et al. (*50*).

In summary, the complex formation of *rac*-DMSA with metal ions has not been studied quantitatively. We have, therefore, initiated comparative studies of *meso*- and *rac*-DMSA ligands and their metal complexing properties. The main objectives of this dissertation are: (1) to understand the structures of the ligands in aqueous solution, and to determine their acid dissociation constants, (2) to understand the structure of zinc and lead complexes of the ligands in aqueous solution, and to determine their formation constants, (3) to assess the relative ability of the ligands to mobilize zinc and lead at physiological pH, (4) to explain, at the molecular level, the *in vivo* results obtained with these ligands, and finally, (5) to propose a more effective regimen for the treatment of lead poisoning.

CHAPTER ONE: SYNTHESIS, STRUCTURES, AND PROPERTIES OF DMSA STEREOISOMERS

Introduction

It has been pointed out in the previous INTRODUCTION section that *meso*-DMSA is soluble only in alkaline solution, very slightly soluble in water and insoluble in ethyl ether. This results in a slow gastrointestinal absorption of the drug after oral administration of *meso*-DMSA. On the other hand, *rac*-DMSA is very soluble in strongly acidic solution, in water, and in ethyl ether, and these unique properties of hydrophilicity and lipophilicity of this stereoisomer of *meso*-DMSA facilitate the absorption of *rac*-DMSA through gastrointestinal membranes, partially account for its higher efficacy in rapid excretion of mercury and cadmium (*56,57*), and also suggest that *rac*-DMSA is a superior and more promising chelating agent than *meso*-DMSA for the treatment of lead poisoning. The efficacy of a chelating agent in the treatment of metal poisoning is, of course, affected by many factors, besides the solubility and structure of the ligand in aqueous solution. Other factors include the stability and solubility of metal chelates of the ligand, rates of excretion and degradation of the ligand, etc. Of all the factors, however, the structure and properties of the ligand alone in aqueous solution are the most fundamental factors because they determine how rapidly the ligand can be delivered to the lead deposit sites in the body. In addition, the

toxicity of a chelating agent, in some instances, is also attributed to inhibition of enzymes by the ligand. The objectives of this chapter, therefore, are to synthesize *rac*-DMSA, to analyze the crystal structures of *rac*-DMSA and its synthetic precursor, to study the interconversion of the *racemo* and *meso* forms, to determine the acid dissociation constants (pK_a's) of *meso*- and *rac*-DMSA, and to determine the conformations of *meso*- and *rac*-DMSA at different protonation stages in aqueous solution.

Experimental Section

Materials.

Acetylenedicarboxylic acid (95%), thiolacetic acid (tech.), potassium bromide (infrared (IR)[1] grade), deuterium oxide, deuterated methanol, and tetramethylammonium hydroxide pentahydrate (99%) were purchased from Aldrich Chemical Co. Inc. (Milwaukee, WI); *Caution:* Acetylenedicarboxylic acid is a highly toxic irritant and readily absorbed through the skin; thiolacetic acid is toxic and has a pungent odor. A face mask was used when weighing acetylenedicarboxylic acid to avoid the inhalation of acetylenedicarboxylic acid dust. Thiolacetic acid should be manipulated in a hood. All organic solvents used were purchased from EM SCIENCE (Gibbstown, NJ); *meso*-DMSA was a gift from Johnson & Johnson Baby Products Co. (Skillman, NJ); tert-butyl alcohol (TBA)[1] was purchased from EM SCIENCE (Gibbstown, NJ) and distilled before use; all other inorganic compounds used were purchased from Mallinckrodt, Inc., Paris, KY, and were of analytical reagent grade. *Caution:* Gloves are necessary in the handling of all the above chemicals to avoid direct contact with skin.

Synthesis of *Rac*-2,3-dimercaptosuccinic Acid (*Rac*-DMSA).

The synthetic route employed is a modification of Gerecke's method (*63*). 18.75 g of acetylenedicarboxylic acid was dissolved in 60 mL ethyl acetate (EA)[1] at 34°C; 25.0 g of thiolacetic acid was added slowly into this

solution over a period of 1 h. The reaction was carried out at 35±1 °C in a Schlenk line under nitrogen to prevent the oxidation of thio-compounds by oxygen in air. A white precipitate formed in approximately 2 h. After 24 h, the suspension in the reaction vessel was cooled slowly to ambient temperature and then chilled and maintained at 7°C overnight. The suspension was filtered and the solid on the filter was washed with 26 mL cold EA / petroleum ether (PE)[1] (1:1, v/v) and dried *in vacuo*; 24.5 g of a pale yellow solid was obtained at this stage and its IR spectrum indicated that it was a mixture of both *meso* and *racemo* forms. The solid was resuspended in 60 mL EA at room temperature for one day with stirring, and finally filtered. Into the above filtrate 30 mL PE was added and the solution was stored at 7°C for 24 h. A crystalline solid was formed, separated by filtration, and washed with cold PE/EA (3:1, v/v), cold PE, and finally the traces of PE present in the solid were removed by evaporation in air. *Racemic*-2,3-bis-(acetylthio)succinic acid (*rac*-BATSA)[1] (4.92 g) was obtained (melting point: 151-153°C; 150-151°C determined by Gerecke (*63*)). Elemental analyses were performed by Desert Analytics, (Tucson AZ), Calcd for $C_8H_{10}O_6S_2$: C, 36.08%; H, 3.79%; S, 24.08%. Found: C, 35.90%; H, 3.78%; S, 24.15%. The purity of the compound was also checked by ^{1}H NMR and IR spectroscopy. The structure of the compound was determined by an X-ray analysis.

Rac-DMSA was synthesized from *rac*-BATSA according to the procedure described by Gerecke et al. (*63*). 4.92 g of *rac*-BATSA was hydrolyzed under basic conditions in an argon atmosphere, acidified with HCl, and extracted with ethyl ether. After a final crystallization from ethyl ether/benzene, 2.91 g of *rac*-DMSA was obtained (melting point: 128.5-130°C; 127-128°C determined by Gerecke (*63*)). Anal. calcd for $C_4H_6O_4S_2$: C, 26.38%; H, 3.32%; S, 35.19%. Found: C, 26.49%; H, 3.27%; S, 34.88. The purity of the compound was also checked by ^{1}H NMR, IR (*50*) and potentiometric titration. The structure of the compound was determined by an X-ray analysis.

Isomerization of *Racemo* to *Meso* Form.

Reactions with the same molar concentrations of the *racemo* and *meso* forms of the compounds were carried out under nitrogen in the presence of 0.5M HCl. Dissolved oxygen was removed from all solvents before use. ^{1}H NMR spectroscopy was used to follow the reaction, and IR spectroscopy was used to identify stereoisomeric products.

X-ray Crystallography.

(A) *Rac*-BATSA($C_8H_{10}O_6S_2$).

Suitable crystals of *rac*-BATSA were obtained from a mixture of acetone and toluene after slow evaporation of acetone. A colorless crystal block with approximate dimensions 0.33 x 0.25 x 0.37 mm was mounted on a glass fiber in

a random orientation. Preliminary examination and data collection were performed with Mo Kα radiation(λ= 0.70930 Å) on an Enraf-Nonius CAD4 (*64*) κ axis diffractometer with a graphite crystal incident beam monochromator.

Cell constants and an orientation matrix for data collection were obtained from least-squares refinement, using the setting angles of 25 reflections in the range $11 < \theta < 17°$. The monoclinic cell parameters and calculated volume are: a= 11.404(3), b=7.531(2), c=13.335(3) Å, β= 93.37(2)°, V= 1143.3(3) Å^3. As a check on crystal quality, ω scans of several intense reflections were measured; the width at half-height was 0.25°, indicative of good crystal quality. From the systematic absences of: $h0l$, $h+l = 2n+1$, $0k0$, $k = 2n+1$; and from subsequent least-squares refinement, the space group was determined to be $P2_1/n$.

2313 reflections were collected, of which 1999 were unique and not systematically absent. As a check on crystal and electronic stability, 3 representative reflections were measured after every 60 minutes. The intensities of these standards remained constant within experimental error throughout data collection. No decay correction was applied.

Lorentz and polarization corrections were applied to the data. The linear absorption coefficient is 4.3 cm^{-1} for Mo Kα radiation. No absorption corrections were made, and the intensities of equivalent reflections were averaged. The

agreement factors for the averaging of the 185 observed and accepted reflections were 1.3% based on intensity and 0.8% based on F_o.

The structure was solved by direct methods. 15 atoms were located from an E-map. The remaining atoms were located in succeeding difference Fourier syntheses. Hydrogen atoms were located and their positions were refined with their isotropic thermal parameters fixed at 5.0 Å (*65*). The structure was refined in full-matrix least-squares. The weights for each reflection were calculated using the counter weighing scheme. The uncertainty factor (*p*) was set at 0.040.

Scattering factors were taken from Cromer and Waber (*65*). Anomalous dispersion effects were included in F_c^3 (*66*); the values for Δf and $\Delta f'$ were those of Cromer (*67*). Details of the structure solution and refinement are given in Table I-S of the supplementary material. All calculations were performed on a VAX computer using SDP/VAX (*68*).

(B) *Rac*-DMSA($C_4H_6O_4S_2$).

Suitable crystals were obtained from a mixture of ethyl ether and benzene after slow evaporation of ethyl ether. A pale yellow irregular fragment of a crystal having approximate dimensions 0.60 x 0.30 x 0.13 mm was mounted on a glass fiber in a random orientation. Preliminary examination and data collection were performed with Mo Kα radiation(λ=0.71073 Å) on a Syntex $P2_1$ diffractometer, with a Crystal Logics control system (*69*).

Cell constants and an orientation matrix for data collection were obtained from least-squares refinement, using the setting angles of 22 reflections in the range $23< 2\theta <37°$. The monoclinic cell parameters and calculated volume are: a= 23.906(4), b=6.262(2), c=10.162(2) Å, β= 103.21(24)°, V= 1481.0 Å^3. As a check on crystal quality, ω scans of several intense reflections were measured; the width at half-height was 0.36°, indicative of moderate crystal quality. From the systematic absences of: $h0l$, $l = 2n+1$; and from subsequent least-squares refinement, the space group was determined to be C2/c.

1470 reflections were collected, of which 1297 were unique and not systematically absent. As a check on crystal and electronic stability, 3 representative reflections were measured after every 97 reflections. The intensities of these standards remained constant within experimental error throughout data collection. No decay correction was applied.

Lorentz and polarization corrections were applied to the data. The linear absorption coefficient is 6.4 cm^{-1} for Mo Kα radiation. No absorption corrections were made. Intensities of equivalent reflections were averaged. The agreement factors for the averaging of the 42 observed and accepted reflections were 1.0% based on intensity and 0.9% based on F_o.

The structure was solved by direct methods. 10 atoms were located from an E-map. Hydrogen atoms were located from difference maps and their positions

were refined with their isotropic thermal parameters fixed at 5.0 Å (*65*). The structure was refined in full-matrix least-squares. The weights for each reflection were calculated using the counter weighing scheme. The uncertainty factor (*p*) was set at 0.040.

Scattering factors were taken from Cromer and Waber (*65*). Anomalous dispersion effects were included in F_c^3 (*66*); the values for Δf and $\Delta f'$ were those of Cromer (*67*). Details on the structure solution and refinement are given in Table II-S of the supplementary material. All calculations were performed on a VAX computer using SDP/VAX (*68*) and XTAL (*69*).

Potentiometry.

Potentiometric measurements of hydrogen ion concentration were performed in a 150 mL glass-jacketed vessel provided with a magnetic stirrer and a tightly fitting rubber stopper. The latter was equipped with inlet and outlet tubes for nitrogen, a buret for delivery of base solution, a glass electrode, a salt-bridge made of 2% agarose gel containing saturated KCl, which was connected to a saturated calomel reference electrode, and a thermometer. During the titration the tip of the buret was positioned right below the surface of the solution; replacement of the NaOH or KOH in the tip of the buret with the titration solution was not observed, because most of the equilibria were established within a minute. The temperature in the titration vessel was controlled by circulation of

thermostated water through the jacket, by using a VWR 1160 refrigerated circulator. To minimize the effect of nitrogen flow on the evaporation of the titration solution, the nitrogen was saturated with water vapor by passing the gas through a 0.1 M $NaNO_3$ solution.

A BECKMAN Φ-72 pH meter equipped with an electrode pair was first calibrated with NIST buffers (pH=4.00 and 7.00). A titration of 9.448×10^{-3} M HNO_3 solution in the presence of 0.10 M $NaNO_3$ or KNO_3 gave an experimental conversion curve of $-\log[H^+]$ vs measured pH. The validity of the conversion curve was checked by the inherent relationships in the Gran plots (*70*) obtained in both acidic and basic regions. These include the equality of the absolute values of the *x*-intercepts, which represent the amount of strong acid present in the initial solution titrated, and the equality of the slopes, which represent the molarity of strong base added, of the Gran plots obtained from both acidic and basic regions. The validity of the conversion curve was also checked by a comparison of pK_w values determined using the conversion curve with the pK_w values calculated using the activity coefficients of hydrogen ion and hydroxide ion which were determined from the extended form of the Debye-Hückel equation. The calculated pK_w value is 13.80 (*71*) and the experimentally determined pK_w value is 13.80±0.01.

Standard NaOH or KOH solutions were prepared from 50% (w/w) NaOH solution or 45% (w/w) KOH solution and CO_2-free double-deionized H_2O. The prepared base solutions were kept under a nitrogen atmosphere to prevent the absorption of CO_2. The carbonate content, determined as described by Martell et al. (*72*), was found to be less than 1.5% in the NaOH solution and 0.7% in the KOH solution; the molarities of NaOH and KOH solutions were determined with potassium acid phthalate with phenolphthalein as indicator. The concentration of a stock HNO_3 solution, prepared from concentrated HNO_3 and CO_2 free double deionized H_2O, was determined with the standard NaOH or KOH. The DMSA stock solutions were prepared by placing a desired amount of the compound, and two equivalents of base if *meso*-DMSA stock solution was being prepared, and CO_2-free double-deionized H_2O in a 50 mL volumetric flask. The concentrations of the DMSA solutions were calculated from the initial weight of the ligands and then confirmed by NaOH or KOH titration with methyl red as indicator. The 1.00 M $NaNO_3$ stock solution was prepared by dissolving 42.50 g $NaNO_3$ in 500 mL CO_2-free double-deionized H_2O. The titration solutions were prepared according to one of the following two procedures: (a) A calculated volume of CO_2-free deionized water was placed in a titration vessel into which a desired volume of the stock solution of DMSA was transferred, followed by addition of a desired volume of standard solution of HNO_3 (if necessary), and a desired amount of

KNO_3 crystals to maintain the ionic strength equal to 0.10±0.01 throughout the titration. (b) A constant volume of the stock solution of DMSA and 5.00 mL of 1.00 M $NaNO_3$ solution were transferred into a 50 mL volumetric flask, followed by addition of a desired volume of standard HNO_3 stock solution (if necessary), and then dilution to the mark with CO_2-free deionized water; 40.00 mL of this solution was then transferred to the titration vessel for potentiometric titration. The titration with each ligand was performed at 25.0 °C at least three times to estimate the uncertainties in the determined pK_a values.

^{1}H NMR Titration of *Rac*- and *Meso*-DMSA.

^{1}H spectra of *rac* and *meso*-DMSA solutions were obtained at ambient temperature (ca. 22°C) with Bruker AM-250 and WM-250 spectrometers, respectively, with digital resolution of 0.365 Hz/pt. The ^{1}H NMR spectra were obtained in 5-mm NMR tubes. The chemical shifts in aqueous solution were recorded relative to TBA and reported relative to sodium 2,2-dimethyl-2-silapentane-5-sulfonate (DSS)[1]. The advantage of using TBA is that its proton signal is independent of pH and ionic strength (*73*). Under our experimental conditions 0.4-1% by volume of TBA gave a good reference signal at 1.010 ppm downfield from DSS.

Rac-DMSA was titrated with tetramethylammonium deuteroxide solution, $(Me)_4NOD$, which was prepared by dissolving $(Me)_4NOH{\cdot}5H_2O$ in D_2O,

evaporating all solvent under vacuum, and redissolving the residual in D_2O. This procedure was repeated to ensure that most of the H_2O was removed. *Meso*-DMSA was titrated with sodium deuteroxide solution, which was prepared by dissolving NaOH in D_2O, evaporating all solvent under vacuum, and redissolving it in D_2O. This procedure was repeated to ensure that most of the hydrogen in NaOH was substituted by deuterium. The concentrations of the $(Me)_4NOD$ and the NaOD stock solutions were determined by titration with the standard HNO_3 solution. A stock solution of *rac*-DMSA was prepared in D_2O by dissolving a weighed amount of the compound in D_2O in a 5 mL volumetric flask and diluting to the mark.

The ^1H NMR titration solutions of *rac*-DMSA solution were prepared by addition of the same volume of the stock solution of *rac*-DMSA to 21 small test tubes, to which 10 μL 10% (v/v) TBA in D_2O and different volumes of $(Me)_4NOD$ stock solution were placed. D_2O was then added to each test tube to make the final volume 600 μL. The prepared solutions were transferred into 5-mm NMR tubes and sealed. After ^1H NMR spectra were recorded, the solutions were transferred to small test tubes for the measurement of p*D*. The ^1H NMR titration solution of *meso*-DMSA was prepared by weighing 14.6 mg of previously vacuum dried *meso*-DMSA in a 5-mm NMR tube followed by addition of 10 μL 10% (v/v) TBA in D_2O and 290 μL D_2O. A suspension was formed in

the tube but it was completely dissolved after two equivalents of NaOD were added. A series of ^{1}H NMR spectra of the resulting Na_2D_2(*meso*-DMSA) were obtained after the successive addition of 0.2 equivalents of NaOD. The pD values of the solution, after each addition of 0.2 equivalents of NaOD, were determined separately by carrying out a parallel experiment in a small test tube. The pD values of NMR titration solutions containing both DMSA stereoisomers were measured using a glass electrode calibrated with two standard buffers (pH= 4.00 and 7.00); the pH meter readings were not converted to -log[D^+]. Transfer of volume was made with the aid of a 200 μL micropipet which had been calibrated previously with deionized water by weighing.

IR Spectroscopy in KBr Pellets.

IR spectra of compounds suspended in KBr pellets were obtained with a Perkin-Elmer 1600 FT-IR spectrophotometer after 16 scans at a resolution of 4.0 cm^{-1}.

IR Spectroscopy in Aqueous Solution.

IR spectra of aqueous solutions were measured with a NICOLET Fourier transform IR spectrometer model 510P at ambient temperature. A calcium fluoride absorption cell, which has a transmission range from 66666 to 1110 cm^{-1}, equipped with a thin teflon spacer was employed, and the thickness of the cell, which was experimentally determined from the interference fringes (*74*), was

31 μm. All experimental IR spectra were recorded after 64 scans against purge nitrogen background and the resolution of the IR measurement was 2 cm^{-1} for all spectra. The processed IR spectra, plotted only in the frequency region between 1660 and 1300 cm^{-1} to show the asymmetric and symmetric stretching bands of the carboxylate groups in the DMSA isomers, were obtained after subtraction of the spectrum of D_2O from the experimental spectra. This was followed by a partial subtraction of the spectrum of a solution with supporting NaCl alone, if additional NaCl was added, and a partial subtraction of the spectrum obtained with 1% H_2O in D_2O. The subtraction of H_2O-in-D_2O spectrum, which displayed one strong band at 3418 cm^{-1} and another weak band at 1462 cm^{-1}, which is located between the two carboxylate stretching bands, was performed until the strong band at 3418 cm^{-1} in the resulting spectrum was completely removed.

Stock solutions of 0.10 M tetrasodium DMSA of the two DMSA isomers were prepared by dissolving 0.40 mmol of the appropriate DMSA in 4.0 mL of D_2O containing 0.40 M NaOD. A stock solution of 4.8 M NaCl was prepared in a 25 mL graduated cylinder by dissolving a weighed amount of NaCl crystals in D_2O. 200 μL solutions, prepared by mixing 0.1 M stock DMSA solution, 4.8 M stock NaCl solution and D_2O in varying ratios with the aid of micropipet, were used for measuring IR spectra.

Results

Synthesis and Isomerization of *Rac*-DMSA.

The synthesis is similar to Gerecke's synthesis (*63*) except that after the addition of thioacetic acid to acetylenedicarboxylic acid, *rac*-BATSA was isolated from the white precipitate formed. An attempt to increase the yield of the racemate was made by using the dimethyl ester of acetylenedicarboxylic acid instead of acetylenedicarboxylic acid; the addition reaction was found to favor the *meso* form and the yield of the *racemo* form was decreased.

^{1}H NMR spectroscopy was used to monitor the acid hydrolysis of *rac*-BATSA, (Fig. 1-1). Spectrum (c) in Fig. 1-2 of the starting material, *rac*-BATSA, showed proton resonance peaks at 4.3 and 2.0 ppm, which corresponded to the methine and methyl protons in *rac*-BATSA, respectively. The ratio of the areas under these two peaks was 1:3. The resonance peaks at 3.54 and 1.64 ppm, shown in spectrum (a) in Fig. 1-2, corresponded to the methine protons in DMSA and methyl protons in the acetic acid products, respectively. The ratio of the areas under these two peaks was 1:3. In all three spectra in Fig. 2, resonance peaks at 4.6, 4.1 and 5.1 ppm were present, which corresponded to protons in DHO and their spinning side bands, respectively.

The stereoisomeric identities of the products at different stages of the acid hydrolysis, shown in Fig. 1-1, were determined by comparing their IR spectra

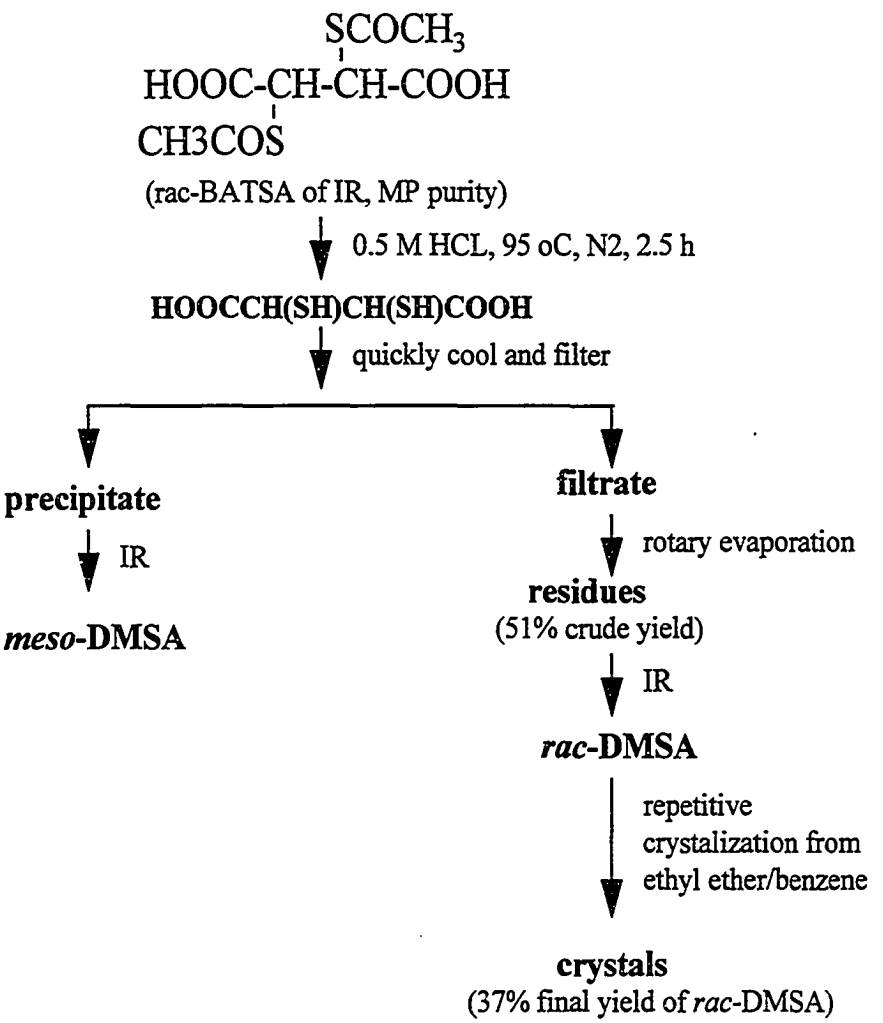

Figure 1-1. Acid hydrolysis of *rac*-BATSA at 95°C.

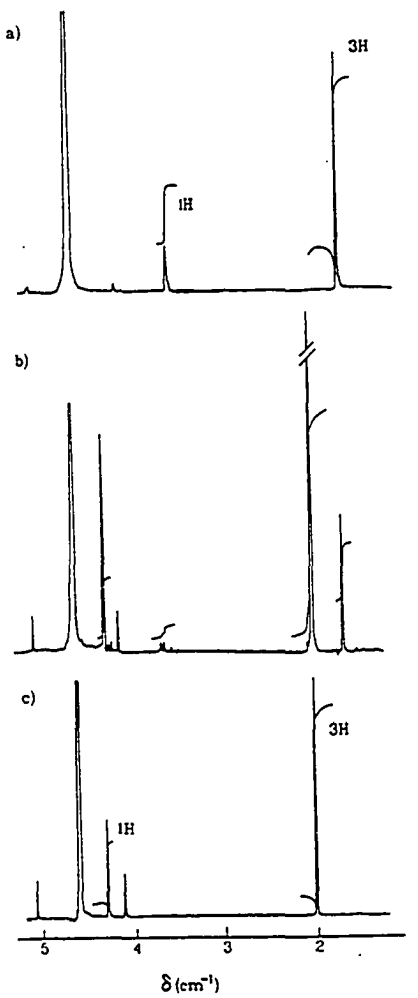

Figure 1-2. ^{1}H NMR spectra of acid hydrolysis of *rac*-BATSA. a) after heating to 95°C for 2.5 h; b) after reaction for 41 h at ambient temperature; c) starting *rac*-BATSA.

with the IR spectra of *rac*- and *meso*-DMSA, which were reported by Rivera et al. (*50*), and the IR spectra of *rac*- and *meso*-BATSA. The IR spectra of *rac*- and *meso*-DMSA and the IR spectra of *rac*- and *meso*-BATSA are shown in Fig. 1-3. The stereoisomeric purity of the starting material in the hydrolysis was established by its IR spectrum and melting point (*63*). The IR spectra of acidic hydrolysis products at different stages in the acid hydrolysis under different conditions are shown in Fig. 1-4; the isomerization of the *racemo* to the *meso* form was evident under our experimental conditions with a 49% crude yield of the *meso*-DMSA at 95°C (spectrum (b) in Fig. 1-4) and 12% crude yield at 50°C (spectrum (d) in Fig. 1-4). *Meso*-BATSA was also used to answer the question: Is the isomerization process reversible? The IR spectrum of the residue obtained by evaporation of the supernatant solutions after the acid hydrolysis of *meso*-BATSA at 95°C is shown in Fig. 1-4 spectrum (f). The IR spectra indicated that the conversion of the *meso* to *racemo* form did not occur.

In order to explore the mechanism of the isomerization observed above a sample of *rac*-DMSA of the same molar concentration of rac-BATSA used in the acidic hydrolysis was prepared in the presence of 0.5 M HCl and exposed to the same experimental conditions used in the acidic hydrolysis of *rac*-BATSA at 95°C. A white precipitate of *meso*-DMSA was formed when the reaction was cooled and maintained at 7 °C overnight. The amount of *meso*-DMSA formed,

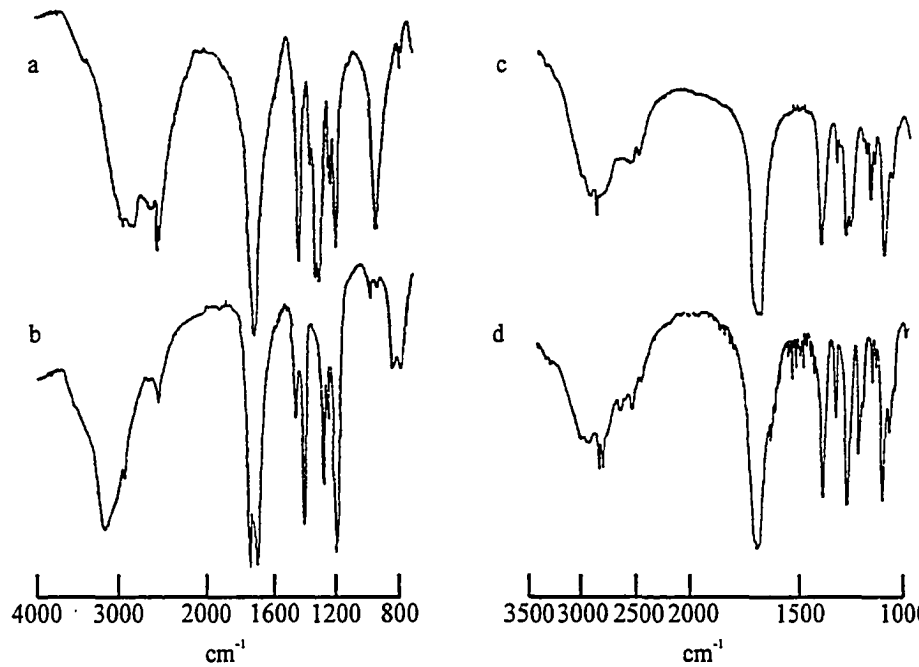

Figure 1-3. IR spectra of a) *meso*-DMSA; b) *rac*-DMSA; c) *meso*-BATSA; d) *rac*-BATSA.

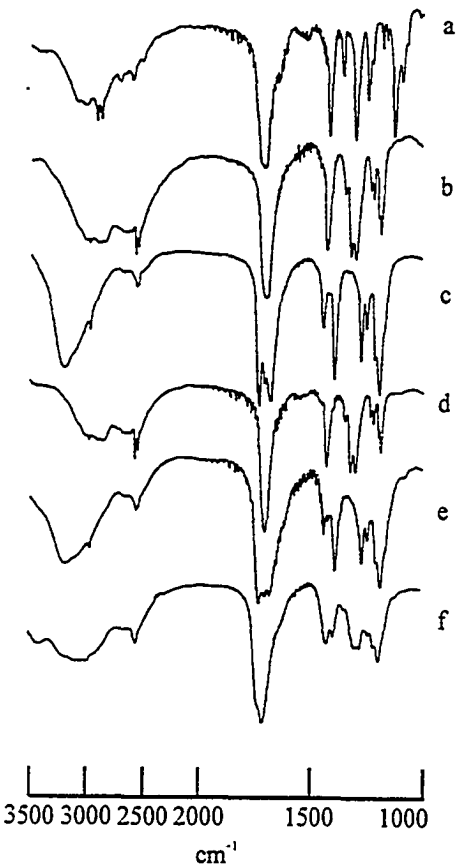

Figure 1-4. IR spectra of a) starting *rac*-BATSA for acid hydrolysis; b) precipitate from the reaction carried out at 95°C(crude yield 49%); c) purified *rac*-DMSA from the reaction carried out at 95°C(final yield 37%); d) precipitate from the reaction carried out at 50°C(crude yield 12%); e) residues from the filtrate from the reaction carried out at 50°C(crude yield 88%); f)residues from the filtrate of the acid hydrolysis reaction, carried out at 95°C starting with *meso*-BATSA (crude yield 5%).

however, was much less than that formed in the acidic hydrolysis of *rac*-BATSA.

X-ray Crystallography.

(A) ***Structure of Rac-BATSA.***

Table II in Appendix A contains the final positional and isotropic thermal parameters for *rac*-BATSA. The bond lengths and angles with standard deviations are listed in Tables 1-1 and 1-2, respectively. The crystal structure of *rac*-BATSA is shown in Fig. 1-5, and a stereoview of the unit cell is shown in Fig. I of the Appendix A.

The structure of *rac*-BATSA can be compared with the structure of dimethyl *meso*-BATSA (*51*), which is centrosymmetric and has a staggered configuration around the central C-C bond, with all torsion angles between equivalent groups equal to 180°. The structure of *rac*-BATSA is not centrosymmetric and the torsion angles for equivalent groups about the central C-C bond are not 180° (Fig. 1-5).

(B) ***Structure of Rac-DMSA.***

Table IV in Appendix A contains the final positional and isotropic thermal parameters for *rac*-DMSA. The bond lengths and angles with standard deviations are listed in Tables 1-3 and 1-4, respectively. The structure of *rac*-DMSA is shown in Fig. 1-6.

Table 1-1. Bond Lengths (Å) for *Rac*-2,3-bis-(acetylthio)succinic Acid[a].

atom 1	atom 2	distance(Å)	atom 1	atom 2	distance(Å)
O1A	HO1	0.85(3)	O1A	C1	1.312(2)
O1B	C1	1.201(2)	C1	C2	1.518(2)
C2	H2	0.98(3)	C2	C3	1.519(2)
C2	S1	1.818(1)	S1	C5	1.781(1)
C5	O5	1.201(2)	C5	C6	1.499(2)
C6	H6C	0.91(3)	C6	H6B	0.85(3)
C6	H6A	0.97(3)	C3	H3	0.94(2)
C3	C4	1.521(2)	C4	O4B	1.214(2)
C4	O4A	1.303(2)	O4A	HO4	0.77(2)
C3	S2	1.812(1)	S2	C7	1.793(1)
C7	O6	1.202(2)	C7	C8	1.496(2)
C8	H8C	0.93(2)	C8	H8B	0.87(3)
C8	H8A	0.86(3)			

[a] Numbers in parentheses are estimated standard deviations in the least-significant digits.

Table 1-2. Bond Angles (deg) for *Rac*-2,3-Bis-(acetylthio)succinic Acid[a].

atom 1	atom 2	atom 3	angle(deg)	atom 1	atom 2	atom 3	angle(deg)
C1	O1A	HO1	109(2)	C5	C6	H6A	108(1)
C4	O4A	HO4	112(2)	H6C	C6	H6B	120(2)
S1	C2	H2	101(1)	H6C	C6	H6A	104(2)
C1	C2	H2	109(1)	H6B	C6	H6A	111(2)
C3	C2	H2	111(1)	C7	C8	H8C	101(1)
S2	C3	H3	103(1)	C7	C8	H8A	111(2)
C2	C3	H3	111(1)	C7	C8	H8B	112(2)
C4	C3	H3	106(1)	H8C	C8	H8A	109(2)
C5	C6	H6C	108(2)	H8C	C8	H8B	119(2)
C5	C6	H6B	106(2)	H8A	C8	H8B	105(2)
C2	S1	C5	99.67(6)	C2	C3	C4	112.2(1)
C3	S2	C7	99.96(6)	O4A	C4	O4B	124.5(1)
O1A	C1	O1B	123.9(1)	O4A	C4	C3	113.0(1)
O1A	C1	C2	112.9(1)	O4B	C4	C3	122.5(1)
O1B	C1	C2	123.1(1)	S1	C5	O5	123.2(1)
S1	C2	C1	109.55(8)	S1	C5	C6	112.8(1)
S1	C2	C3	113.98(8)	O5	C5	C6	124.1(2)
C1	C2	C3	112.1(1)	S2	C7	O6	122.5(1)
S2	C3	C2	113.42(9)	S2	C7	C8	111.9(1)
S2	C3	C4	110.73(8)	O6	C7	C8	125.6(1)

[a] Numbers in parentheses are estimated standard deviations in the least-significant digits.

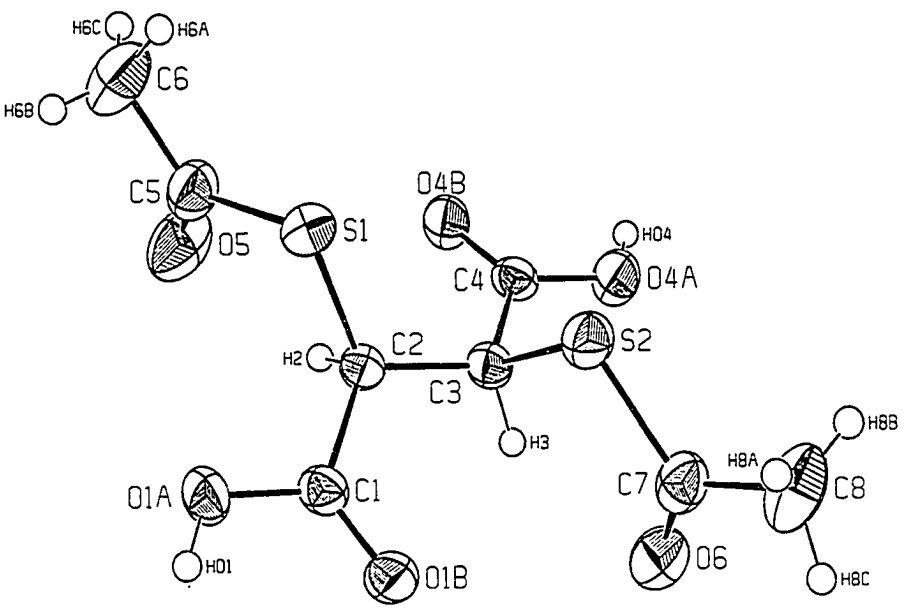

Figure 1-5. ORTEP of *rac*-2,3-bis-(acetylthio)succinic acid (*rac*-BATSA).

Table 1-3. Bond Lengths (Å) for *Rac*-DMSA[a].

atom 1	atom 2	distance(Å)	atom 1	atom 2	distance(Å)
S1	C2	1.803(3)	O4A	C4	1.306(3)
S2	C3	1.814(3)	C1	C2	1.511(4)
O1A	C1	1.320(3)	C2	C3	1.539(4)
O1B	C1	1.202(3)	C3	C4	1.509(4)
O4B	C4	1.214(3)	S1	HS1	1.17(4)
O4A	HO4A	0.78(4)	S2	HS2	1.07(4)
C2	HC2	0.99(4)	O1A	HO1A	0.87(4)
C3	HC3	0.91(4)			

[a] Numbers in parentheses are estimated standard deviations in the least-significant digits.

Table 1-4. Bond Angles (deg) for *Rac*-DMSA[a].

atom 1	atom 2	atom 3	angle(deg)	atom 1	atom 2	atom 3	angle(deg)
O1A	C1	O1B	125.3(2)	S2	C3	C2	112.4(2)
O1A	C1	C2	111.3(2)	S2	C3	C4	108.7(2)
O1B	C1	C2	123.4(2)	C2	C3	C4	111.1(2)
S1	C2	C1	108.6(2)	O4B	C4	O4A	125.1(2)
S1	C2	C3	112.5(2)	O4B	C4	C3	122.7(2)
C1	C2	C3	110.3(2)	O4A	C4	C3	112.2(2)
C2	S1	HS1	94(2)	C1	C2	HC2	113(2)
C3	S2	HS2	99(2)	C3	C2	HC2	108(2)
C1	O1A	HO1A	108(3)	S2	C3	HC3	106(2)
C4	O4A	HO4A	105(3)	C2	C3	HC3	108(3)
S1	C2	HC2	104(2)	C4	C3	HC3	111(2)

[a] Numbers in parentheses are estimated standard deviations in the least-significant digits.

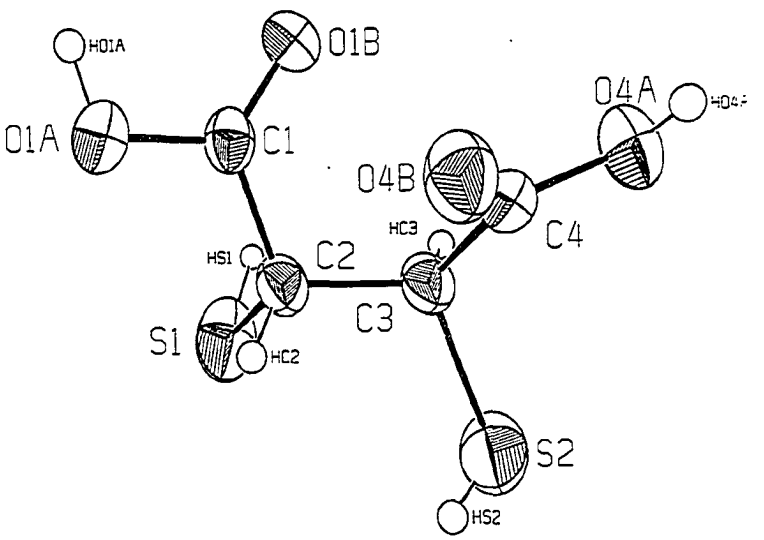

Figure 1-6. ORTEP of *rac*-2,3-dimercaptosuccinic acid (*rac*-DMSA).

Determination of Acid Dissociation Constants of *Rac*- and *Meso*-DMSA.

The pH meter readings at an ionic strength of 0.10 and 25.0°C were converted into hydrogen ion concentrations, $[H^+]$, and $-\log[H^+]$ (i.e. pH_{calc}) values by carrying out a titration of a standard solution of HNO_3 vs a standard solution of NaOH at the same ionic strength (0.10) and calculating the $[H^+]$ at every point on the titration curve. A linear plot of $-\log[H^+]$ vs pH measured was generated by a least-squares regression. The slopes of the generated straight lines were found to be always slightly larger, 0.5 to 0.2%, than the slopes displayed on the pH meter. This is an indication that sodium ions interfere in the measurement of high pH values. The propagated errors in the $-\log[H^+]$ values obtained from the above straight line are less than ±0.01 pH.

The dissociation constants K_{a1} to K_{a4} are given by

$$K_{a1} = \frac{[H^+][H_3L^-]}{[H_4L]} \qquad (1\text{-}1)$$

$$K_{a2} = \frac{[H^+][H_2L^{2-}]}{[H_3L^-]} \qquad (1\text{-}2)$$

$$K_{a3} = \frac{[H^+][HL^{3-}]}{[H_2L^{2-}]} \qquad (1\text{-}3)$$

$$K_{a4} = \frac{[H^+][L^{4-}]}{[HL^{3-}]} \qquad (1\text{-}4)$$

where H_4L represents the fully protonated DMSA.

The acid dissociation constants K_{a1} and K_{a2} were calculated from the titration data in the low pH buffer region by employing a linear least-squares method (Equations 1-5 and 1-6).

$$\frac{S[H^+]^2}{(S - 2C_a)} = - K_{a1} \frac{[H^+](S - C_a)}{(S - 2C_a)} - K_{a1}K_{a2} \qquad (1\text{-}5)$$

where $$S = [Na^+] + [H^+] - [OH^-] \qquad (1\text{-}6)$$

All concentration terms, in square brackets, are expressed in moles per liter; C_a is the analytical concentration of the DMSA. The values of K_{a1} and K_{a2} were obtained from the slope and Y-intercept of the straight line defined by Equation 1-5. Similarly the acid dissociation constants K_{a3} and K_{a4} were calculated from the titration data in the high pH buffer region by employing a linear least-squares method (Equations 1-7 and 1-8).

$$\frac{(S - 2C_a)[H^+]^2}{(S - 4C_a)} = - K_{a3} \frac{[H^+](S - 3C_a)}{(S - 4C_a)} - K_{a3}K_{a4} \qquad (1\text{-}7)$$

where $$S = [Na^+] + [H^+] - [OH^-] \qquad (1\text{-}8)$$

The values of K_{a3} and K_{a4} were given by the slope and Y-intercept of the straight line defined by Equation 7. The pK_a values of DMSA were also calculated using a non-linear fitting program entitled "PKAS" (*72*). The pK_a values obtained in our laboratory are compared with the pK_a values reported previously

(*75,76,77,78*), which are listed in Table 1-5, as well as used to simulate the potentiometric titration curves with the aid of the "BEST" program (*72*). The simulated curves are shown as solid lines in Fig. 1-7. Based on the pK_a values determined in our laboratory, species distributions of *rac*-DMSA as a function of pH are plotted in Fig. 1-8 to help later to identify the conformations of DMSA stereoisomers at different pD values in aqueous solution.

^{1}H NMR Titration of *Rac*- and *Meso*-DMSA.

The chemical shifts of the methine protons of the DMSA stereoisomers as a function of pD are plotted in Fig. 1-8. It was difficult to measure the chemical shifts of *meso*-DMSA when less than 2 equivalents of base was added because precipitates formed in the solution. Therefore, the chemical shifts of *meso*-DMSA were reported only after 2 equivalents of base were added. The chemical shifts of methine protons in *meso*-DMSA, shown in Fig. 1-8, remain almost constant in the course of deuteration of the two thiolate groups, when the pD was decreased from 12 to 4.2. In contrast to *meso*-DMSA, the chemical shift of the methine protons of *rac*-DMSA varies with pD in the course of the addition of 4 equivalents of base, shown in Fig. 1-8. When one deuterium ion is added to the *rac*-DMSA ligand, L^{4-}, DL^{3-} reaches a maximum concentration at pD 10.48, and the chemical shift of the methine protons increases from 3.081 to about 3.220 ppm, resulting in a 0.139 ppm downfield shift of the methine protons due to the

Table 1-5. Acid Dissociation Constants of *Meso-* and *rac*-DMSA at an Ionic Strength of 0.10 and 25.0 °C.

	Acid Dissociations	pK_a			
meso- DMSA	$H_4L \rightleftharpoons H^+ + H_3L^-$	2.45±0.01[a]	3.16(*76*)	2.71(*75*)	2.39(*78*)
	$H_3L^- \rightleftharpoons H^+ + H_2L^{2-}$	3.44±0.01[a]	4.55(*76*)	3.48(*75*)	3.58(*78*)
	$H_2L^{2-} \rightleftharpoons H^+ + HL^{3-}$	9.65±0.01[a]	9.45(*76*)	8.89(*75*)	9.33(*78*)
	$HL^{3-} \rightleftharpoons H^+ + L^{4-}$	11.89±0.01[a]	12.8(*76*)	10.79(*75*)	12.0(*78*)
rac- DMSA	$H_4L \rightleftharpoons H^+ + H_3L^-$	2.36±0.01[a]	2.25(*76*)	2.25±0.15(*77*)	
	$H_3L^- \rightleftharpoons H^+ + H_2L^{2-}$	3.87±0.04[a]	3.96(*76*)	4.13±0.15(*77*)	
	$H_2L^{2-} \rightleftharpoons H^+ + HL^{3-}$	9.42±0.02[a]	9.61(*76*)	9.54±0.10(*77*)	
	$HL^{3-} \rightleftharpoons H^+ + L^{4-}$	12.51±0.03[a]	> 11(*76*)	11.34±0.20(*77*)	

[a] The values were determined in our laboratory, and the errors were estimated from several sets of repetitive titration data.

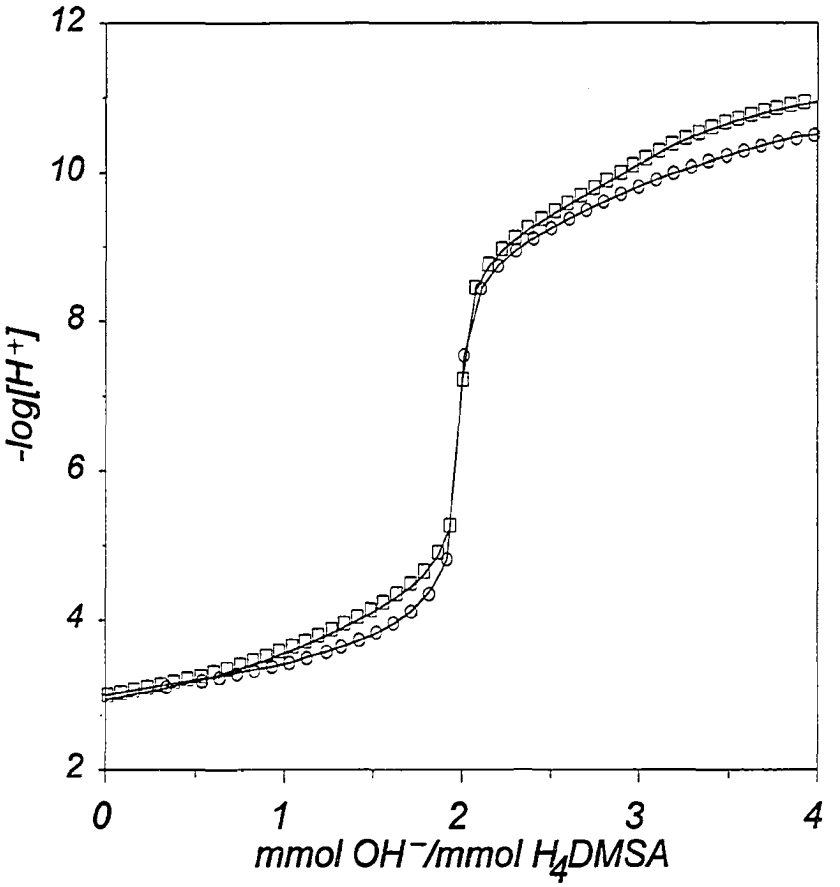

Figure 1-7. Potentiometric titration of 1.206 mM of *meso*-DMSA (○), and 1.405 mM of *rac*-DMSA (□). The solid lines represent the simulated titration curves for *meso*- and *rac*-DMSA solutions by the BEST program using the pK_a values determined in our laboratory.

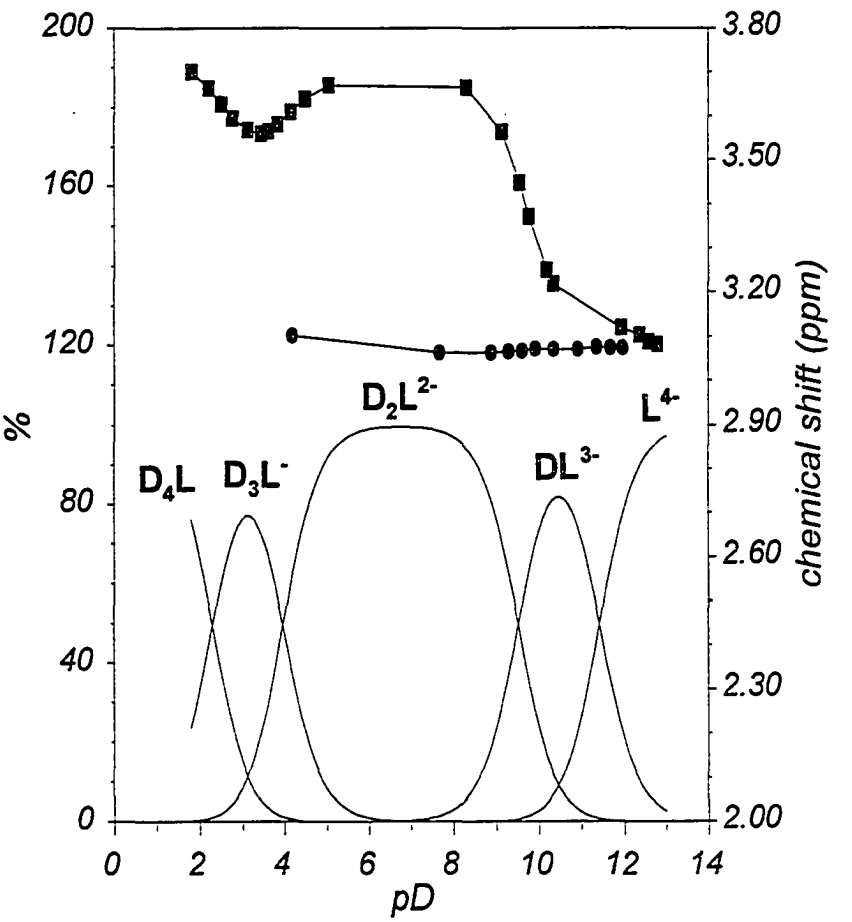

Figure 1-8. ■ : Chemical shift of methine protons of *rac*-DMSA versus pD; • : Chemical shift of methine protons of *meso*-DMSA versus pD; solid line: Distribution curves of *rac*-DMSA versus pD.

deuteration of one thiolate group. When the second deuterium ion is added on the *rac*-DMSA ligand, D_2L^{2-} reaches a maximum concentration around pD 6.75, and the chemical shift of the methine protons increases from 3.220 to 3.671. The net downfield chemical shift caused by deuteration of the second thiolate group is about 0.451 ppm, which significantly exceeds the chemical shift caused by the deuteration of the first thiolate group. At pD below 5.04, however, an "abnormal" upfield shift was observed as a result of deuteration of the first carboxylate group. When the third deuterium ion is added, the chemical shift of the methine protons moves upfield and reaches a minimum of 3.560 ppm at pD 3.46, where the concentration of the D_3L^- form is almost a maximum. The chemical shift caused by the deuteration of the first carboxylate group of *rac*-DMSA is -0.111 ppm, which obviously does not match the reported value of the chemical shift (0.20 ppm) (*73*) caused by deuteration of methylene protons directly attached to a carboxylate group. Decreasing pD from 3.46 to 1.82 results in a 75% deuteration of the second carboxylate group of *rac*-DMSA and moves the methine proton peak back to 3.702 ppm, with a net downfield chemical shift of 0.142.

Interpretation of ^{1}H NMR Results.

The use of proton magnetic resonance spectroscopy in combination with potentiometric titrations in the study of protonation sites and conformations of aminopolycarboxylic acids in aqueous solution has been described by Letkeman

and Martell (*79*). The deshielding effect of deuteration in NMR has been reported since the 1960's and deuteration of methylene protons directly attached to carboxylate groups causes a downfield shift by 0.20 ppm (*73*). An "abnormal" upfield shift of methylene protons directly attached to carboxylate groups, however, was also observed for aminopolycarboxylic acids in the low pD region (*80,81*). Letkeman and Martell (*79*) attributed this upfield shift to a positive long-range shielding effect of the carbonyl group because the carbonyl group has a negative as well as a positive long-range shielding effect that depends on the orientation and distance of a hydrogen atom from the carbonyl group (*82,83*). The positive shielding region of a carbonyl group is close to the *x* axis at the "carbon end" of the bond as well as above and below the plane of the bond, in the vicinity of the *z* axis.

The chemical shift of the methine protons in DMSA molecules depends on the electronic environment, which is determined by the overall deuteration status of the molecule, as well as the position of the methine protons relative to the carbonyl double bond of either carboxylate or carboxylic groups in the molecule, if the carboxylate or carboxylic acid groups in the molecule are restricted from free rotation around the central C-C bond. The two methine protons in the individual DMSA stereoisomer are magnetically equivalent in the

^{1}H NMR spectrum, and recorded as a singlet, and therefore, no information of site selective protonation is obtained from the NMR work.

Deuteration of one thiolate group of the *rac*-DMSA ligand causes a 0.139 ppm downfield shift of the methine proton peak, but deuteration of the second thiolate group causes a 0.451 ppm downfield shift of the methine proton peak. The additional 0.312 ppm downfield chemical shift must be induced by a change in conformation of the ligand upon the deuteration of the second thiolate group. In the resulting conformation of D_2L^{2-} of the *rac*-DMSA the two carboxylate groups must be restrained from free rotation and be positioned where a negative shielding effect is experienced by the methine protons. The estimated chemical shift resulting from this conformational change is about 0.312 ppm on the assumption that the contribution to the overall chemical shifts from the deuteration of the basic sites and steric restriction of the carbonyl group are additive. The reported value of the change in chemical shift of methylene protons is 0.20 ppm (*73*) upon deuteration of its directly attached carboxylate group, but the observed change in the chemical shift of the methine protons caused by the deuteration of the first carboxylate group of *rac*-DMSA is -0.111 ppm. The overall additional change in the chemical shift is -0.311, which is very close to the chemical shift caused by the conformational change after the deuteration of the second thiolate group. This indicates that D_3L^- of *rac*-DMSA assumes the

conformation of the completely deprotonated species, L^{4-}, of *rac*-DMSA after one of the two carboxylate groups of *rac*-DMSA is deuterated.

The downfield chemical shift due to the deuteration of two thiolate groups of the *rac*-DMSA molecule was not observed for *meso*-DMSA. Similarly, this has to be attributed to the change in the conformation of *meso*-DMSA in the course of addition of two deuterium ions. In the resulting conformations the carboxylate groups of *rac*-DMSA must be restrained from free rotation and positioned where a positive shielding effect is experienced by the methine protons in order to cancel out the deshielding effect resulting from the deuteration.

IR of *Rac*- and *Meso*-DMSA in Aqueous Solution.

The IR spectra of *rac*- and *meso*-DMSA tetrasodium salts in aqueous solutions at concentrations ranging from 0.1 to 0.01 M are shown in Fig. 1-9, and the IR spectra of 0.02 M *rac*- and *meso*-DMSA ligands, L^{4-}, at sodium ion concentrations ranging from 0.08 to 3.9 M are shown in Fig. 1-10.

Rac-DMSA is composed of equal amounts of two enantiomers (R,R-2,3-dimercaptosuccinic acid, (R,R-DMSA)[1], and S,S-2,3-dimercaptosuccinic acid, (S,S-DMSA)[1]). The IR stretching frequencies of the carboxylate groups, however, should not be affected by the chiral centers in the ligand because they are not chiral. The observed absorption bands in the spectra of tetrasodium *rac*-DMSA are unsymmetrical and composed of peaks at 1578 and 1553 cm^{-1}, under the

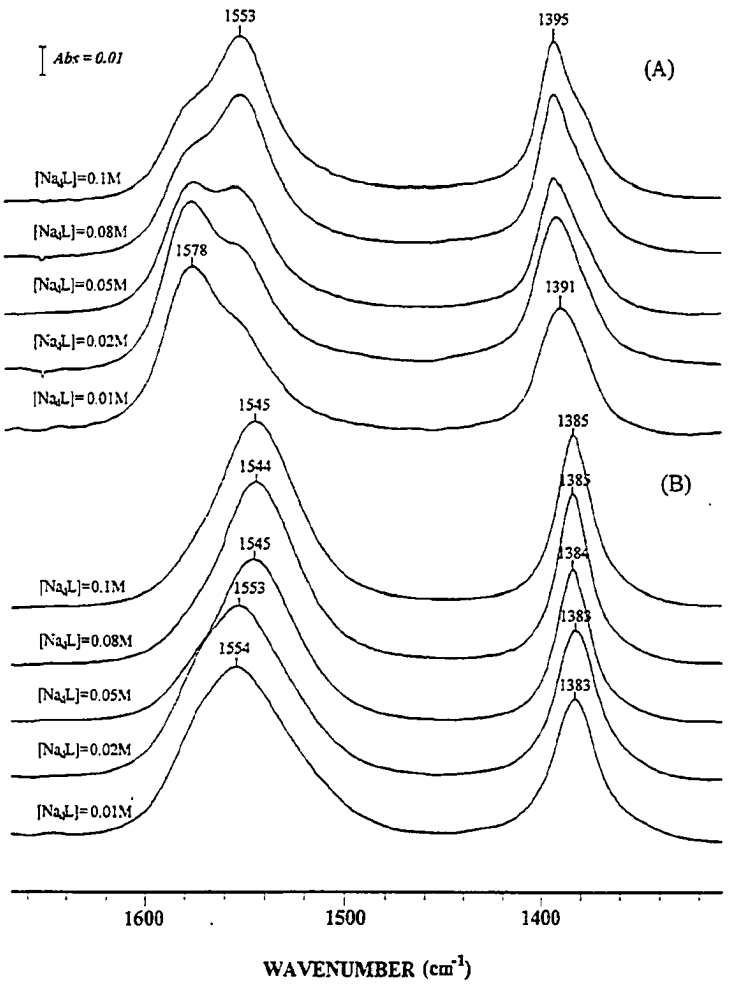

Figure 1-9. IR spectra of tetrasodium DMSA solutions at different concentrations. (A) *rac*-DMSA; (B) *meso*-DMSA.

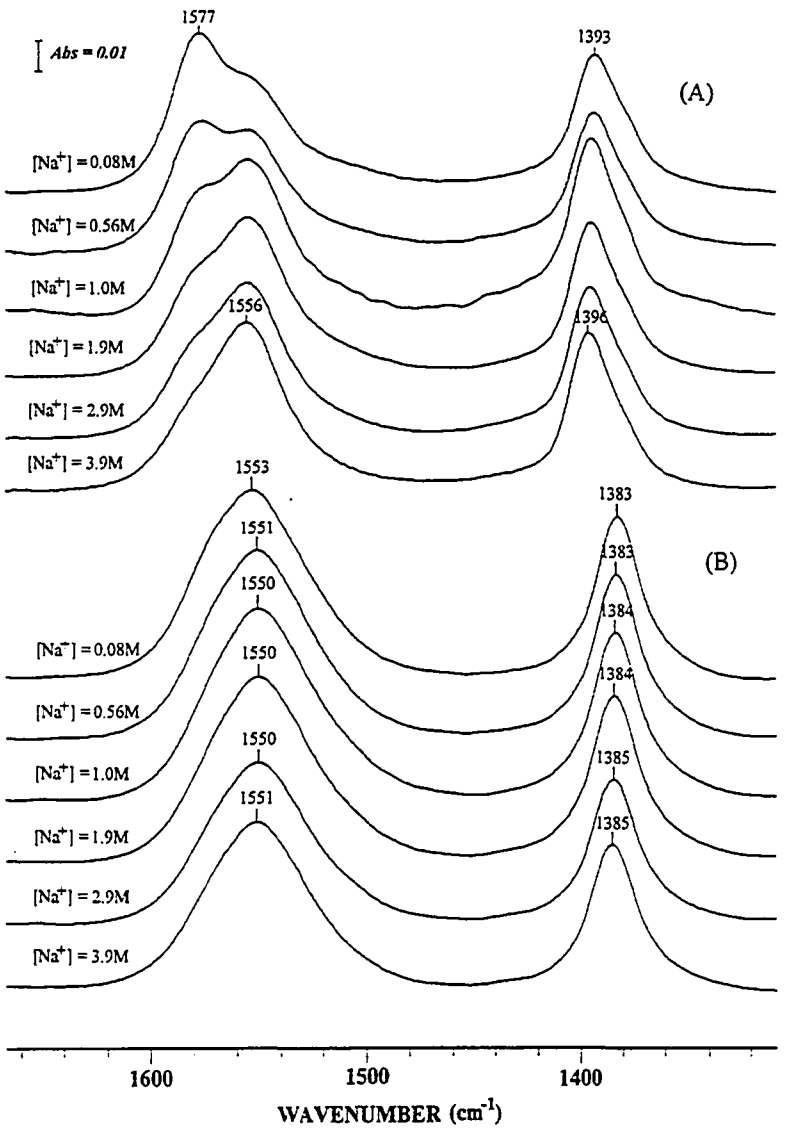

Figure 1-10. IR spectra of 0.02 M DMSA ligand, L^{4-}, solutions at different concentrations of sodium ion. (A) *rac*-DMSA; (B) *meso*-DMSA.

asymmetric stretching bands, and peaks at 1394 and 1380 cm^{-1} shown as small shoulders under the symmetric stretching bands. The ratio of the intensity of the 1553 cm^{-1} peak to the 1578 cm^{-1} peak increases with the concentration of *rac*-DMSA, and so does the ratio of the intensity of the 1394 cm^{-1} peak to the 1380 cm^{-1} peak (Fig. 1-9 (A)). The intensity change of the latter, however, is much smaller, and this may be explained by interaction of overtones of low frequency vibrations in the *rac*-DMSA with the symmetric stretching band. The exact positions of the four peaks also vary slightly with the change in the relative intensities because of the significant overlapping of the peaks. A similar change in the spectrum was observed for 0.02 M *rac*-DMSA solutions with addition of NaCl (Fig. 1-10 (A)). This indicates that the *rac*-DMSA ligands, L^{4-}, formed a comparatively stable ion-pair complex with sodium ions in the solution. The peak at 1553 cm^{-1} under the asymmetric stretching band can be safely assigned to the sodium ion-paired *rac*-DMSA ligand, and the peak at 1394 cm^{-1} is mainly due to the sodium ion-paired ligand as well.

Shown in Fig. 1-9 (B), the IR spectra of tetrasodium *meso*-DMSA remain almost unchanged at concentrations below 0.02 M, with the asymmetric and symmetric stretching bands of its carboxylate groups at 1553 and 1383 cm^{-1}, respectively. When the concentration increases from 0.02 to 0.05 M, both asymmetric and symmetric stretching bands become narrowed and shifted to 1545

and 1385 cm^{-1}, respectively. The peak narrowing and shifting may not be attributed to the formation of ion-paired complexes with sodium ions, because addition of NaCl to 0.02 M *meso*-DMSA tetrasodium solutions does not induce any noticeable changes in the spectra (Fig. 1-10 (B)). The origin of the sudden frequency shifts as a result of dilution is still not clear, and may be related to the change of solvation of the carboxylate groups. The *meso*-DMSA ligands are mainly present in the non-ion-paired form.

Discussion

Rac-DMSA Irreversibly Converts to *Meso* Form at Elevated Temperature in Acidic Condition.

Although Gerecke et al. (*63*) reported the synthesis of both the *racemo* and *meso* forms of DMSA, their synthesis has been used almost exclusively for the synthesis of *rac*-DMSA. The optimum yield of the racemate was, however, only 10.5%. The purification of the *rac*-BATSA from the filtrate after carrying out the addition reaction, as described by Gerecke et al. (*63*), is very difficult. The basic hydrolysis of *rac*-BATSA is affected by traces of oxygen because the resulting thiol compounds are readily oxidized under basic conditions to form disulfides and sulfonic acids (*84*). Attempts were made to improve the yield of *rac*-DMSA by modifying the procedures used in the isolation and purification of *rac*-BATSA, and by hydrolyzing *rac*-BATSA under acidic conditions.

It was found that the acid hydrolysis reaction was extremely slow at ambient temperature. When the reaction mixture was heated for about an hour at 95°C, most of the *rac*-BATSA was converted to DMSA, and after 2½ hours the conversion was complete. The product was *meso*-DMSA which precipitated as a white solid. The ^{1}H NMR spectrum showed only peaks at 3.54 and 1.64 ppm (Fig. 1-2). The conversion of *rac*- to *meso*-DMSA was clearly demonstrated by recording the infrared spectra, shown in Fig. 1-4, of the reaction product during

the course of the acid hydrolysis. Based on the results of the acid hydrolysis experiments, which are summarized in Table 1-6, the following conclusions have been made:

1) The acid hydrolysis of *rac*-BATSA did not improve the yield obtained by hydrolyzing under basic conditions; the yield was about 90% when the hydrolysis was performed in 3M NaOH at 0°C.

2) Isomerization of the *racemo* form to the *meso* form occurred at high temperature, and the extent of isomerization increased with an increase in temperature.

3) The isomerization is irreversible.

The isomerization of the *racemo* form to the *meso* form of DMSA in acidic aqueous solution has not been reported previously. There are two possible mechanisms (Fig. 1-11) for the isomerization. Both involve the participation of a neighboring group. Mechanism (A) is based on the formation of a five-membered intermediate via the carbonyl oxygen in the thioacetyl group of *rac*-BATSA, but mechanism (B) suggests a simple migration of a neighboring hydrogen. Mechanism (A) requires a thioacetyl group for the isomerization to occur, whereas mechanism (B) does not require a thioacetyl group; therefore, the isomerization should occur with *rac*-DMSA. The isomerization of *rac*-DMSA, under the same conditions as *rac*-BATSA, indicated that the thioacetyl group is

Table 1-6. Isomerization of DMSA in Acidic Aqueous Solution.

BATSA	DMSA crude yield		Temperature	Reaction time
	meso	*racemo*		
racemo	49%[a]	51%[b], 37%[c]	95°C	2.5 hr
meso	85%[a]	5%[b]	95°C	2.5 hr
racemo	12%[a]	88%[b]	50°C	36 hr
racemo	no reaction	no reaction	room temperature	36 hr

[a] The values were estimated from the weight of precipitate.
[b] The values were estimated from the weight of the residue obtained by evaporation of the filtrate.
[c] The value was estimated from the weight of final purified *rac*-DMSA.

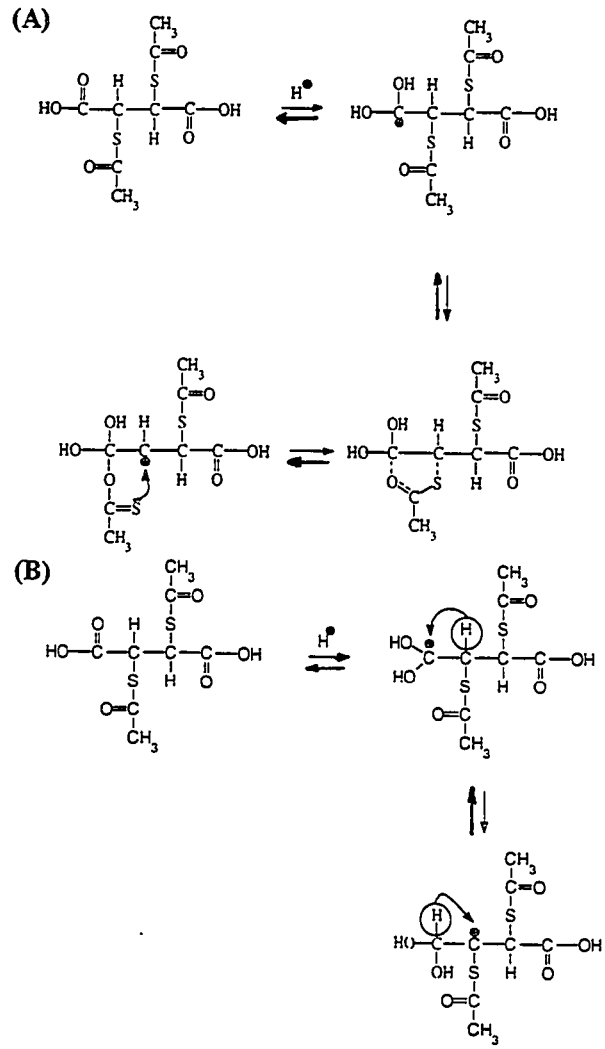

Figure 1-11. Possible mechanisms of the isomerization of *racemo* to *meso* form in an acidic aqueous solution.

not necessary for the reaction to occur, although the reaction is much slower in the absence of the thioacetyl group. Both mechanisms (A) and (B) may be involved, therefore, in the isomerization during the acid hydrolysis of *rac*-BATSA.

Meso-DMSA Is More Stable in The Crystalline Form and Less Soluble Than _Rac_-DMSA.

The solubilities of the DMSA stereoisomers are determined, at least in part, by the stabilities of the crystal lattice structures of the isomers. The single crystal X-ray analysis of *rac*-DMSA shows that the *rac*-DMSA molecule adopts a staggered gauche-conformation, Fig. 1-6, in which the two carboxylic acid groups are positioned on one side of the molecule and the two thiol groups are positioned on the other side. The arrangement of *rac*-DMSA molecules in the crystal lattice is shown in Fig. 1-12. The individual *rac*-DMSA molecules in the crystal lattice form four intermolecular hydrogen-bonds with their neighbouring *rac*-DMSA molecules, through carboxylic acid groups, to form a double-stranded structure with all the thiol groups of the *rac*-DMSA, which participate in the double-strand formation, pointed towards the outside. The double-stranded units then stack on each other by van der Waals forces to form a three-dimensional structure in the *rac*-DMSA crystal. The structure of *meso*-DMSA in the pure solid state has not been reported in the literature, but the structure of *meso*-DMSA in

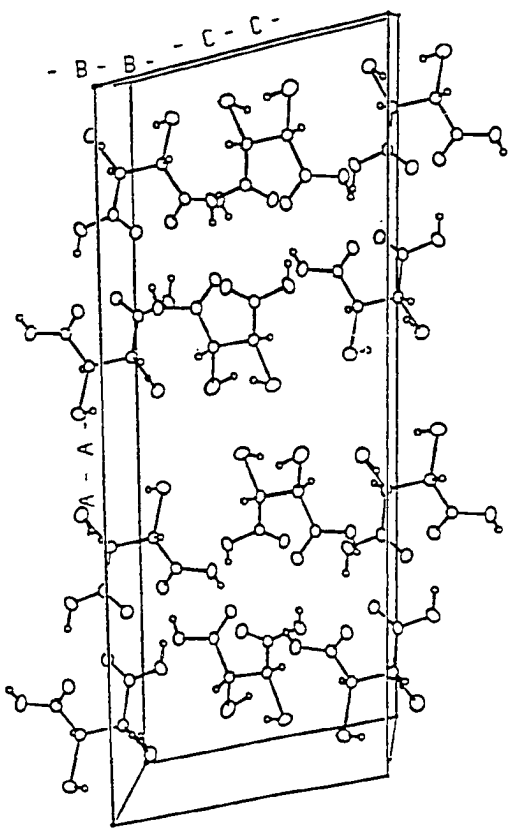

Figure 1-12. Molecular packing in the unit cell of *rac*-2,3-dimercaptosuccinic acid (*rac*-DMSA).

a single crystal of 1:2 adduct of *meso*-DMSA and *N,N*-dimethylformamide has been determined *(85)*. The structure of the dimethyl ester of *meso*-DMSA in the solid state has also been determined (*86*). It was found that the *meso*-DMSA in the adduct adopts a staggered anti-conformation, in which the two carboxylic acid groups are opposite each other as are the two thiol groups, and so does its dimethyl ester. Therefore, it is reasonable to assume that the *meso*-DMSA adopts the same staggered anti-conformation in the pure solid state as it does in the solid state in its adduct with dimethylformamide. The most energetically favorable arrangement of *meso*-DMSA molecules in a single crystal is illustrated in Fig. 1-13, in which the individual *meso*-DMSA molecules are stabilized by maximizing the interactions with their neighbouring *meso*-DMSA molecules. Each *meso*-DMSA molecule in the postulated crystal lattice structure forms four hydrogen-bonds, through the two carboxylic acid groups, with its four neighbouring *meso*-DMSA molecules to form a three-dimensional network structure. The postulated three-dimensional structure of *meso*-DMSA is much more stable than that determined for *rac*-DMSA because the three-dimensional lattice structure of *meso*-DMSA is stabilized by the hydrogen-bonds between the individual molecules, whereas, the three dimentsional structure of *rac*-DMSA is stabilized by van der Waals forces between the double-stranded units; in addition, the stacking of the double-stranded units of *rac*-DMSA

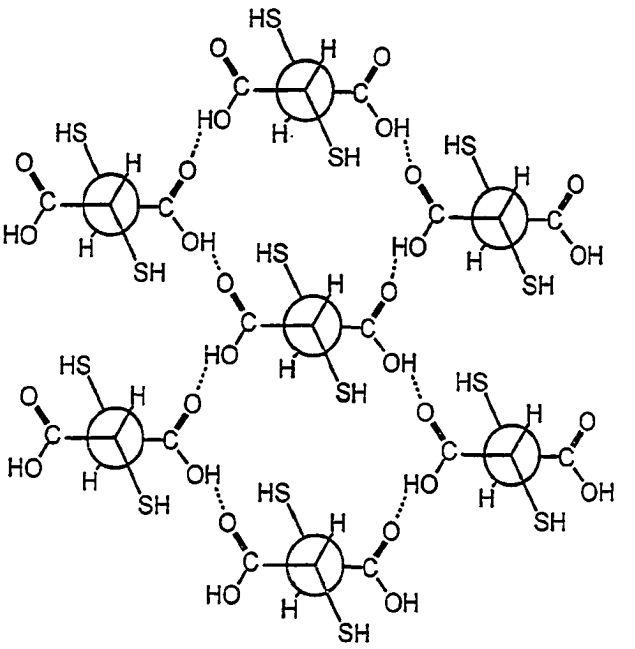

Figure 1-13. Postulated arrangement of *meso*-DMSA molecules in the solid state.

is further weakened as a result of the repulsions between the thiol groups which are all located outside the double-stranded units of *rac*-DMSA. This accounts for the higher solubility of *rac*-DMSA in aqueous solution.

Conformations of *Rac*-DMSA at Different Protonation Stages in Aqueous Solution.

The conformations of *rac*-DMSA at different protonation stages are proposed in Fig. 1-14, using S,S-DMSA as an example, according to the following considerations: firstly, the proposed conformations must explain the results obtained from ^{1}H NMR and IR experiments; secondly, the proposed conformations are energetically favorable. To obtain an energetically favorable conformation three factors must be considered in the following order: (1) the number of intramolecular hydrogen-bonds is maximized, (2) the repulsion between the carboxylate or carboxylic acid groups and thiolate or thiol groups is minimized, and (3) the interaction between sodium ions and the ligands is increased. It is also reasonable to assume that the sodium ions only bind with the carboxylate groups in the sodium ion-pairs of the *rac*-DMSA.

The *rac*-DMSA ligands, L^{4-}, have been shown in the results section to form ion-paired complexes, and the formation of ion-pairs results in a shift of 25 cm^{-1} of the asymmetric stretching of the carboxylate group to a lower frequency. The 25 cm^{-1} red shift may be rationalized by the electrostatic interaction between

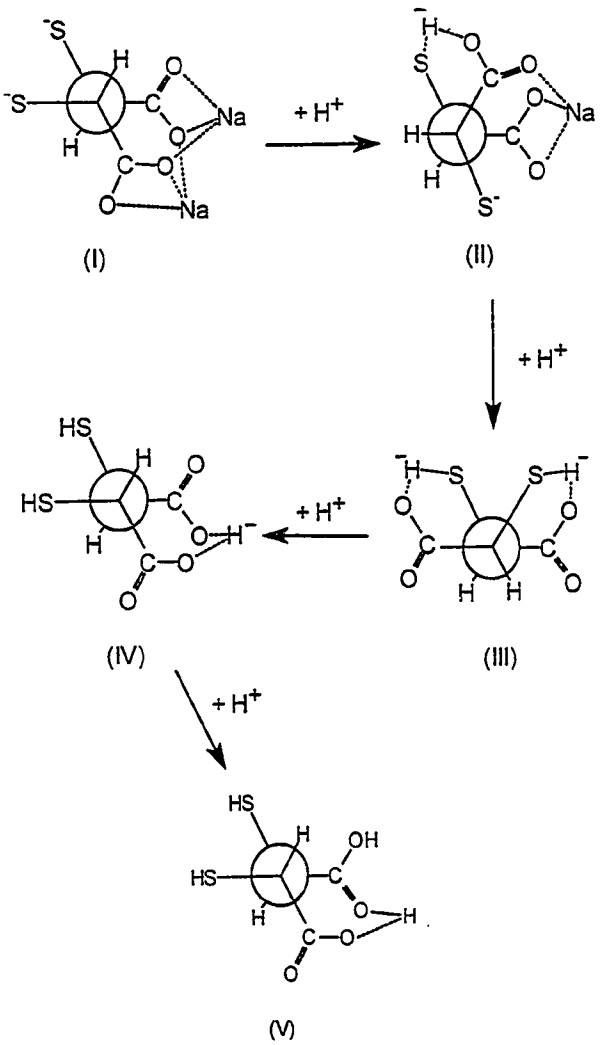

Figure 1-14. Conformations of the species (I) Na_2L^{2-}, (II) $NaHL^{2-}$, (III) H_2L^{2-}, (IV) H_3L^- and (V) H_4L of *rac*-DMSA.

the sodium ion and the carboxylate group involved. The carboxylate groups of the *rac*-DMSA ligands, L^{4-}, in the ion-paired state are almost as symmetrical as in the "free" state, with the two oxygen atoms of any individual carboxylate group being equivalent with respect to their local electron environments. The electrostatic attraction between positively-charged sodium ions and "free" carboxylate groups simply induces a withdrawal of electrons from the carboxylate groups and results in a reduction of the strength of the stretching vibration of the carboxylate groups, which accounts for the red shift of the asymmetric stretching frequency in the IR spectra of the *rac*-DMSA ligands in solutions.

The proposed fomula for the sodium ion-paired complex of *rac*-DMSA ligand, L^{4-}, is Na_2L^{2-}. This complex adopts a conformation, shown in Fig. 1-14 (I), in which each carboxylate group is located at a staggered anti-position with respect to a thiolate group of the ligand. This conformation is energetically most favorable because both carboxylate groups and both thiolate groups of the ligand are located in different hemispheres, so that the repulsion between them is minimized. The proposed ion-paired complex is also stable by adopting the conformation, shown as Fig. 1-14 (I), in which each sodium ion is linked to three oxygen atoms of the two carboxylate groups, so that the electrostatic attraction between sodium ions and carboxylate groups is maximized. As a result of the ion-pair formation, the carboxylate groups of the ligand in Na_2L^{2-} are restrained from

free rotation and the methine protons of the ligand are located outside the deshielding planes of the carboxylate groups. The monoprotonated *rac*-DMSA exists in the ion-paired form, i.e. $HNaL^{2-}$, and adopts a conformation (Fig. 1-14 (II)) in which the thiol group forms an intramolecular hydrogen-bond with one of the two ion-paired carboxylate groups to form a single six-membered ring in the ligand. As a result of the hydrogen-bond formation, one of the two sodium ions initially bound in the Na_2L^{2-} of the ligand is depleted from the ligand. By comparing the conformations of Na_2L^{2-} and $HNaL^{2-}$(Fig. 1-14 (I) and (II)), it is found that the front carboxylate group in $HNaL^{3-}$ rotates 120 degrees anti-clockwise around the central C-C bond, with respect to the conformation of Na_2L^{2-}, however, the relative orientations of the methine protons to the carbonyl bond planes of the carboxylate groups do not vary significantly from Na_2L^{2-} to $HNaL^{2-}$. Therefore, in the ^1H NMR experiment with the *rac*-DMSA ligands, the change in the chemical shift of the methine protons, observed after the addition of one deuterium ion to the ligand, is caused only by the deshielding effect of the deuteration and by some shielding effect resulting from the release of one sodium ion. The diprotonated *rac*-DMSA exists as H_2L^{2-} and adopts a conformation (Fig. 1-14 (III)) in which two intramolecular hydrogen-bonds are formed via one thiol group and one carboxylate group of the ligand, respectively. By comparing the conformations of H_2L^{2-} and Na_2L^{2-} (Fig. 1-14 (III) and (I)), it is found that the

front carboxylate group in H_2L^{2-} rotates 120 degrees clockwise around the cntral C-C bond, with respect to the conformation of Na_2L^{2-}, and the relative orientations of the methine protons to the carbonyl bond planes of the carboxylate groups undergo a significant change from Na_2L^{2-} to H_2L^{2-}. As a result of the formation of two intramolecular hydrogen-bonds, both sodium ions initially bound in the Na_2L^{2-} of the ligand are released from the ligand and two six-membered rings are formed in the ligand. Both six-membered rings adopt energetically more favorable chair conformations in which both methine protons of the ligand are located within the plane of the carbonyl double bond, where the deshielding effect of the carbonyl double bond reaches a maximum. This accounts for the additional downfield shift of 0.312 ppm, observed in the ^1H NMR experiments with *rac*-DMSA when the second thiolate group of the ligand was deuterated. The triprotonated *rac*-DMSA exists as H_3L^- and adopts a conformation (Fig. 1-14 (IV)) in which one intramolecular hydrogen-bond is formed via two oxygen atoms from the different carboxylate groups of the ligand. By comparing the conformations of H_3L^- and Na_2L^{2-} (Fig. 1-14 (IV) and (I)), it is found that H_3L^- of the *rac*-DMSA assumes the conformation of Na_2L^{2-} of *rac*-DMSA, and the methine protons of the ligand are again positioned outside the deshielding planes of the carboxylate groups. This accounts for the additional upfield shift of 0.311 ppm, observed in the ^1H NMR experiments with *rac*-DMSA when the first

carboxylate group of the ligand was deuterated. Fully protonated *rac*-DMSA adopts a conformation (Fig. 1-14 (V)) similar to that of H_3L^- of the *rac*-DMSA. The formation of one intramolecular hydrogen-bond between the two carboxylic acid groups of the ligand prevents the relative orientation of the methine protons to the carbonyl bond planes of the carboxylic acid groups from changing as a result of protonation of H_3L^- of the *rac*-DMSA. This explains why the observed change in the chemical shift of the methine protons due to the deuteration of H_3L^- of *rac*-DMSA agrees with the value reported in the literature for the deuteration of a carboxylate group.

Conformations of *Meso*-DMSA at Different Protonation Stages in Aqueous Solution.

In contrast to *rac*-DMSA ligand, as shown in Fig. 1-10 (B), both asymmetric and symmetric stretching bands of tetrasodium *meso*-DMSA in solution are not affected by the addition of sodium ions, which indicates that *meso*-DMSA does not form an ion-paired complex with sodium ions under our experimental conditions. Fully deprotonated *meso*-DMSA exists as L^{4-} and adopts a conformation (Fig. 1-15 (I)) in which the two carboxylate groups are located at a staggered anti-position and so are the two thiolate groups of the ligand. The carboxylate groups of the ligand are free to rotate in the proposed conformation of L^{4-} of *meso*-DMSA. The repulsion between the carboxylate groups and the

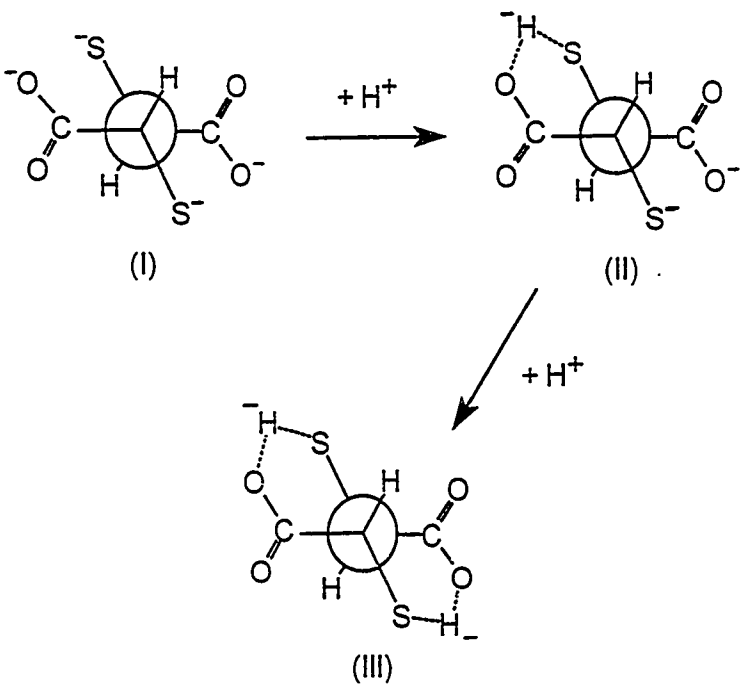

Figure 1-15. Conformations of the species (I) L^{4-}, (II) HL^{3-} and (III) H_2L^{2-} of *meso*-DMSA.

thiolate groups is minimized in the proposed structure because the four negatively-charged groups are positioned in two hemispheres. Because the two carboxylate groups of the ligand have a staggered anti-relation, each sodium ion in the ion-paired complex of *meso*-DMSA binds with only two oxygen atoms of each carboxylate group, and therefore, the resulting ion-paired complex is less stable than that of *rac*-DMSA. This explains why the sodium ion-paired complexes of *meso*-DMSA were not observed in our IR experiments. Monoprotonated *meso*-DMSA exists as HL^{3-} and adopts a conformation (Fig. 1-15 (II)) similar to that of L^{4-} of *meso*-DMSA. The thiol group in the HL^{3-} of *meso*-DMSA forms an intramolecular hydrogen-bond with one of the two carboxylate groups to form a single six-membered ring in the ligand. The six-membered ring adopts an energetically favorable chair conformation. As a result of the hydrogen-bond formation, the carboxylate group which participates in the hydrogen-bonding is restrained from free rotation, and its adjacent methine proton is located in the shielding zone of the carbonyl bond planes (*82,83*) of this carboxylate group. This induces an additional shielding effect on the methine proton and cancels out the deshielding effect caused by protonation of one of the thiolate groups. This explains why, in the ^1H NMR experiments with *meso*-DMSA ligands, the observed chemical shift of the methine protons of *meso*-DMSA does not change significantly upon addition of one deuterium ion to the ligand, L^{4-}. The

diprotonated *meso*-DMSA exists as H_2L^{2-} and adopts a conformation (Fig. 1-15 (III)) similar to that of HL^{3-} of *meso*-DMSA. Two intramolecular hydrogen-bonds are formed in the proposed conformation for H_2L^{2-}. This results in the formation of two six-membered rings which are in the chair conformations in the ligand. In this case, both carboxylate groups are restrained from free rotation and both methine protons in the ligand are located in the shielding zone of the carbonyl bond planes of the carboxylate groups. The induced additional shielding effect on the methine protons again cancels out the deshielding effect caused by protonation of both of the thiolate groups of *meso*-DMSA. This explains why, in the ^1H NMR experiments with *meso*-DMSA, the observed chemical shift of the methine protons of remains almost unchanged in the course of the addition of the second deuterium ion to the ligand.

In summary, the conformations of the species H_4L, H_3L^- and L^{4-} of *rac*-DMSA in aqueous solution are similar to that of H_4L of *rac*-DMSA in the solid state, whereas the conformations of the species H_2L^{2-} and HL^{3-} of *rac*-DMSA in aqueous solution are different from that of H_4L of *rac*-DMSA in the solid state; the conformations of the species H_2L^{2-}, HL^{3-} and L^{4-} of *meso*-DMSA in aqueous solution are similar to that of H_4L of *meso*-DMSA in the solid state.

CHAPTER TWO: STRUCTURES AND PROPERTIES OF ZINC CHELATES OF DMSA STEREOISOMERS IN AQUEOUS SOLUTION

Introduction

The unique properties of hydrophilicity and lipophilicity of *rac*-DMSA account for its higher efficacy in the rapid excretion of mercury and cadmium (*56,57*), and also indicate that *rac*-DMSA can be a superior and more promising chelating agent than *meso*-DMSA for lead poisoning. An increased urinary excretion, by approximately a factor of 2, of zinc by *rac*-DMSA was also reported (*57,62*) when identical doses of *meso*- and *rac*-DMSA were administered to rats. The various aspects of the physiological and biological functions of zinc in humans have been reviewed in a book entitled "Zinc" (*87*), and the following introduction is based on the literature cited in this book.

Zinc is found in every human tissue and tissue fluid, although concentrations vary. The mean serum concentration of zinc is approximately 100 μg/dL. Zinc is also an important constituent of red blood cells, representing approximately 10 times the amount of zinc found in serum. Zinc in serum is mainly bound to either proteins, forming macromolecular zinc complexes, or small ligands, forming micromolecular zinc complexes. Approximately 32% of the zinc circulating in blood serum is bound to an α_2-macroglobulin, forming a tight complex with a formation constant of 10^{10}. It has been proposed that the

zinc-α_2-macroglobulin complex is formed and metabolized only in the liver. About 66% of the serum zinc is bound to albumin, forming a loose complex with a formation constant of 10^6, presumably to one of the histidine moieties of this molecule. The albumin-bound zinc is in equilibrium with amino acid zinc complexes that comprise about 1-2% of the serum zinc. The amino acid-zinc complexes, which are almost exclusively composed of the amino acids histidine and cysteine, are available for transport to all tissues, including body organs, red cells, and brain. Histidine and cysteine easily cross the blood-brain barrier (*88*).

An increase in the concentration of micromolecular zinc complexes, that readily cross the renal glomerulus, could lead to an excessive loss of endogenous zinc. Observations of several investigators indicate that under normal conditions about 0.5 mg zinc is excreted in urine daily, although extrapolations from model studies suggest that excretion of micromolecular zinc-amino acid complexes by renal glomerular filtration of 183 liters contributes to 2 mg zinc in 24 hr. This suggests that the major part of the normal filtered load of amino acid-complexed zinc must be reabsorbed by the kidney. It has been postulated that metallothionein, which contains both zinc and cadmium, may play an important role in the conservation of zinc.

Zinc is an integral component of DNA polymerase, and therefore, any rapidly dividing cellular system has an important requirement for zinc. Zinc as a

cofactor with many enzymes has been well known. Zinc also plays an important role in the stabilization of biological membranes, participation in electron transfer processes and in enzyme-substrate interactions (*89*). Hormonal activity can be influenced by zinc-interactions at several levels of action, including synthesis, secretion, target-organ binding, and function. The LD_{50} of *rac*-DMSA is 10.84 mmol/kg (*58*), which is a little higher than that of *meso*-DMSA (LD_{50}=13.73 or 10.9 mmol/kg, i.p., depending on the source of the drug (*58*)). The higher toxicity of *rac*-DMSA could be, at least in part, attributed to the high extent of excretion of endogenous zinc by *rac*-DMSA. It is important to understand the reasons for these differences in the depletion of endogenous zinc when different chelating agents or the stereoisomers of the same chelating agent are administered in the treatment of heavy metal poisoning. A knowledge of the chemistry of zinc complex formation with the diastereoisomers of DMSA can also help in selecting the conditions under which these chelating ligands are employed for the treatment of heavy metal poisoning. A knowledge of the interaction between zinc and the diastereoisomeric DMSA molecules will also assist in designing derivatives of *rac*-DMSA which do not excrete endogenous zinc to a significant extent but are more effective in mobilizing *in vivo* heavy metals. A knowledge of the structure of zinc complexes with DMSA molecules will also provide important information on the mechanism of *in vivo* mobilization of endogenous zinc by DMSA.

In this chapter the results of comparative experiments that have been performed with *meso*- and *rac*-DMSA are described. A speciation model that includes a series of complexes formed in aqueous solutions containing Zn^{2+} and *meso*- or *rac*-DMSA has been proposed, and experimental evidence which confirms this speciation model is presented. The conformations of various dimeric and monomeric zinc complexes have been determined in aqueous solutions and the distributions of these zinc complexes in solution have been calculated as a function of pH, and their formation constants have been determined. On the basis of the distributions of these zinc complexes formed with *meso*- and *rac*-DMSA, the reason why *rac*-DMSA excretes endogenous zinc to a greater extent than its *meso* isomer has been demonstrated. The difference in the depletion of endogenous zinc by the DMSA stereoisomers has also been rationalized, at a molecular level, by analysis of the structures of the zinc complexes formed in aqueous solutions with the two isomers. Finally, *rac*-DMSA has been proposed to be used clinically as an effective prophylactic for the prevention of lead poisoning; the ZnL_2 complex of *rac*-DMSA has been proposed as a better therapeutic antidote for lead poisoning than *meso*-DMSA alone.

Experimental Section

Materials.

Deuterium oxide, deuterated methanol, zinc bromide (98+%) and tetramethylammonium (TMA)[1] hydroxide pentahydrate (99%) were purchased from Aldrich Chemical Co. Inc. (Milwaukee, WI). ***Caution:*** *tetramethylammonium hydroxide is a very strong base and corrosive, it has a strong ammonia-like odor, and should be manipulated in a hood.* Tert-butyl alcohol was purchased from EM (Gibbstown, NJ) and distilled before use; all organic solvents used were purchased from EM; *rac*-DMSA was synthesized as described in Chapter One; *meso*-DMSA was a gift from Johnson & Johnson Baby Products Co. (Skillman, NJ); all other inorganic compounds used were purchased from Mallinckrodt, Inc. (Paris, KY), and were of analytical reagent grade. ***Caution:*** *Gloves are necessary in the handling of all the above chemicals to avoid direct contact with skin.*

Potentiometry.

The apparatus and procedures used for potentiometric measurement of hydrogen ion concentration have been described in Chapter One. The standard NaOH or KOH solutions, HNO_3 solution and DMSA solutions were prepared in the same way as those used in Chapter One. A stock Zn^{2+} solution was prepared

from $Zn(NO_3)_2xH_2O$ and CO_2-free double-deionized H_2O, and its concentration was determined by EDTA titration.

The titration solutions were prepared according to one of the following two procedures: (a) A calculated volume of CO_2-free deionized water was placed in a titration vessel into which a desired volume of the stock solution of DMSA was transferred, followed by addition of a desired volume of standard solution of HNO_3 (if necessary), and a desired volume of zinc nitrate stock solution, and finally a desired amount of KNO_3 was weighed and placed in the titration vessel to maintain the ionic strength equal to 0.10±0.01 throughout the titration. (b) A constant volume of the stock solution of DMSA and 5.00 mL of 1.00 M $NaNO_3$ solution were transferred into a 50 mL volumetric flask, a desired volume of standard solution of HNO_3 (if necessary) was added, followed by addition of a desired volume of zinc nitrate stock solution and then dilution to the mark; 40.00 mL of this solution was transferred to the vessel for potentiometric titration. By changing the volume of zinc nitrate stock solution added, a series of titration curves at different ligand:Zn^{2+} stoichiometric ratios were obtained. The potentiometric titrations were performed at 25.0 °C.

Synthesis of $[(Me)_4N]_6[Zn(rac\text{-}DMSA)_2]$.

The synthesis of this ion association complex was carried out under argon

to prevent oxidation of the mercapto compounds to disulfides. Stoichiometric amounts of *racemic*-DMSA, (H_4L), zinc nitrate, and tetramethylammonium hydroxide shown below were used in the synthesis:

$$2H_4L + Zn(NO_3)_2 + 8(Me)_4NOH \rightarrow [ZnL_2]^{6-} + 8(Me)_4N^+ + 2NO_3^- + 8H_2O$$

rac-DMSA (273.3 mg = 1.5 mmol) was dissolved in 10 mL of oxygen-free double-deionized H_2O. 2.72 mL (0.75 mmol) of 0.2763 M $Zn(NO_3)_2$ solution, previously standardized with EDTA, was added, and finally 2.56 mL of 2.343 M $(Me)_4NOH$ solution, standardized previously with standard HNO_3 solution, was added slowly with stirring. The clear solution was allowed to react with continuous stirring for 30 min under an argon atmosphere. After the solvent was evaporated in a rotatory evaporator under vacuum, a white sticky precipitate was left behind. This precipitate was treated with a deaereated mixture of 50% v/v ethanol-acetone, filtered, and dried in vacuum. The purification procedure was repeated three times and the final product was rinsed with ethyl ether. The stoichiometry and purity of the final product were determined by proton NMR spectroscopy. The compound was dissolved in deuterated methanol (99.8 atom% deuterium) containing 0.03% tetramethylsilane (TMS) (v/v), and chemical shifts were measured with respect to the TMS signal. In the proton NMR spectrum of the purified compound (Fig. 2-1) a large singlet was observed at 4.92

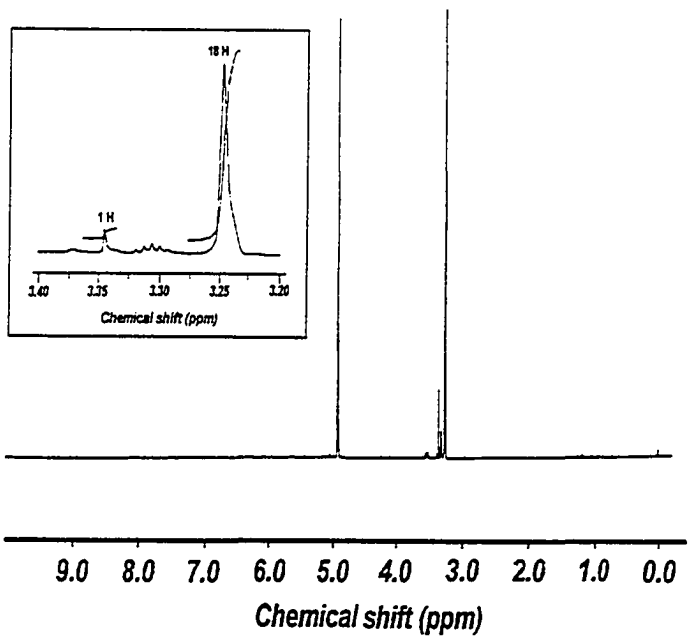

Figure 2-1. Proton NMR spectrum of $[(Me)_4N]_6[Zn(rac\text{-}DMSA)_2]$ in methanol-d_4.

ppm and a small pentet at 3.31 ppm, which originated from the residual protons in the deuterated methanol solvent. The singlet at 3.25 ppm was attributed to the methyl protons in the tetramethylammonium cation and the singlet at 3.35 ppm was attributed to the methine protons in *rac*-DMSA. The small peaks around 1.2 and 3.5 ppm probably originated from a trace amount of solvent residue introduced in the purification process. The integrated peak ratio of tetramethylammonium protons to DMSA methine protons was 1:18, shown in the scale-up of the chemical shift region around 3.3 ppm (inset of Fig. 2-1). These observations supported the expected stoichiometry of the compound, $[(Me)_4N]_6[Zn(rac\text{-}DMSA)_2]$.

NMR Measurements.

Proton and ^{13}C NMR spectra were obtained with either a Bruker WM-250 or AM-250 spectrometer. All experiments were carried out at ambient temperature (22°C) unless specified in the text. The proton spectra were obtained in 5-mm NMR tubes and the digital resolution was 0.365 Hz/pt. ^{13}C spectra were obtained in a 5-mm NMR tube, and the digital resolution was 1.850 Hz/pt. The chemical shifts in aqueous solution were measured with respect to TBA but reported with respect to DSS.

Proton NMR Spectroscopy of (Rac-DMSA)$^{4-}$ and (Meso-DMSA)$^{4-}$ at Different L^{4-}/Zn^{2+} Ratios.

A $Zn(NO_3)_2$ stock solution in D_2O was prepared by dissolving $Zn(NO_3)_2xH_2O$ in D_2O, (the depletion of water of hydration in the solid $Zn(NO_3)_2xH_2O$ with D_2O is difficult due to its hydrolysis), and standardized with EDTA. A titration solution was prepared in a 5-mm NMR tube by mixing a weighed amount of *rac*- or *meso*-DMSA, four equivalent amounts of NaOD solution, 10 μL 10% TBA, and a calculated volume of D_2O to bring the final volume to 300 μL. A calculated volume of the stock solution of zinc nitrate containing 10% of the total number of millimoles of *rac*- or *meso*-DMSA was added and the proton NMR spectrum was acquired. The sequential addition of the zinc nitrate solution was continued until a zinc:ligand ratio of 1.2:1 was reached.

Proton NMR Titration of Zn^{2+}-rac-DMSA System with NaOD.

A solution for proton NMR spectroscopy was prepared in a 5-mm NMR tube by mixing a weighed amount of *rac*-DMSA, a measured volume of zinc nitrate stock solution corresponding to half the number of millimoles of *rac*-DMSA, 10 μL 10% TBA, and a calculated volume of D_2O to bring the final volume to 300 μL. A volume of NaOD corresponding to 20% of the number of millimoles of *rac*-DMSA was added to the NMR tube, successively before the proton NMR spectra were acquired after swirling the solution in the tube. The pD

values of the above solutions at the various points in the proton NMR titration were determined with the aid of a glass calomel electrode pair by carrying out a parallel experiment under exactly the same conditions in a small test tube. The glass electrode was calibrated in the same manner as described in Chapter One, and the pD values reported are pH meter readings and have not been converted to $[D^+]$ values in moles/L.

Variable-Temperature ^{13}C NMR of $[(Me)_4N]_d[Zn(rac\text{-}DMSA)_2]$ in Methanol-d_4.

The variable-temperature ^{13}C NMR studies were carried out with a solution containing 25 mg of the compound in 0.7 mL of deuterated methanol containing 0.03% TMS (v/v). Peaks arising from methanol do not interfere with peaks arising from the ion association complex in the aliphatic carbon region. The carbonyl carbon signal was not detected in the background noise because the methyl carbon signal of the TMA cation was so intense that it raised the detection limit of the analog-to-digital converter, and the acquisition time was not set long enough to record the slow relaxation of the carbonyl carbon signal under our experimental conditions. The chemical shifts were recorded relative to the TMS signal.

IR Spectroscopy of (Rac-DMSA)$^{4-}$ and (Meso-DMSA)$^{4-}$ at Different L^{4-}/Zn^{2+} Ratios.

IR spectra of aqueous solutions containing varying ratios of zinc to ligand were measured with a NICOLET Fourier transform IR spectrometer model 510 P at ambient temperature. A calcium fluoride absorption cell, which has a transmission range from 66666 to 1110 cm^{-1}, equipped with a thin teflon spacer was employed, and the thickness of the cell, which was experimentally determined from the interference fringes (*74*), was 31 μm. Since liquid water possesses strong IR absorption bands near 3300 and 1600 cm^{-1} (*90,91*), all solutions were prepared in D_2O which shifts the angular vibration frequency of O-H from 1640 to 1210 cm^{-1} as a result of the replacement of hydrogen atoms with deuterium. This left the carboxylate stretching vibration free of the solvent absorption band. The sample chamber was purged with nitrogen during the measurements and all spectra of the IR titration solutions were recorded using air as background. The resolution of the IR spectra was 2 cm^{-1}. The spectra of IR titration solutions were plotted after subtraction of the spectrum of D_2O containing 0.20 M H_2O from the recorded spectra followed by subtraction of the water vapor spectrum.

Stock solutions of 0.10 M tetrasodium DMSA of the two DMSA isomers were prepared by dissolving 0.40 mmol of the appropriate DMSA in 4.0 mL of

D_2O containing 0.40 M NaOD. L^{4-}:zinc 1:1 stock solutions of 0.10 M for the two DMSA isomers were prepared by dissolving 32.3 mg (0.143 mmol) of zinc bromide in 1.43 mL of 0.10 M tetrasodium DMSA solution. IR spectroscopic studies of DMSA solutions containing varying L^{4-}:zinc ratios were carried out by acquiring the IR spectra of solutions which were prepared by mixing 0.10 M stock ligand, L^{4-}, with 0.10 M stock L^{4-}: zinc 1:1 solution in different ratios.

Results

Formation Constants of Zinc Chelates of *Meso-* and *Rac*-DMSA.

The potentiometric titration points for *meso-* and *rac*-DMSA in the presence of Zn^{2+} at various DMSA:Zn^{2+} ratios are shown in Figs. 2-2 and 2-3, respectively. The complexation of zinc with *meso*-DMSA has been studied by Jones et al. (*92*) and Harris et al. (*93*). It was concluded by both groups, after the analysis of potentiometric titration curves by non-linear least-squares methods and as a consequence of the cross-over and non-superimposability of the formation function curves, that a variety of polynuclear complexes were formed in aqueous solution, although there were differences in the speciation models proposed by the two groups.

The complexation of zinc with *rac*-DMSA has not been investigated quantitatively. In the systems containing the completely deprotonated DMSA ligand, L^{4-}, and Zn^{2+} ion, the equilibria governing complex formation are described by equation 1 on the assumption that no protonated metal complexes are formed.

$$pM^{2+} + qL^{4-} \rightleftharpoons (M_pL_q)^{2p-4q} \qquad (2\text{-}1)$$

where p and q are integers and each complex has an overall stability constant β_{pq}, defined by:

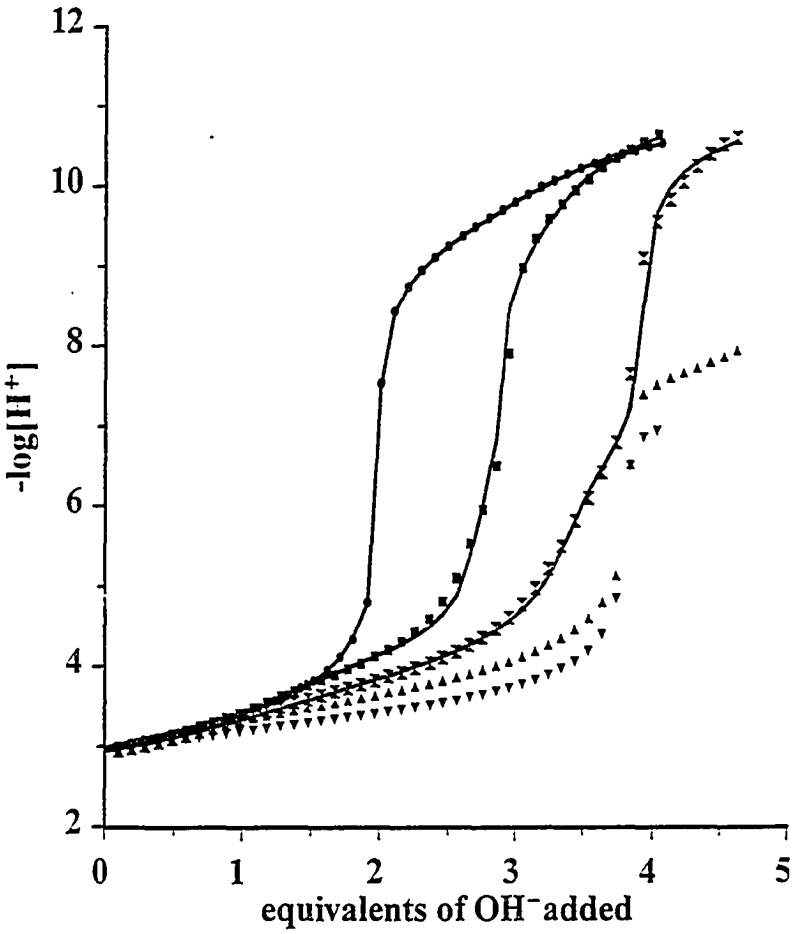

Figure 2-2. Potentiometric titration curves of 1.295 mM *meso*-DMSA only (•); and 1.206 mM *meso*-DMSA in the presence of Zn^{2+} at 0.6026 mM (2:1) (■), 1.205 mM (1:1) (X), 2.410 mM (1:2) (▲) and 6.024 mM (1:5)(▼) at T = 25.0°C and ionic strength(μ) = 0.10. The solid lines are the titration curves simulated by "PKAS" for *meso*-DMSA, and by "BEST" for *meso*-DMSA in the presence of zinc ions.

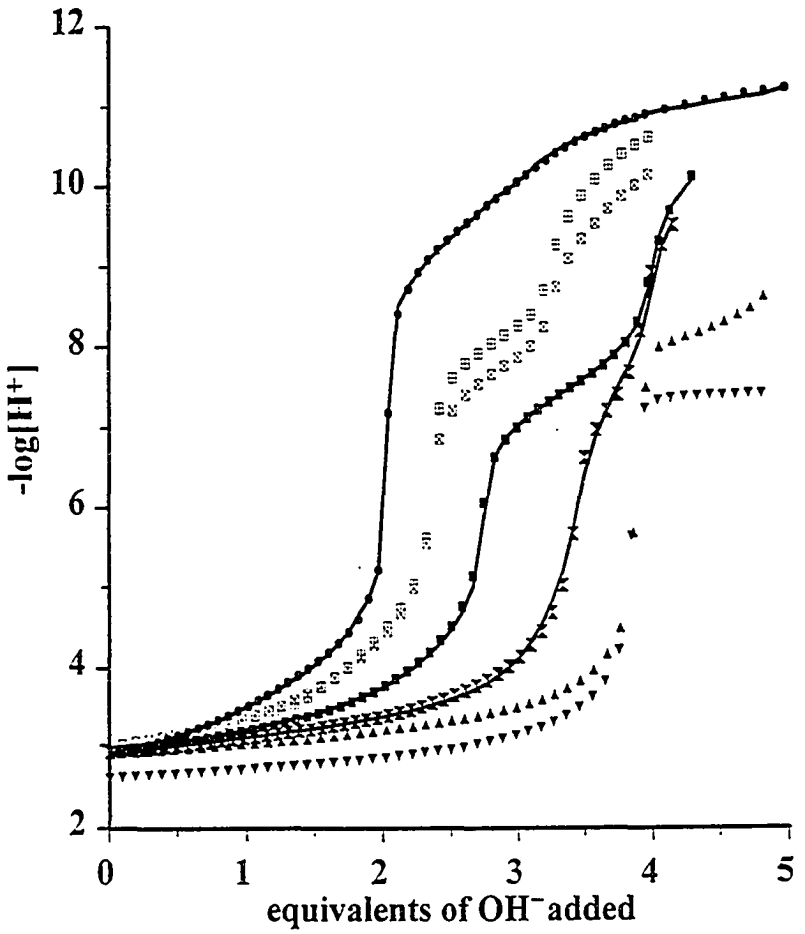

Figure 2-3. Potentiometric titration curves of 1.412 mM *rac*-DMSA only (•); and of 1.232 mM *rac*-DMSA in the presence of Zn^{2+} at 0.6024 mM (2:1) (▪), 1.205 mM (1:1) (X), 2.410 mM (1:2) (▲), 6.024 mM (1:5) (▼); and of 1.201 mM *rac*-DMSA in the presence of 0.4016 mM Zn^{2+} (1:3) (squares with plus inside); and of 0.9745 mM *rac*-DMSA in the presence of 0.3258 mM Zn^{2+} (1:3) (squares with X inside) at T = 25.0°C and ionic strength (μ) = 0.10. The solid lines are the titration curves simulated by "PKAS" for *rac*-DMSA, and by "BEST" for *rac*-DMSA in the presence of zinc ion.

$$\beta_{pq}=\frac{[M_pL_q]^{2p-4q}}{[M^{2+}]^p[L^{4-}]^q} \tag{2-2}$$

The formation function, ñ, which can be used to determine the average stoichiometric composition of a metal ligand complex, is defined by the ratio of the total number of moles of complexed ligand to the total number of moles of metal species present in the solution. By assuming that no polynuclear complexes were formed in the system, (i.e. p = 1), the formation function, ñ, can be simplified by the equation:

$$\bar{n}=\frac{\sum_{i=1}^{q} i[ML_i^{(4i-2)-}]}{C_M} \tag{2-3}$$

where C_M represents the analytical concentration of the metal ion, Zn^{2+}. The value of the formation function, ñ, as well as the free ligand concentration, $[L^{4-}]$, at any point on the titration curve can be calculated from known or experimentally measurable quantities using the following equations:

$$\bar{n}=\frac{C_{H_4L}-[L^{4-}]\alpha_{L_H}}{C_M} \tag{2-4}$$

$$[L^{4-}]=\frac{2C_{H_4L}-[Na^+]-[H^+]+[OH^-]}{K_1[H^+]+2K_1K_2[H^+]^2+3K_1K_2K_3[H^+]^3+4K_1K_2K_3K_4[H^+]^4} \quad (2\text{-}5)$$

$$\alpha_{L_H}=1+K_1[H^+]+K_1K_2[H^+]^2+K_1K_2K_3[H^+]^3+K_1K_2K_3K_4[H^+]^4 \quad (2\text{-}6)$$

where C_{H4L} represents the analytical concentration of the ligand, and K_1, K_2, K_3 and K_4 are the first, second, third and fourth protonation constants, respectively, of DMSA. All concentrations in the above equations, in square brackets, are expressed in moles per liter. It was postulated at first that ZnL^{2-} and ZnL_2^{6-} were the chelated species formed in the system. In order to prove that these zinc complexes were formed with *rac*-DMSA, titrations of *rac*-DMSA in the presence of Zn^{2+} and ligand in a ratio of 3:1 were carried out and the titration curves were analyzed by means of eqs 2-4 to 2-6. The formation curves were obtained by plotting the formation function, ñ, versus $p[L^{4-}]$, the values of the negative log of the free ligand concentration. There are several important features in the formation curves in Fig. 2-4: First, the inflection in the curve occurred at a ñ value of 0.57 rather than 1.0 as would be the case if two complexes, ZnL^{2-} and ZnL_2^{6-}, were formed, with well-separated formation constants. The inflection at ñ < 1 led us to the conclusion that a protonated form of ZnL^{2-} was formed. Second, the inflections at ñ ca. 1.85 were observed as the values of $-\log[L^{4-}]$ decreased, in

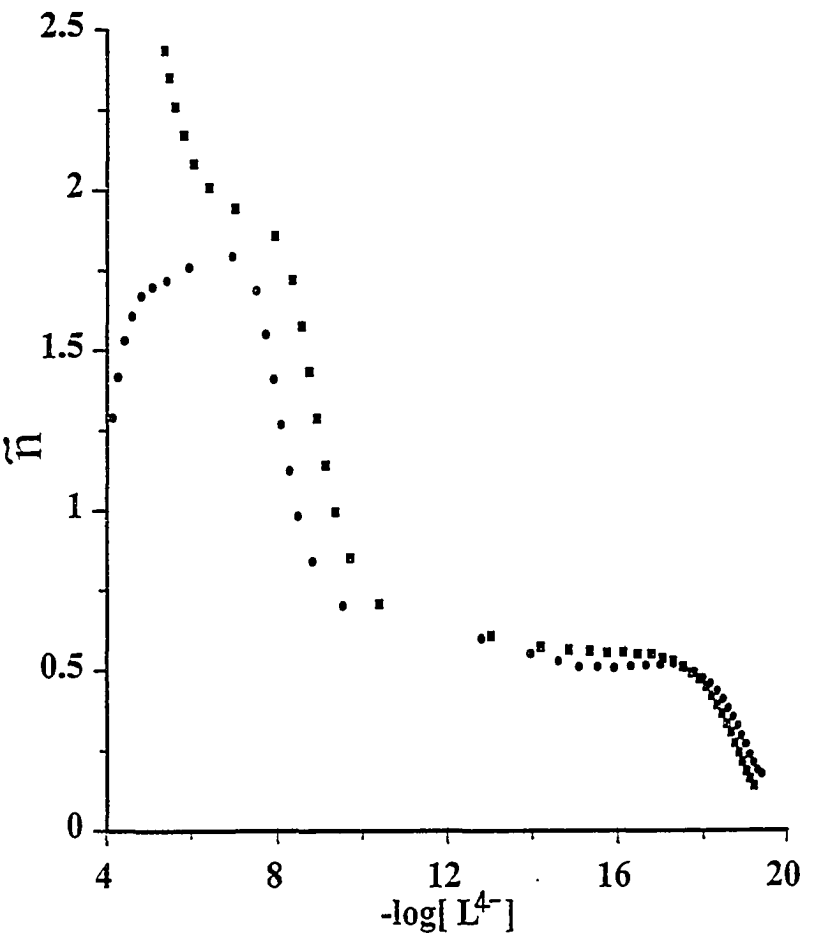

Figure 2-4. Formation curves of *rac*-DMSA-Zn^{2+} (3:1) •: $[L^{4-}]$ = 1.201 mM and $[Zn^{2+}]$ = 0.4016 mM; ▪: $[L^{4-}]$ = 0.9745 mM and $[Zn^{2+}]$ = 0.3258 mM.

both formation function curves with a decrease in ñ value for the curve obtained with the higher initial concentration (filled-in circles in Fig. 2-4) and an increase in ñ value for the curve with the lower initial concentration (filled-in squares in Fig. 2-4). This observation led us to propose that protonated ZnL_2^{6-} species were formed in the system. The "abnormal" decrease in ñ values with higher initial concentration (filled-in circles in Fig. 2-4), at low values of $-\log[L^{4-}]$, corresponding to pH values between 8.7 and 10.6, probably implies that the species ZnL_2^{6-} undergoes an internal configuration exchange equilibrium. In the case of the low initial concentration (filled-in squares in Fig. 2-4), there are less uncoordinated thiolate groups available in ZnL_2^{6-} for protonation to form a significant amount of HML_2^{5-}. Uncoordinated carboxylate groups may exist, but no protonation would occur between pH 8.7 and 10.6. In the case of high initial concentration (filled-in circles in Fig. 2-4), the internal configuration equilibrium shifts towards the side which produces ZnL_2^{6-} with more uncoordinated thiolate groups which can be protonated between pH 8.7 and 10.6 to form a significant amount of HML_2^{5-}. This can result in an "abnormal" decrease in apparent ñ values, defined by eq 2-3 at low values of $-\log[L^{4-}]$ along the formation curve. The net effect of the change in protonation sites in ZnL_2^{6-} on the ñ value is a decrease in the ñ value caused by the invalidity of eq 2-3, since all protonated metal complexes were not taken into account in the numerator of eq 2-3. The

shape of the formation curve is dependent on the initial concentration and the curves are obviously not superimposable; this suggests that polynuclear complexes are also formed in the zinc-*rac*-DMSA system.

Since protonated as well as polynuclear complexes are formed in the zinc-*meso*-DMSA and zinc-*rac*-DMSA systems, eqs 2-3 to 2-5 are no longer valid, and no simple procedures exist for proving the presence of such complexes and for determining the formation constants of these complexes. The computer program "BEST" was therefore used (*72,94*), which employs an iterative process of nonlinear fitting by calculating the equilibrium pH value at each point in the potentiometric titration and refining the equilibrium constants in the selected model until the weighted discrepancies between the experimental and the calculated pH values are minimized (*72*).

The titration curves for both *meso*- and *rac*-DMSA with a ligand:zinc ratio of 2:1 and 1:1 were analyzed using the BEST program because these ratios closely approximated the true stoichiometry of the zinc complexes formed in the system, based on the analysis of the formation function curves. The titration curves for the zinc-*meso*-DMSA system were analyzed by the "BEST" program; the complex species formed in the L:Zn system are $Zn_2L_2OH^{5-}$, $Zn_2L_2^{4-}$, $Zn_2L_2H^{3-}$, and $ZnLH^{-}$; and in the 2L:Zn system are $Zn_2L_2^{4-}$, $Zn_2L_2H^{3-}$, ZnL_2^{6-} and ZnL_2H^{5-}. The formation constants and the protonation constants of various zinc complexes

with *meso*-DMSA are listed in Tables 2-1 and 2-2 and the titration curves simulated by the "BEST" program for *meso*-DMSA:zinc ratios of 2:1 and 1:1 are shown in Fig. 2-2 (solid lines). The titration curves for *rac*-DMSA were analyzed by the "BEST" program and, of the many models that were evaluated, the data for the statistically favorable models are summarized in Table 2-3. The protonation constants of various zinc complexes with *rac*-DMSA are listed in Table 2-4. The titration curves simulated by the "BEST" program for *rac*-DMSA:zinc ratios of 2:1 and 1:1 are shown in Fig. 2-3 (solid lines). In the potentiometric titration of both L:M and 2L:M systems, zinc interacted with *rac*-DMSA to form dimeric complexes at different stages of protonation: $Zn_2L_2OH^{5-}$, $Zn_2L_2^{4-}$, $Zn_2L_2H^{3-}$, $Zn_2L_2H_2^{2-}$ in the 1:1 system and $Zn_2L_2H^{3-}$, $Zn_2L_2H_2^{2-}$ in the 2:1 system.

NMR Spectroscopy.

The utility of proton NMR spectroscopy for probing the protonation sites of polyfunctional ligands and the conformations of metal complexes in aqueous solution has been amply demonstrated during the past three decades. Kinetic and mechanistic information on ligand exchange may be extracted (*95,96,97*) from the linewidths or bandshapes of the NMR signals at varying temperatures. In our studies the proton NMR spectra of *rac*- or *meso*-DMSA were recorded as a function of zinc:ligand ratio. The completely deprotonated ligand, L^{4-}, was

Table 2-1. Formation Constants of the Zinc Complexes of *Meso*-DMSA at μ = 0.10 and T = 25.0°C. L^{4-} represents completely deprotonated *meso*-DMSA.

Ratio of L:Zn	Species			log β_{pqr}[a]	
	p	*q*	*r*		
2:1	1	2	0	19.7[b]	19.46±0.06(*92*)[d]
	1	2	1	30.6[b]	
	2	2	0	33.8[b]	33.6±0.5(*93*)
	2	2	1	39.8[b]	39.6±0.3(*93*)
1:1	1	1	1	20.3[c]	
	2	2	0	33.6[c]	34.08±0.08(*92*)[d]
	2	2	1	40.1[c]	40.07±0.02(*92*)[d]
	2	2	-1	22.7[c]	23.6±0.8(*93*)

[a] $\beta_{pqr} = [Zn_pL_qH_r^{-(4q-2p-r)}]/[Zn^{2+}]^p[L^{4-}]^q[H^+]^r$.
[b] Values determined in our laboratory with a minimum $\sigma(pH)_{fit}$ of 0.016 (*72*).
[c] Values determined in our laboratory with a minimum $\sigma(pH)_{fit}$ of 0.022 (*72*).
[d] Values reported at an ionic strength of 0.15.

Table 2-2. Protonation Constants of the Zinc Complexes of *Meso*-DMSA at μ = 0.10 and T = 25.0°C. L represents completely deprotonated *meso*-DMSA.

protonation	log K	
$Zn_2L_2^{4-} + H^+ \rightleftharpoons Zn_2L_2H^{3-}$	6.0[a]	6.5[b]
$ZnL_2^{6-} + H^+ \rightleftharpoons ZnL_2H^{5-}$	10.9[a]	

[a] Values derived from the β_{pqr} values determined from a 2:1 solution of ligand:zinc.
[b] Values derived from the β_{pqr} values determined from a 1:1 solution of ligand:zinc.

Table 2-3. Formation Constants of Zinc Complexes of *Rac*-DMSA at μ = 0.10 and T = 25.0°C. L^{4-} represents the completely deprotonated *rac*-DMSA.

Ratio of L:Zn	Species			log β_{pqr}[a]
	p	*q*	*r*	
2:1	1	2	0	25.3[b]
	1	2	1	32.9[b]
	1	2	-1	14.7[b]
	2	2	1	42.3[b]
	2	2	2	46.5[b]
1:1	1	2	2	43.1[c]
	2	2	0	34.8[c]
	2	2	1	42.3[c]
	2	2	2	46.2[c]
	2	2	-1	24.6[c]

[a] $\beta_{pqr} = [Zn_pL_qH_r^{-(4q-2p-r)}]/[Zn^{2+}]^p[L^{4-}]^q[H^+]^r$.
[b] Values determined in our laboratory with a minimum $\sigma(pH)_{fit}$ of 0.0116 (*72*).
[c] Values determined in our laboratory with a minimum $\sigma(pH)_{fit}$ of 0.0076 (*72*).

Table 2-4. Protonation Constants of the Zinc Complexes of *Rac*-DMSA at μ = 0.10 and T = 25.0°C. L represents the completely deprotonated *rac*-DMSA.

Protonation					log K	
$Zn_2L_2^{4-}$	+	H^+	⇌	$Zn_2L_2H^{3-}$	7.5[b]	
$Zn_2L_2H^{3-}$	+	H^+	⇌	$Zn_2L_2H_2^{2-}$	4.2[a]	3.9[b]
ZnL_2^{6-}	+	H^+	⇌	ZnL_2H^{5-}	7.6[a]	
ZnL_2H^{5-}	+	H^+	⇌	$ZnL_2H_2^{4-}$	10.2[c]	

[a] Values derived from the β_{pqr} values obtained from a 2:1 solution of ligand:zinc.
[b] Values derived from the β_{pqr} values obtained from a 1:1 solution of ligand:zinc.
[c] Values derived by combining the β_{pqr} values which were determined from the 2:1 and 1:1 solutions of ligand:zinc.

titrated with zinc nitrate and the spectra are plotted in Fig. 2-5 for *rac*-DMSA and in Fig. 2-6 for *meso*-DMSA to show the change in bandwidth in the course of the titration; the chemical shifts of methine proton peaks are plotted as a function of millimolar ratios of zinc and DMSA isomers in Fig. 2-7. The possible reaction of DMSA ligands, L^{4-}, with zinc ion in the course of addition of zinc nitrate solution is schematically illustrated in Fig. 2-8. The D_2O solution of zinc nitrate is acidic and can be reasonably represented as a mixture of $ZnOD^+$ and D^+ for a discussion of the chemical shifts that are observed when aliquots of the zinc nitrate solution were added to the solution of L^{4-}.

The methine proton resonance of the L^{4-} of *rac*-DMSA alone occurred as a singlet at 3.08 ppm (A0 in Fig. 2-5). Addition of zinc nitrate ((a) in Fig. 2-8) gave rise to another peak at 3.14 ppm (A1 in Fig. 2-5), i.e. a 0.06 ppm downfield shift as a result of the complexation. The methine protons in ZnL_2OD^{7-} underwent a slow exchange with the L^{4-} and its protonated form, DL^{3-}, and the uncomplexed ligand resonance was shifted slightly downfield supporting the formation of the DL^{3-} and its fast exchange with the L^{4-}. After the addition of 0.5 equivalents of zinc nitrate ((b) in Fig. 2-8), the resonance signal arising from the L^{4-} and the DL^{3-} completely disappeared, indicating that all the uncomplexed ligand was converted to ZnL_2^{6-} which gave rise to the singlet at 3.19 ppm (A5 in Fig. 2-5). Further addition of zinc nitrate caused a downfield chemical shift and a significant

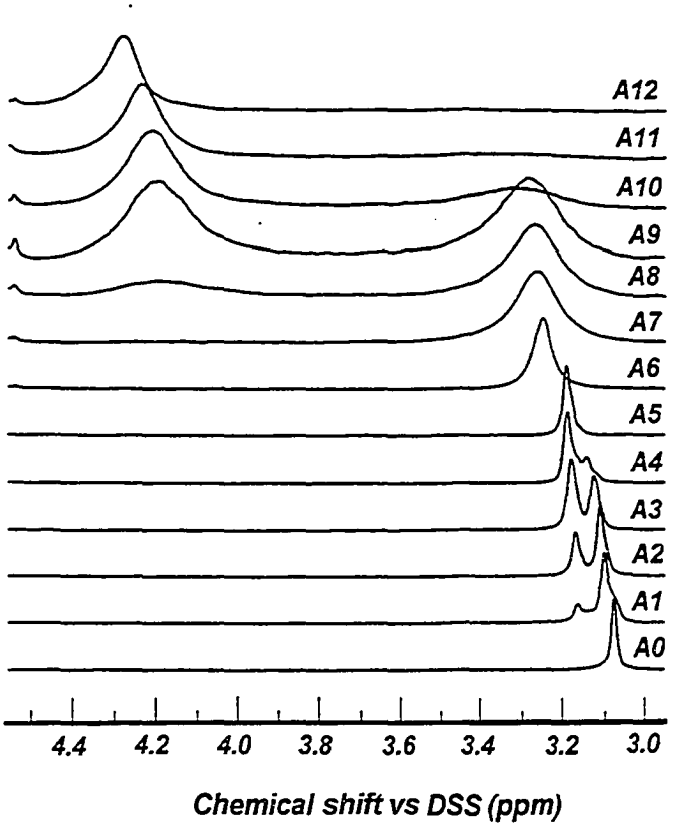

Figure 2-5. Proton NMR spectra of the aliphatic region of 0.081 mmol of *rac*-DMSA, L^{4-}, at zinc:ligand molar ratios ranging from 0.0 to 1.2 (spectra A0 through A12); the increment of the zinc:ligand ratio is 0.1.

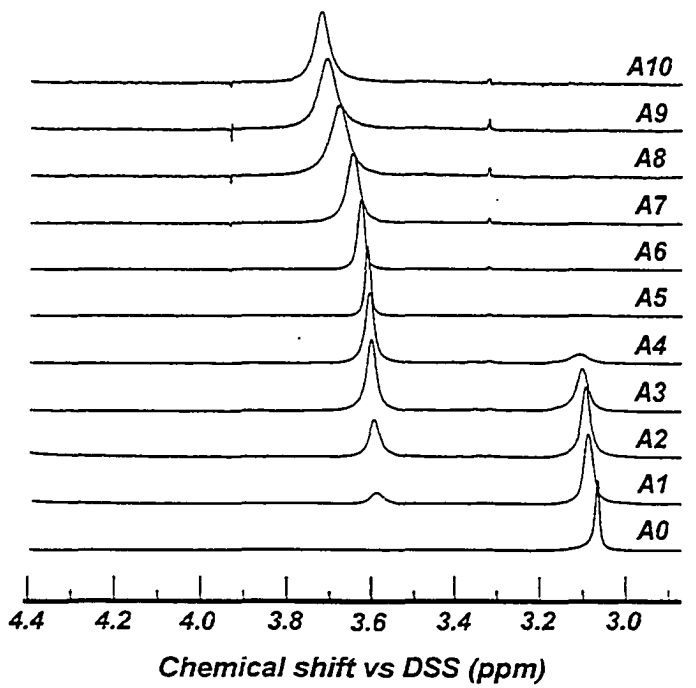

Figure 2-6. Proton NMR spectra of the aliphatic region of 0.081 mmol of *meso*-DMSA, L^{4-}, at zinc:ligand molar ratios ranging from 0.0 to 1.0 (spectra A0 through A10); the increment of the zinc:ligand ratio is 0.1.

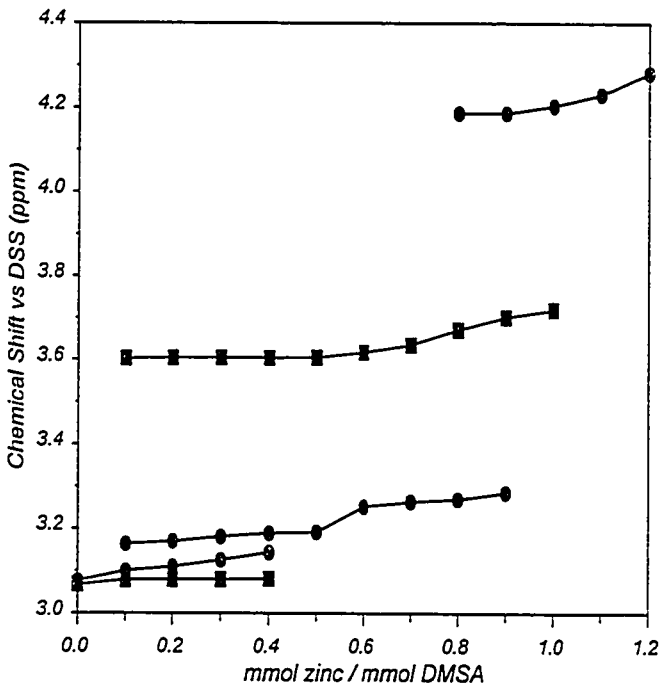

Figure 2-7. Chemical shift of the methine protons as a function of zinc:ligand molar ratio. (■): observed for the zinc-*meso*-DMSA solutions; (•): observed for the zinc-*rac*-DMSA solutions.

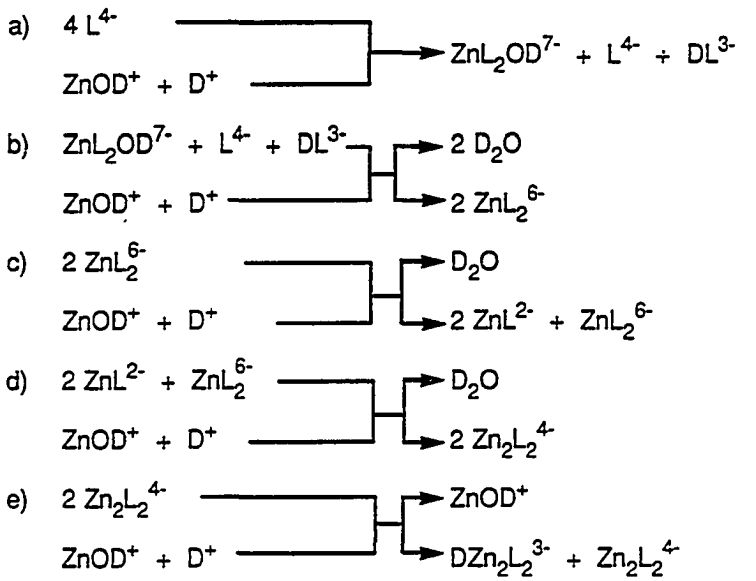

Figure 2-8. Proposed reactions of DMSA, L^{4-}, with zinc nitrate after addition of (a) 0.25 equivalents zinc, (b) 0.5 equivalents zinc, (c) 0.75 equivalents zinc, (d) 1.0 equivalent zinc, and (e) 1.25 equivalents.

broadening of the peak (A6 - A10 in Fig. 2-5). This was attributed to the formation of ZnL^{2-} ((c) in Fig. 2-8), which was likely undergoing a ligand exchange with ZnL_2^{6-} at an intermediate rate at the experimental temperature, relative to the NMR timescale (200 ms) of methine protons in the ligand. Therefore, no separate peaks were resolved for ZnL^{2-} and ZnL_2^{6-}, but instead, peak coalescence was observed. After 0.75 equivalents of zinc nitrate was added, a new peak, well separated from the resonance peak due to ZnL^{2-} and ZnL_2^{6-}, emerged at 4.20 ppm (A8 in Fig. 2-5), which corresponded to the formation of a dimeric complex, $Zn_2L_2^{4-}$ ((d) in Fig. 2-8). A ligand exchange phenomenon was observable between ZnL^{2-}, ZnL_2^{6-} and $Zn_2L_2^{6-}$, which resulted in peak broadening, and the resonance peak due to ZnL^{2-} and ZnL_2^{6-} gradually diminished, leaving only one peak due to $Zn_2L_2^{4-}$ at 4.21 ppm (A10 in Fig. 2-5). When more than one equivalent of zinc nitrate was added, the resonance peak shifted slightly downfield to 4.28 ppm (Fig. 2-5), as a result of formation of the protonated dimeric complex $DZn_2L_2^{3-}$ ((e) in Fig. 2-8).

The interaction of the *meso*-DMSA ligand, L^{4-}, with zinc ion in the course of the addition of zinc nitrate solution is assumed to be similar to that of the *rac*-DMSA ligand, as illustrated in Fig. 2-8. The methine proton resonance of the L^{4-} alone occurred as a singlet at 3.07 ppm (A0 in Fig. 2-6). Addition of zinc nitrate yielded another peak at 3.59 ppm, i.e. a 0.52 ppm downfield shift as a result of

the complexation, (A1 in Fig. 2-6). The proton resonance resulting from pure ligand completely disappeared upon addition of 0.5 equivalent of zinc nitrate, indicating the formation of ZnL_2^{6-} (A5 in Fig. 2-6). Further addition of zinc nitrate up to 1.0 equivalent caused a slight downfield shift of the peak to 3.72 ppm; however, a significant peak broadening occurred after 0.7 equivalent of zinc nitrate was added, and reached a maximum at a zinc:ligand ratio around 0.8 (A7 - A8 in Fig. 2-6). This might be an indication that only $Zn_2L_2^{4-}$ was formed upon addition of zinc nitrate to ZnL_2^{6-}, and that it underwent an intermediate ligand or metal exchange with ZnL_2^{6-}, resulting in a maximized peak broadening when the concentrations of both species were close to each other. There was no conclusive evidence, however, to exclude the formation of the monomeric complex, ZnL^{2-}.

A proton NMR titration of *rac*-DMSA with NaOD, shown in Fig. 2-9, was carried out for *rac*-DMSA in the presence of Zn^{2+} at a ligand:zinc ratio of 2:1 to confirm the formation of the zinc complexes of *rac*-DMSA, which were predicted by the potentiometric studies. The chemical shifts plotted as a function of pD values are shown in Fig. 2-10. With the aid of the proton NMR results previously obtained from the titration of L^{4-} with zinc nitrate and from the titration of H_4L with NaOD (*55*), the proton NMR results obtained from the titration of Zn^{2+}-*rac*-DMSA with NaOD are interpreted as follows: at pD values greater than 12.5 only one sharp signal from the methine protons in *rac*-DMSA was observed at 3.15

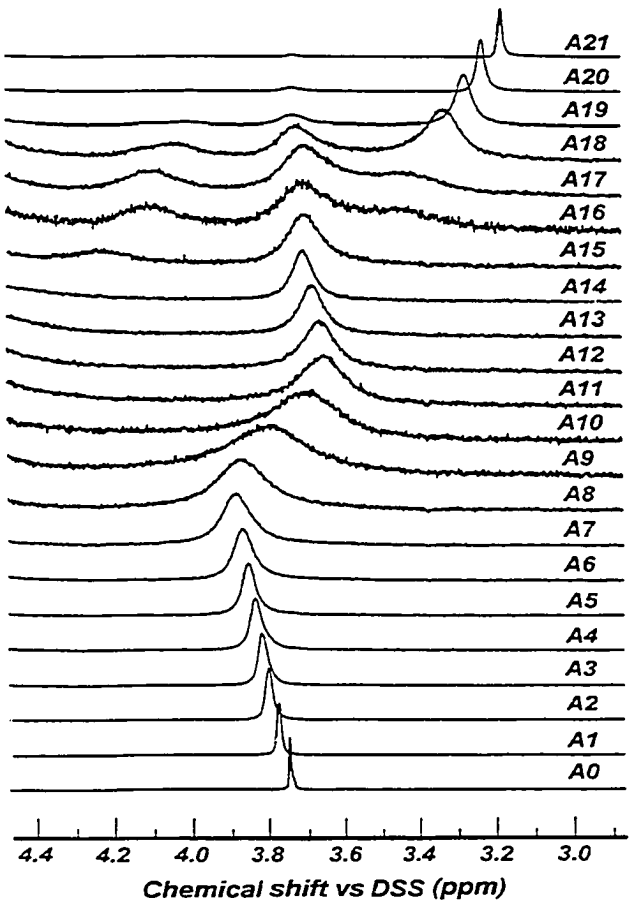

Figure 2-9. Proton NMR spectra of the aliphatic region of 0.08 mmol *rac*-DMSA in the presence of 0.04 mmol Zn^{2+} at NaOD:*rac*-DMSA ratios ranging from 0.0 to 4.2 (spectra A0 through A21); the increment of the molar ratio of NaOD:*rac*-DMSA is 0.2.

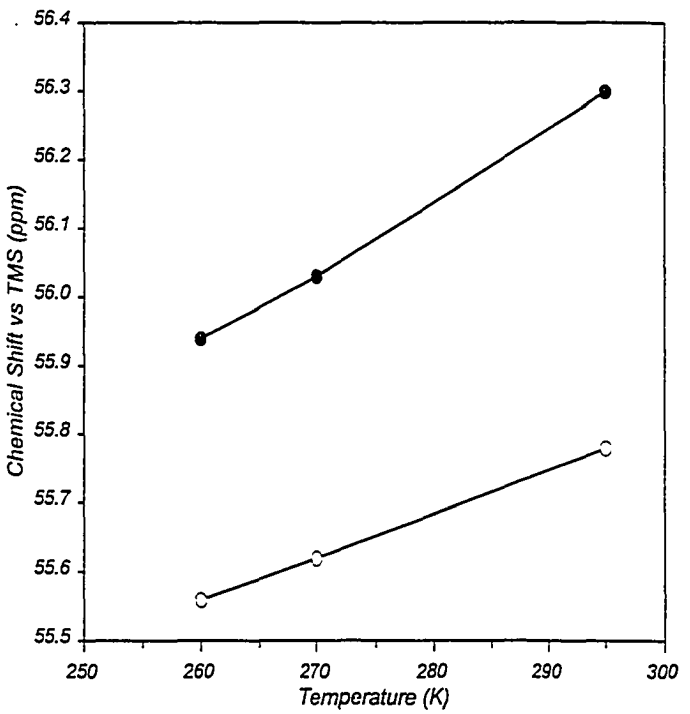

Figure 2-10. ^{13}C chemical shifts in the aliphatic region of $[(Me)_4N]_6[Zn(rac\text{-}DMSA)_2]$ versus temperature, (•): methyl carbon of TMA; (○): methine carbon of Zn-*rac*-DMSA complex.

ppm (shown in Fig. 2-10, but not in Fig. 2-9), which indicated that ZnL_2OD^{7-} was the predominant species in solution; when pD was reduced, the resonance peak started to broaden and shift downfield as a result of the loss of the deuteroxyl group of ZnL_2OD^{7-} and the subsequent formation of ZnL_2^{6-}; at pD about 7.3 (A21 in Fig. 2-9), another resonance peak emerged at 3.75 ppm which corresponds to the protonation of ZnL_2^{6-}; a decrease in pD from 7.0 to 6.0 resulted in another new resonance peak at 4.01-4.24 ppm which is direct evidence for the presence of dimeric complexes in this pD region. The change in the chemical shift and in the width of the methine proton peak located between 4.01 and 4.24 ppm implied that the protonated dimeric complexes may be present and undergo an intermediate ligand exchange among themselves as well as with the various protonated forms of the free ligand in this pD region. A further decrease in pD resulted in the disappearance of the two resonance peaks upfield and downfield, leaving only the middle resonance peak around 3.74 ppm which arose from the free ligand in its various stages of protonation as deduced from the proton NMR studies of *rac*-DMSA (*55*). By comparing the species distribution model and NMR results of the NaOD titration, an "abnormal" upfield shift from around 4.19 to around 3.69 ppm (i.e. the disappearance of the resonance peak around 4.2 ppm) was observed for the dimeric complex, $D_2Zn_2L_2^{2-}$. This will be discussed later in the Discussion section.

Variable-temperature ^{13}C NMR.

This experiment was originally designed to study the structures of the zinc-DMSA complexes on the basis of the splitting pattern of the ^{13}C resonance peaks in the coordination complexes (*98*). It was observed that in the aliphatic region of $[(Me)_4N]_6ZnL_2$ there were only two resonance peaks at ambient temperature, which corresponded to the methyl carbon in the TMA cation and the methine carbon in the ligand. As shown in Fig. 2-10, both resonance peaks shifted upfield with a decrease in temperature from 295 to 260 K; however, the expected splitting of the resonance peak in the ZnL_2^{6-} of *rac*-DMSA was unfortunately not observed even at 260 K. The upfield shift of methyl carbon in the TMA cation was caused by neutralization of the positive charge on the TMA cation. This indicates that the ion pair association equilibrium between the TMA cation and the ZnL_2^{6-} complex anion shifts towards the formation of the ion pair when the temperature decreases. As a result of ion pair association, a deshielding effect was expected on the methine carbon in ZnL_2^{6-} and the methine carbon resonance in the ligand should, therefore, shift downfield; an upfield shift was observed instead. The extent of the shift of the methine carbon resonance with temperature (0.0063 ppm/K), however, is not as great as that of the methyl carbon (0.01 ppm/K) (Fig. 2-10). This "abnormal" upfield shift could be a result of change in the conformation of the complex with a decrease in temperature, but its exact origin is still in question.

IR Spectroscopy.

The correlation between the asymmetric stretching frequency (ν_a) and symmetric stretching frequency (ν_s) of a carboxyl group and their separation ($\Delta\nu$) with the nature of the coordination of a carboxylate group has been well established (*99*), and used in the interpretation of the strength of the metal-oxygen bond (*100,101*) since the early 1960's. It has been summarized by Deacon et al. (*99*) that $\Delta\nu$ values ≥ 200 cm^{-1} appear to be generally associated with unidentate coordination of a carboxylate group, in which only one oxygen atom of the carboxylate group participates in the metal-oxygen bonding. The correlation between molecular structure and band intensity of the carbonyl group was demonstrated by Ramsay and Jones et al. (*102,103*) in the early 1950's; the use of band intensity, however, has not received significant attention since then, because its application is limited to bands free from overlap with other bands. The ratio of the intensity of the asymmetric stretching band to that of the symmetric stretching band is about 0.8 (*104*) for a saturated sodium acetate aqueous solution, and about 1.4 (*105*) for a 50/50 (mol/mol) acetic acid/water mixture. An increase in the ratio of intensity of the asymmetric band to that of the symmetric band relative to the ratio for the sodium carboxylate, in which the

metal-oxygen bond is assumed to be completely ionic, can be an indication of an increase in the covalency of the metal-oxygen bond.

By use of the PC/IR software 3.10 supplied with the NICOLET FT-IR spectrometer model 510P, it is possible to obtain the spectrum of an unknown component from a spectrum of a multicomponent solution if the composition of the solution and the spectra of the other components are known. The frequencies and the intensity ratios of the asymmetric and symmetric bands have been used to elucidate the nature of the coordination bonds in the zinc complexes of DMSA. In our studies, the IR spectra of *rac*- or *meso*-DMSA were obtained as a function of zinc:ligand ratio. The IR spectra in the frequency range between 1740 and 1260 cm^{-1} of the 0.1 M DMSA titration solutions in which the ratios of Zn:L range from 0 to 1 are shown in Figs. 2-11 and 2-12. The asymmetry of the absorption peak at 1376 cm^{-1} (C10 in Fig. 2-12), for the $Zn_2L_2^{4-}$ of *meso*-DMSA, is attributed to the possible conformational isomers of $Zn_2L_2^{4-}$ of *meso*-DMSA.

With successive addition of zinc ion to the *rac*-DMSA solution the asymmetric band of *rac*-DMSA shifted to a higher frequency and the symmetric band of the ligand shifted to a lower frequency (solid lines A0 through A10 in Fig. 2-11), which indicated that new complexes were formed in the course of addition of zinc ions. As indicated by NMR results, before the zinc:ligand ratio reached 0.5 only ZnL_2^{6-} was formed in the titration solution. The IR spectra for

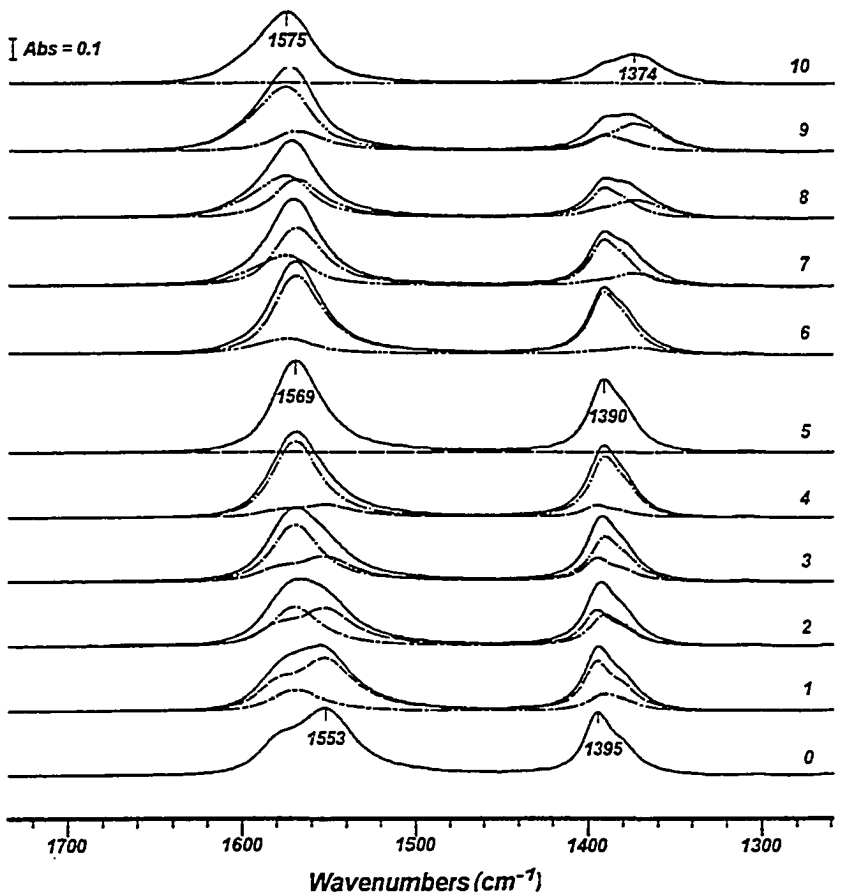

Figure 2-11. IR spectra of 0.1 M zinc-*rac*-DMSA solutions at zinc:ligand molar ratios ranging from 0.0 to 1.0; the increment of the zinc:ligand ratio is 0.1. Solid lines 0 through 10, represented as A0 to A10, are the experimental spectra; dot-dashed lines 1 through 5, represented as B1 to B5, are the calculated spectra for the ZnL_2^{6-} complex; broken lines 1 through 5 are the spectra resulting from the presence of the ligand in the solutions; double-dot-dashed lines 6 through 10, represented as C6 to C10, are the calculated spectra for the $Zn_2L_2^{4-}$ complex; dot-dashed lines 6 through 10 are the spectra resulting from the presence of ZnL_2^{6-} in the solutions.

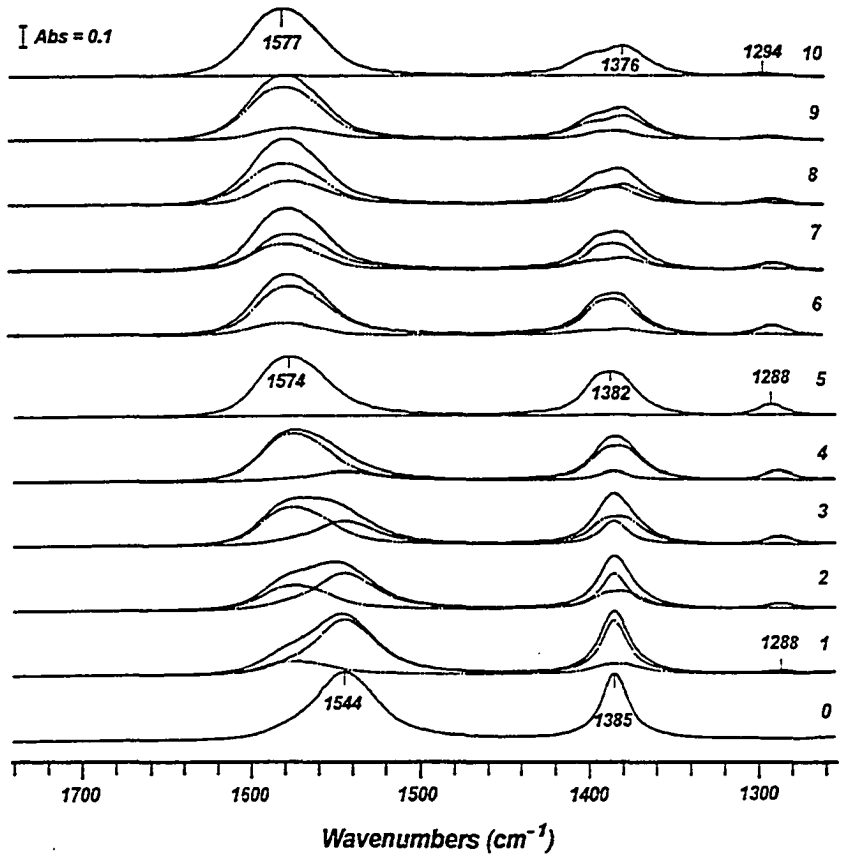

Figure 2-12. IR spectra of 0.1 M zinc-*meso*-DMSA solutions at zinc:ligand molar ratios ranging from 0.0 to 1.0; the increment of the zinc:ligand ratio is 0.1. Solid lines 0 through 10, represented as A0 to A10, are the experimental spectra; dot-dashed lines 1 through 5, represented as B1 to B5, are the calculated spectra for the ZnL_2^{6-} complex; broken lines 1 through 5 are the spectra resulting from the presence of the ligand in the solutions; double-dot-dashed lines 6 through 10, represented as C6 to C10, are the calculated spectra for the $Zn_2L_2^{4-}$ complex; dot-dashed lines 6 through 10 are the spectra resulting from the presence of ZnL_2^{6-} in the solutions.

ZnL_2^{6-} were obtained by subtraction of the ligand spectrum proportionally from the spectra obtained with the titration solutions at zinc:ligand ratios ranging from 0.1 to 0.5. The resulting spectra were the same, confirming that ZnL_2^{6-} of *rac*-DMSA indeed was the only species formed in the solution. After more than 0.5 equivalents of zinc ion was added, $Zn_2L_2^{4-}$ or ZnL^{2-} may be formed. Since the stoichiometry of the two complexes was the same, their IR spectra could be obtained by subtraction of the ZnL_2^{6-} spectrum (B5 in Fig. 2-11) proportionally from the spectra obtained with the titration solutions at zinc:ligand ratios ranging from 0.6 to 1.0. The resulting spectra were the same with respect to the asymmetric stretching bands, although the left shoulder of the peaks of the symmetric stretching bands varied slightly. The separation between the asymmetric stretching band and the symmetric stretching band of the carboxylate groups in the *rac*-DMSA alone (L^{4-}) was 158 cm^{-1} and their intensity ratio was 1.08 (A0 in Fig. 2-11). The separation between the asymmetric stretching band and the symmetric stretching band of the carboxylate groups in ZnL_2^{6-} of *rac*-DMSA was 179 cm^{-1} and their intensity ratio was 1.26 (B5 in Fig. 2-11). The increase in both the intensity ratio and the band separation indicated that the zinc ion in the complex was bound to the carboxylate group of *rac*-DMSA. On the basis of an increase in the intensity ratio by 0.18 and an increase in the overall band separation by 21 cm^{-1}, it was concluded that only one of the two carboxylate

groups in *rac*-DMSA participated in an unidentate coordination with the zinc ion in the complex. The separation between the asymmetric band and the symmetric band of the carboxylate groups in $Zn_2L_2^{4-}$ of *rac*-DMSA was 201 cm^{-1} and their intensity ratio was 2.39 (C10 in Fig. 2-11). This indicated that both carboxylate groups in *rac*-DMSA participated in unidentate coordination with zinc ions in $Zn_2L_2^{4-}$.

IR spectra obtained for the titration of *meso*-DMSA with zinc ion are shown in Fig. 2-12. A changing pattern, similar to that obtained with *rac*-DMSA, of the asymmetric and symmetric bands with the addition of zinc ions was observed. The same approach was used as with *rac*-DMSA to interpret the IR spectra of the titration solution at various zinc:ligand ratios. The species ZnL_2^{6-} was formed before the zinc:ligand ratio reached 0.5, and species $Zn_2L_2^{4-}$ (or ZnL^{2-}) was formed in the titration solutions when the zinc:ligand ratio was greater than 0.5. Similarly to its racemic isomers, the separation between the asymmetric band and the symmetric band of the carboxylate groups in *meso*-DMSA alone (L^{4-}) was 159 cm^{-1} and their intensity ratio was 1.06 (A0 in Fig. 2-12). The separation between the asymmetric band and the symmetric band of the carboxylate groups in ZnL_2^{6-} of *meso*-DMSA was 193 cm^{-1} and their intensity ratio was 1.35 (B5 in Fig. 2-12). Since the $\Delta\nu$ value was very close to 200 cm^{-1}, it was concluded that both carboxylate groups of *meso*-DMSA were bound to the zinc ion in the

complex. The intensity ratio, however, is close to that observed for the ZnL_2^{6-} of *rac*-DMSA and the $\Delta\nu$ value was slightly less than 200 cm^{-1}. On this basis it may be postulated that one of the two carboxylate groups of *meso*-DMSA in the complex may be bound to the zinc ion in an unsymmetrical bidentate manner, in which the asymmetry of this bound carboxylate group is slightly reduced with respect to a carboxylate group which is bound in an unidentate manner. Similarly to the corresponding complex of its racemic isomers, the separation between the asymmetric band and the symmetric band of the carboxylate groups in $Zn_2L_2^{4-}$ of *meso*-DMSA was 201 cm^{-1} and their intensity ratio was 2.17 (C10 in Fig. 2-12). This indicated that both carboxylate groups in *meso*-DMSA participated in unidentate coordination with zinc ions in $Zn_2L_2^{4-}$. A small absorption peak that appeared at 1288 cm^{-1} is an artifact resulting from spectrum subtraction.

Discussion

Speciation Models for Zinc-*meso*-DMSA.

Ligands containing mercapto groups, such as *meso*-DMSA (*93*), the dimethyl ester of *meso*-DMSA (*98*), Unithiol (*92*), and mercaptoacetic acid (*106*), have been reported to form dimeric complexes with zinc. The speciation models proposed for the zinc-*meso*-DMSA system by Harris et al. (*93*) was used to refine the potentiometric titration data obtained for the zinc-*meso*-DMSA system, in which L:Zn=1:1, and it was found be the statistically favorable model for the system. The formation constants (Table 2-1) of the dimeric complexes, $Zn_2L_2^{4-}$ and $Zn_2L_2H^{3-}$, which are determined from both L:M and 2L:M systems, agree very well with each other, within the margin of error of the computations with the "BEST" program (*72,94*). This strongly supports the models that define the zinc complex species that are present in solution in the course of the potentiometric titrations of the two systems in which the *meso*-DMSA:zinc ratio is 1:1 and 2:1. The average values of the log formation constants determined by us for the $Zn_2L_2^{4-}$ and $Zn_2L_2H^{3-}$ are 33.70±0.14 and 39.95±0.21, respectively, which are in good agreement with the values reported by Harris et al. (*93*), 33.6±0.5 and 39.6±0.3, respectively; and by Jones et al. (*92*), 34.08±0.03 and 40.07±0.02, respectively, despite the differences in ionic strength, and temperature used by Jones et al. The log formation constant of $Zn_2L_2OH^{5-}$

determined by us, 22.7, is also in good agreement with the value reported by Harris et al. (*93*), 23.6±0.8; Jones et al. (*92*) have postulated the formation of ZnL_2^{6-} on the basis of a statistically most favorable model obtained from MINIQUAD (*107*); however, Harris et al. (*93*), did not include this complex in their statistically most favorable model. The log formation constant of ZnL_2^{6-} determined by us is 19.7, which is, once again, in good agreement with the value reported by Jones et al., 19.46±0.06. The formation of ZnL_2 has been confirmed by IR and proton results. Although Jones et al. also postulated the formation of protonated forms of ZnL_3^{10-}, it was not confirmed in the proton NMR and IR experiments.

Speciation Models for Zinc-*rac*-DMSA.

It has been shown in Table 2-3 that the complexation of zinc with *rac*-DMSA is much more complicated than complexation with its *meso* isomer. Egorova et al. (*77*) suggested that *rac*-DMSA had a higher formation constant than *meso*-DMSA in the formation of ZnL_2^{6-}. This qualitative observation was made on the basis of the suppression of the buffer region, which was observed after 3 equivalents of base were added, in the potentiometric titration of a *rac*-DMSA solution containing a 2:1 ligand:zinc ratio. No quantitative calculations were performed for zinc-*rac*-DMSA systems and no dimeric complexes were included in their interpretation of the potentiometric titrations of the zinc-*meso*-

DMSA systems. The shapes of the potentiometric titration curves obtained with a 2:1 ratio of ligand:zinc, for zinc-*meso*-DMSA and zinc-*rac*-DMSA systems, in our laboratory are exactly the same as those obtained by Egorova et al. (*77*). The proposed speciation models for zinc-*rac*-DMSA (Table 2-3) were calculated with the aid of the computer program "BEST" (*72,94*) and shown to be the most favorable on a statistical basis. The log formation constants (Table 2-3) of the dimeric complexes, $Zn_2L_2H^{3-}$ and $Zn_2L_2H_2^{2-}$, which are determined from both L:M and 2L:M systems, agree very well with each other, within the margin of error of the computations with the "BEST" program. This strongly supports the models that define the zinc complex species that are present in solution in the course of the potentiometric titrations of the two systems in which the *rac*-DMSA:zinc ratios are 1:1 and 2:1. The ZnL_2^{6-} species of *rac*-DMSA is extraordinarily stable with a log formation constant of 25.3, in comparison with the ZnL_2^{6-} of *meso*-DMSA, which has a log formation constant of 19.7. The proposed speciation model for the zinc-*rac*-DMSA system was confirmed by independent NMR and IR studies. By ignoring the isotope effect of deuterium on the pK_a values of *rac*-DMSA, the distributions of various ionic and molecular species as a function of pD in the Zn^{2+}-*rac*-DMSA system used in the NMR titration are calculated and shown in Fig. 2-13 by using the speciation model and the stability constants obtained from the potentiometric studies. The NMR results confirmed the model

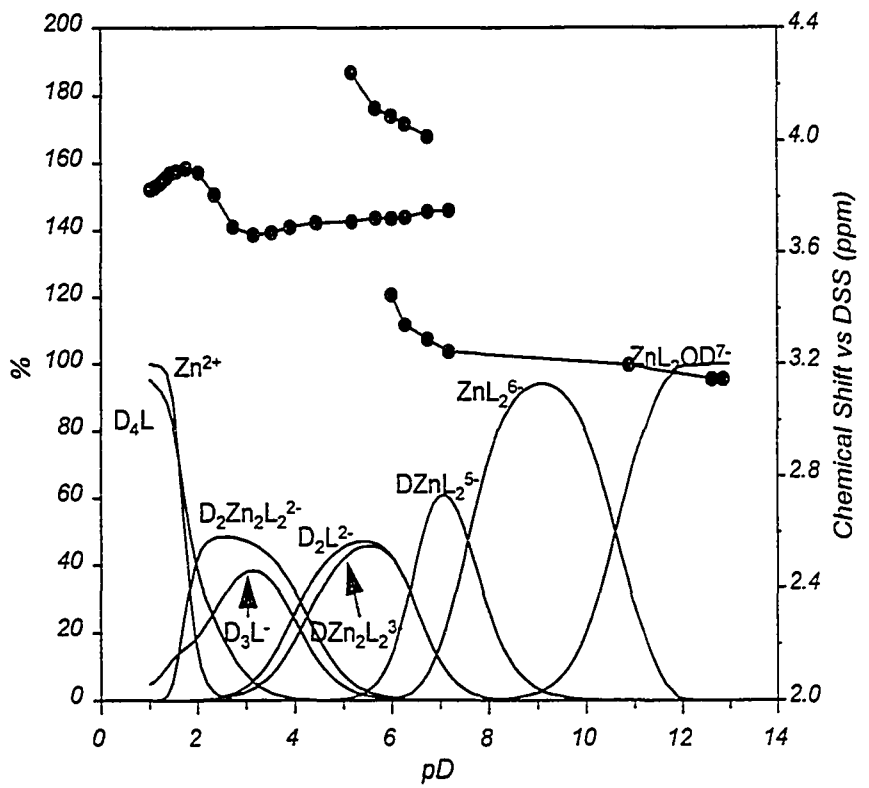

Figure 2-13. Plots of the chemical shift of the methine protons and the speciation curves, calculated by the "BEST" program, as a function of pD for solutions containing 0.08 mmol *rac*-DMSA and 0.04 mmol Zn^{2+}.

because the model predicts, as shown in Fig. 2-13, that ZnL_2OD^{7-} and ZnL_2^{6-} predominate at high pD values; $DZnL_2^{5-}$ predominates at pD around 7.3; dimeric complexes are formed at pD between 6.0 and 7.0; and various protonated ligand species are predominant in the low pD region; and the NMR results, reported in the Results section do predict the formation of these species at these pD. The chemical shifts of the methine protons of DMSA in some zinc complexes are summarized in Table 2-5. Formation of ZnL_2 complexes of *rac*-DMSA is also supported by proton NMR and IR results, shown in Figs. 2-5 and 2-11.

Rac-DMSA Mobilizes More Zinc Than _Meso_-DMSA at Physiological pH.

As indicated by the potentiometric titration curves and confirmed by the speciation models for *meso*- and *rac*-DMSA, the complex formation behavior of *rac*-DMSA is dramatically different from that of *meso*-DMSA. Therefore, it is not valid to predict the extent of zinc complexation with the two isomers of DMSA on the basis of a naive comparison of formation constants. The distribution of zinc complexes *in vivo* varies as a result of the large pH variation in the various *in vivo* compartments. It is reasonable, however, to select a pH of 7.4 as a general physiological pH value. In order to compare the extent of formation of zinc complexes with *meso*- and *rac*-DMSA at physiological pH, the program "SPE" (*72*) was used to calculate the distribution of various zinc complexes formed in the presence of both *meso*- and *rac*-DMSA under various conditions, as a function

Table 2-5. Chemical Shifts of the Methine Protons in Zinc Complexes of *Rac*- and *Meso*-DMSA vs DSS.

	meso-DMSA			*rac*-DMSA				
species	L^{4-}	ZnL_2^{6-}	$Zn_2L_2^{4-}$	L^{4-}	ZnL_2^{6-}	$DZnL_2^{5-}$	$Zn_2L_2^{4-}$	$DZn_2L_2^{3-}$
ppm	3.07	3.59	3.72	3.08	3.19	3.75	4.21	ca. 4.28

of pH by using the formation constants listed in Tables 2-1 and 2-3. It was assumed in the calculation, that all the zinc complexes of *meso*- and *rac*-DMSA, shown in Tables 2-1 and 2-3, were present. The concentrations of the ligands used in the calculation ranged from 0.1 to 1.0 mM, which covers the typical concentration range of a chelating agent used clinically. The concentration of zinc used in the calculation ranged from 0.001 to 1.0 mM in order to cover the biological levels of zinc. The concentrations of *meso*- and *rac*-DMSA were varied simultaneously and always kept the same in our computer calculations. It is shown in Fig. 2-14 that in a solution containing (2*meso*-DMSA + 2*rac* - DMSA):Zn, only two types of zinc complexes are present in the vicinity of pH 7.4, Zn(*rac*-DMSA)$_2$H$_2^{4-}$ and Zn$_2$(*meso*-DMSA)$_2^{4-}$, with about 88% of zinc bound in *rac*-DMSA and about 12% of zinc bound in *meso*-DMSA. When the zinc concentration was increased by a factor of 2 while the DMSA concentrations were kept constant, a protonated zinc complex of *meso*-DMSA, Zn$_2$(*meso*-DMSA)$_2$H^{3-}, was formed in the vicinity of pH 7.4 along with an increase in the concentration of Zn$_2$(*meso*-DMSA)$_2^{4-}$ and a decrease in the concentration of Zn(*rac*-DMSA)$_2$H$_2^{4-}$ (Fig. 2-15). As a consequence, only about 47% of the zinc is bound in *rac*-DMSA and about 53% of zinc in *meso*-DMSA. A further increase in the concentration of zinc to a ratio of (*meso*-DMSA + *rac*-DMSA):2Zn did not result in any change in the concentrations of the individual zinc complexes with *meso*-

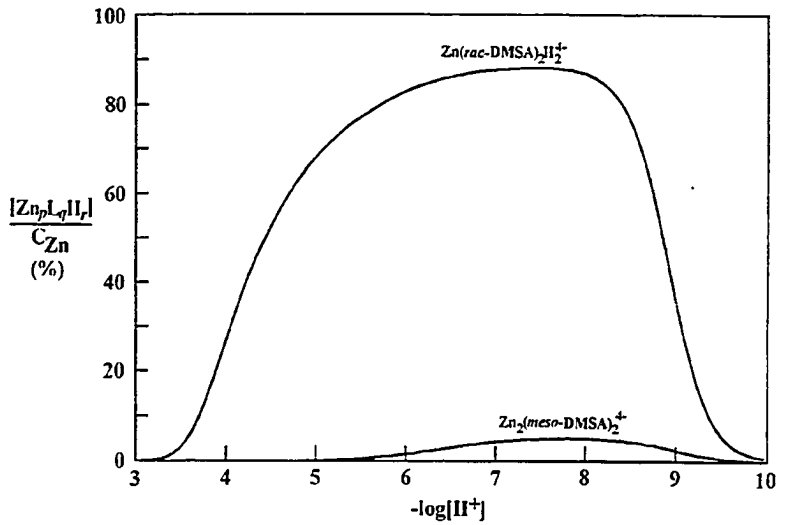

Figure 2-14. Distribution curves of zinc species in a solution containing 0.25 mM Zn^{2+}, 0.50 mM *rac*-DMSA and 0.5 mM *meso*-DMSA, (i.e. L:Zn=4:1). The zinc species plotted are only those which contribute to the total amount of zinc by more than 0.2% in the vicinity of pH 7.4.

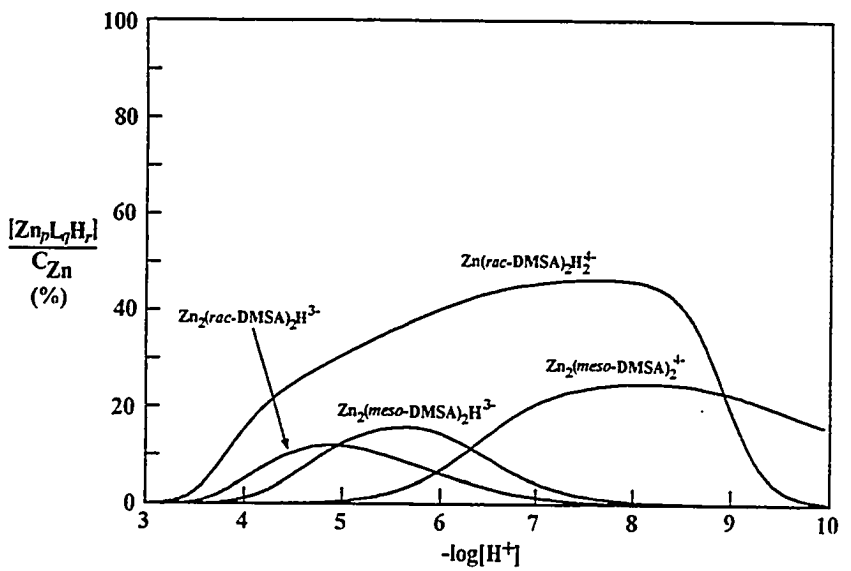

Figure 2-15. Distribution curves of zinc species in a solution containing 0.50 mM Zn^{2+}, 0.50 mM *rac*-DMSA and 0.50 mM *meso*-DMSA (i.e. L:Zn=2:1). The zinc species plotted are only those which contribute to the total amount of zinc by more than 0.2% in the vicinity of pH 7.4.

DMSA; however, the concentration of the zinc complexes formed with *rac*-DMSA were drastically changed as a result of the formation of two dimeric complexes, $Zn_2(rac\text{-DMSA})_2^{4-}$ and $Zn_2(meso\text{-DMSA})_2H^{3-}$, and the disappearance of $Zn(rac\text{-DMSA})_2H_2^{4-}$ (Fig. 2-16). The amount of zinc bound in *rac*-DMSA remained unchanged at about 47%. It is evident from Figs. 2-13, 2-14 and 2-15 that the ratio of zinc complexed by the two DMSA isomers depends on the concentration of zinc present in the solution and also depends on the concentrations of the DMSA isomers. The term, Plasma Mobilizing Index (PMI) (*92,108*), has been used to assess the efficacy of a chelating agent in mobilizing a metal ion from a labile metal protein complex in blood plasma. A similar term, Relative Plasma Mobilizing Index (RPMI), which is defined as:

$$\text{RPMI} = \frac{\text{(the total concentration of zinc bound in } rac\text{-DMSA)}}{\text{(the total concentration of zinc bound in } meso\text{-DMSA)}}$$

has been used to compare the relative extent of the depletion of zinc by *rac*-over *meso*-DMSA. The advantage of using RPMI is that the metal-mobilizing ability in plasma of a chelating agent can be evaluated without a knowledge of the metal-complexing properties of plasma constituents, if the mobilizing ability of any chelating agent has been known. RPMI values at pH 7.4 were calculated by using

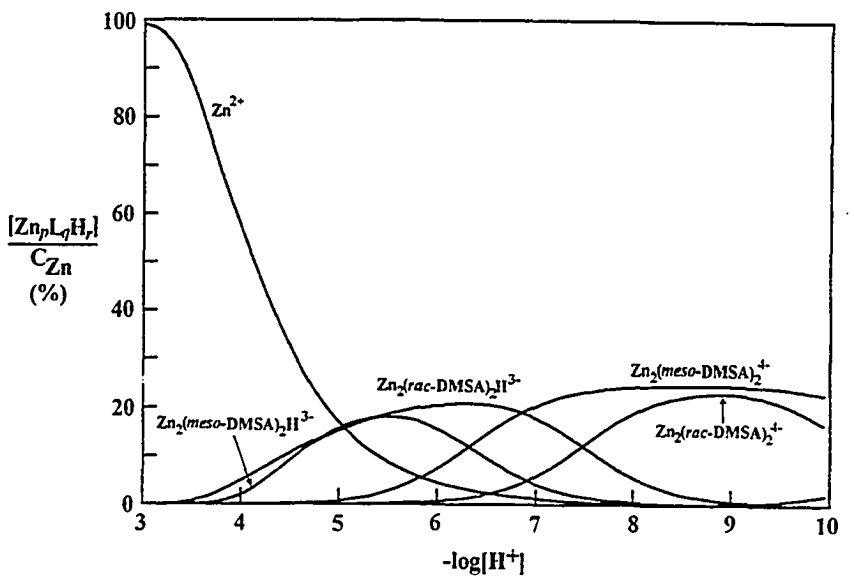

Figure 2-16. Distribution curves of zinc species in a solution containing 1.0 mM Zn^{2+}, 0.5 mM *rac*-DMSA and 0.5 mM *meso*-DMSA (i.e. L:Zn=1:1). The zinc species plotted are only those which contribute to the total amount of zinc by more than 0.2% in the vicinity of pH 7.4.

the program "SPE" over a wide range of zinc concentration and total DMSA concentration, but the individual concentrations of *rac*- and *meso*-DMSA were always kept the same. The results of the calculations were plotted in Fig. 2-17 as log(RPMI) versus the log of the molar ratio of *rac*-DMSA to zinc. It is evident from Fig. 2-17 that the RPMI value is affected by the DMSA to zinc ratio and the absolute concentration of the DMSA. The RPMI value is independent of the absolute concentration of DMSA (Fig. 2-17), before the ratio of *rac*-DMSA:zinc approaches 1:1 which corresponds to a total DMSA:zinc ratio of 2. There is no significant difference in the depletion of zinc by the two isomers at a log(RPMI) value of around 0 despite the difference in the chemical nature of zinc-*rac*-DMSA complexes (Fig. 2-16). A significant increase by 3 to 4 powers of ten in the depletion of zinc by *rac*- over *meso*-DMSA occurs when log(*rac*-DMSA/zinc) increases from 0 to 1.0, which corresponds to an increase in the ratio of total DMSA to zinc between 2 and 20. A further increase in the ratio of total DMSA to zinc from 20 to 200 does not cause a significant additional increase in the depletion of zinc by *rac*- over *meso*-DMSA. A high dosage of DMSA is commonly used in the treatment of acute heavy metal poisoning. Hence, the ratio of DMSA:zinc is between 20 and 200 or even higher, and the zinc depletion by *rac*-DMSA is expected to be much greater than the zinc depletion by *meso*-DMSA. Animal studies (*57*) showed that *rac*-DMSA only increased urinary

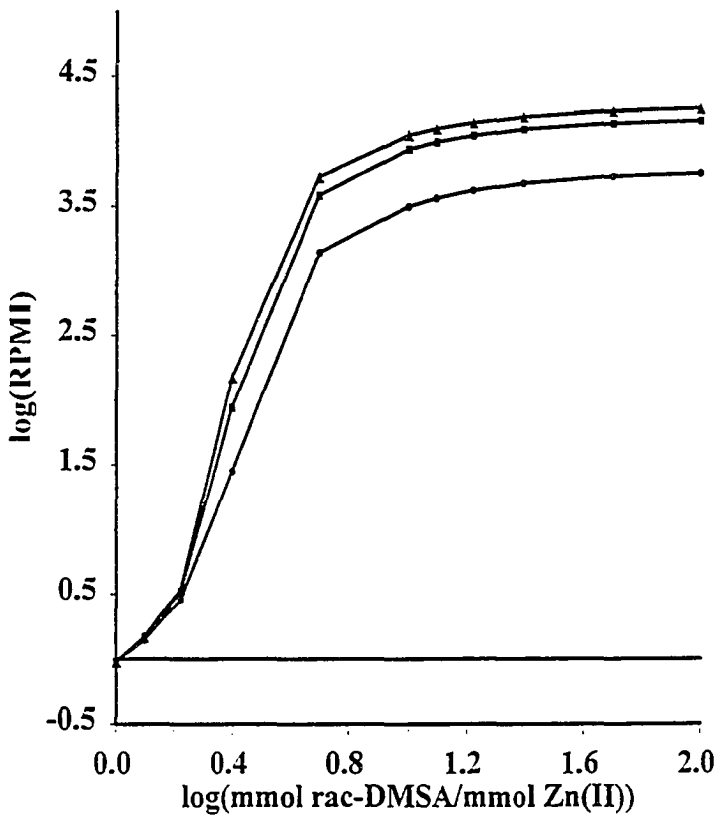

Figure 2-17. Curves for log of zinc(II) relative plasma mobilizing index (RPMI) of *rac*- over *meso*-DMSA versus the log of molar ratio of *rac*-DMSA to zinc(II) at the concentrations of *rac*-DMSA of 0.1 mM (•), 0.5 mM (■) and 1.0 mM (▲). Note: The total concentration of *meso*-DMSA is always equal to the total concentration of *rac*-DMSA present.

excretion of zinc by 2-fold, which is obviously lower than that predicted by the speciation model. This implies that *rac*-DMSA complexes as a whole are more readily reabsorbed after normal glomerular filtration. If this is true, the structure of the complexes may play an important role in the reabsorption mechanism.

Rac-DMSA alone is superior to *meso*-DMSA if the drug is administered to children and pregnant women as a prophylactic for the prevention of lead poisoning. In this case the required dosage of the drug is low. Lead blood levels as low as 10-15 μg/dL (*26*), i.e. 0.48-0.72 μM and possibly lower, are linked with impaired neurobehavioral development in human fetuses and children. In order to maintain the lead blood level under 0.48 μM, a DMSA concentration of a few μM is required in the blood, which brings the DMSA:zinc ratio to the vicinity of 1.0 or even lower, where the extent of zinc depletion by the two DMSA isomers is approximately equal. The administration of *rac*-DMSA, therefore, is advantageous because of the higher lead mobilizing capability of *rac*- over *meso*-DMSA.

Rac-DMSA may be superior to *meso*-DMSA in the treatment of acute heavy metal poisoning, e.g. cadmium, lead poisoning etc., if the zinc complex, $Zn(rac\text{-}DMSA)_2^{6-}$, is administered instead of the pure ligand, *rac*-DMSA. At pH 7.4 a low level of free zinc ion is expected to be maintained by the administered zinc chelate of *rac*-DMSA in the solution, and this ensures that there is practically no depletion of endogenous zinc by *rac*-DMSA. On this basis, it may be

postulated that Zn(*rac*-DMSA)$_2^{6-}$ is more efficacious and much less toxic than either *meso*- or *rac*-DMSA in the treatment of acute lead poisoning. The detailed assessment of this idea is performed in Chapter Three.

Conformations of Various Zn-*rac*- and Zn-*meso*-DMSA Chelates in Solution.

Zinc-DMSA solution is a dynamic system in which there are many conformations of zinc complexes of DMSA. The complexation of *rac*-DMSA with zinc ion is even more complicated than that of *meso*-DMSA because *rac*-DMSA is a mixture of equal amounts of two enantiomers, i.e. R,R-DMSA and S,S-DMSA. Despite the complexity of the system the NMR and IR spectra of zinc complexes are mainly influenced by the major conformations present in solution and can provide conformational information on the complexes. Potentiometry is another experimental probe which can determine whether thiolate groups in DMSA complexes are free or coordinated to a metal ion. In the DMSA ligand, L^{4-}, there are two types of protonation sites, carboxylate groups and thiolate groups, the protonation constants (log*K* values) of which are typically less than 4.0 and greater than 9.0, respectively. If a protonation constant larger than 9.0 is obtained potentiometrically for a zinc complex, there must be a free thiolate group present in the complex. If a protonation constant between 5.0 and 8.0 is obtained for a zinc complex, there is no free thiolate group available, and only coordinated thiolate groups are present in the complex. The decrease in the protonation

constant of a coordinated thiolate group, compared with a free thiolate group in the zinc complexes, results when the protonation of the thiolate group is preceded by an energetically unfavorable coordination bond-breaking process. On the basis of NMR and IR results presented in the Results Section and with the aid of a molecular model, the representative and energetically favorable conformations of various zinc complexes of *rac*- and *meso*-DMSA are shown in Figs. 2-18 and 2-19.

Although the conformation of Zn(R,R-*rac*-DMSA)(S,S-*rac*-DMSA) purports to represent ZnL_2^{6-} (Fig. 2-18 (I)), Zn(R,R-*rac*-DMSA)$_2$ and Zn(S,S-*rac*-DMSA)$_2$ are also present in solution, and their conformations are very similar to the conformation of Zn(R,R-*rac*-DMSA)(S,S-*rac*-DMSA) shown in Fig. 2-18. The coexistence of three types of the ZnL_2 may be responsible for the unsymmetrical shape of the IR symmetric stretching band of the complex (Fig. 2-11, solid line 5). As shown in Fig. 2-7, the net downfield shift resulting from the formation of ZnL_2^{6-} of *rac*-DMSA is only 0.11 ppm, which is smaller than that due to the protonation of a thiolate group, 0.14 ppm, as found in Chapter One, or smaller than that due to the protonation of a carboxylate acid group, 0.20 ppm (*73*), or smaller than that due to the formation of ZnL_2^{6-} with *meso*-DMSA, 0.53 ppm. This implies that the deshielding effect by Zn^{2+} is not the only effect responsible for the chemical shift change. The ZnL_2^{6-} most likely adopts a conformation in

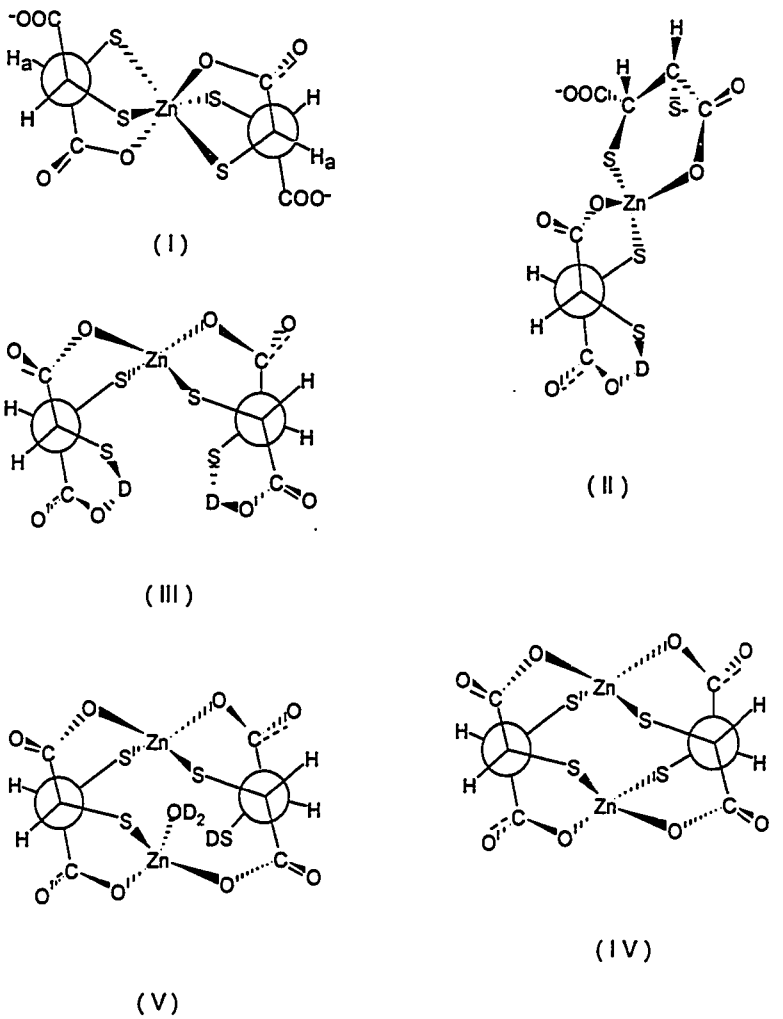

Figure 2-18. Proposed conformations of zinc-*rac*-DMSA complexes in an aqueous solution. (I) ZnL_2^{6-}; (II) $DZnL_2^{5-}$; (III) $D_2ZnL_2^{4-}$; (IV) $Zn_2L_2^{4-}$; (V) $DZn_2L_2^{3-}$.

which the methine proton of the ligand is oriented in the shielding region of the carbonyl double bond, which to some extent cancels out the deshielding effect of Zn^{2+}. As illustrated in Fig. 2-18 (I) each ligand in the complex forms one five-membered ring in which one carboxylate group and its adjacent thiolate group are bound to the zinc ion, another five-membered ring in which both thiolate groups are bound to the zinc ion, and a six-membered ring in which one carboxylate group and one thiolate group, at the β-position relative to the carboxylate group, are bound to the zinc ion. The unbound carboxylate group can rotate freely around the C-C single bond as it does in the free ligand (L^{4-}). With the aid of a molecular model, it is found that the methine protons (Ha in Fig. 2-18 (I)) are located out of the deshielding plane of the C=O bond of their contiguous carboxylate groups, where they are exposed to an additional shielding effect because the six-membered ring adopts a rigid boat conformation as a result of zinc-sulfur bridging through the thiolate group at the α position relative to the carboxylate group participating in the six-membered ring. This cancels out in part the deshielding effect of the zinc ion on the methine protons of *rac*-DMSA, and accounts for the small downfield shift, 0.11 ppm, of the methine proton peak in the ZnL_2^{6-} from that in the pure *rac*-DMSA ligand. The *meso*-DMSA ligand in ZnL_2^{6-}, as shown in Fig. 2-19 (I), uses two carboxylate groups and one thiolate group to form a five-membered ring, a six-membered ring and a seven-membered

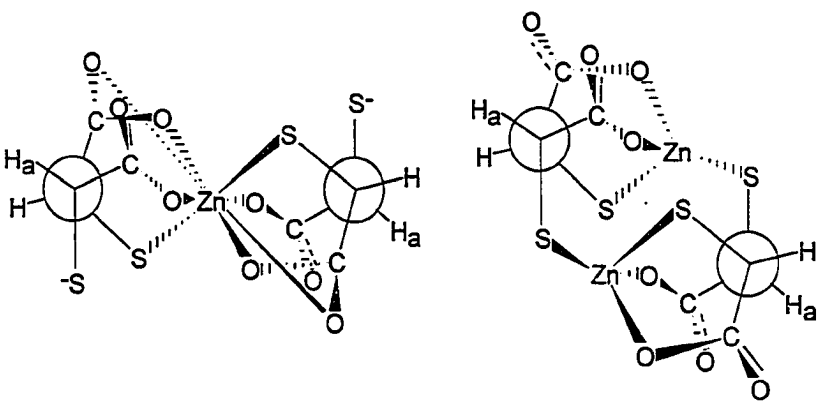

(I) (II)

Figure 2-19. Proposed conformations of zinc-*meso*-DMSA complexes in an aqueous solution. (I) ZnL_2^{6-}; (II) $Zn_2L_2^{4-}$.

ring. It is found with the aid of a molecular model that, in contrast to the ZnL_2^{6-} of *rac*-DMSA, the methine protons (Ha in Fig. 2-19 (I)) are located in the deshielding plane of the C=O bond of its contiguous carboxylate groups, where they are exposed to an additional deshielding effect, because the six-membered ring adopts a chair conformation to minimize the electrostatic repulsion between the oxygen of the carboxylate group and the negatively charged free thiolate group. This accounts for the drastic downfield shift, 0.52 ppm (Fig. 2-7), of the methine proton peak in the ZnL_2^{6-} from that in the pure *meso*-DMSA ligand. The proposed conformations of ZnL_2^{6-} of *rac*- and *meso*-DMSA are also cross confirmed by the results obtained from the potentiometric results. The protonation constant (log*K* value) of ZnL_2^{6-} of *meso*-DMSA is 10.9, which indicates that a free thiolate group must be available in the complex for protonation, whereas the protonation constant (log*K* value) of ZnL_2^{6-} of *rac*-DMSA is 7.6, which indicates that the thiolate groups in the complex are all bound to the zinc ion.

As shown in Fig. 2-18 (IV), each zinc ion in the dimeric complex $Zn_2L_2^{4-}$ of *rac*-DMSA is tetrahedrally coordinated with two carboxylate groups and two thiolate groups, forming two six-membered rings of the same type. In each six-membered ring structure, one carboxylate group and one thiolate group, at the β-position relative to the carboxylate group of the same ligand, are bound to the same zinc ion. There are four six-membered rings formed in the complex, and all

the six-membered rings adopt rigid boat conformations as a result of cross-linking via two central zinc ions between two ligands. It is evident in a molecular model that all the methine protons are located in the deshielding planes of the C=O bonds of the carboxylate groups in this conformation of $Zn_2L_2^{4-}$ of *rac*-DMSA. This accounts for the drastic downfield shift, 1.02 ppm, observed after addition of one more zinc ion on ZnL_2^{6-} of *rac*-DMSA (Fig. 2-7). Although the conformation of Zn(S,S-*rac*-DMSA)$_2$ represents $Zn_2L_2^{4-}$ in Fig. 2-18 (IV), Zn_2(R,R-*rac*-DMSA)$_2$ and Zn_2(S,S-*rac*-DMSA)(R,R-*rac*-DMSA) are likely present in the solution, and their conformations are very similar to each other. The shoulder at the symmetric stretching band in the sample with zinc:ligand 1:1 (solid line 10 in Fig. 2-11) may be attributed to other conformations of the ZnL_2^{6-} chelate which exist in the solution at less significant concentrations, or to the experimental error associated with sample preparation, which gives a small portion of ZnL_2 in the sample. The IR spectrum of $Zn_2L_2^{4-}$ of *meso*-DMSA also exhibits a split of the symmetric stretching band, and the frequency of the relatively small left peak is higher than the frequency of the symmetric stretching vibration of the ligand alone. Therefore, it is more reasonable to attribute this peak to an interference with an overtone of some low frequency vibration in the complex. The zinc ion in the dimeric complexes of *meso*-DMSA (Fig. 2-19, (II)) is coordinated with two carboxylate groups and two thiolate groups. Each ligand

uses two carboxylate groups and one thiolate group to bind to one zinc ion, and uses the other thiolate group to bind to the other zinc ion. Compared with the conformations of the ligand in the ZnL_2^{6-} of *meso*-DMSA, there is not much change in the magnetic environment of the methine protons after the formation of $Zn_2L_2^{4-}$, except that the free thiolate group in the ZnL_2^{6-} is coordinated with a zinc ion in the $Zn_2L_2^{4-}$. This accounts for the small downfield shift, 0.13 ppm (Fig. 2-7), of the methine proton peak, after addition of another zinc ion to ZnL_2^{6-} of *meso*-DMSA. The absence of free thiolate groups in the conformations of the dimeric complexes of $Zn_2L_2^{4-}$ of both *rac*- and *meso*-DMSA is also cross confirmed by the results obtained from potentiometric studies. The protonation constants, (log*K* values), of $Zn_2L_2^{4-}$ of *meso*- and *rac*-DMSA are 6.3 and 7.5, respectively, which indicates that all thiolate groups in both complexes are coordinated to zinc ions.

The appearance of new peaks at 3.75 ppm (A21 - A19 in Fig. 2-9), which are assigned to $DZnL_2^{5-}$ by the speciation model (Fig. 2-17), implies that the conformation of the ligand in the complex $DZnl_2^{5-}$ of *rac*-DMSA may be similar to that in the ligand, D_2L^{2-}, because the chemical shift of the methine protons in the D_2L^{2-} of *rac*-DMSA is 3.67 ppm. It is postulated, therefore, that in $DZnL_2^{5-}$ the zinc ion is tetrahedral bound to two ligands via one thiolate group and one carboxylate group from each ligand as shown in Fig. 2-18 (II). The presence of

the free thiolate group in the $DZnl_2^{5-}$ complex is also confirmed by its protonation constant (log*K* value), 10.2. The conformation of $D_2ZnL_2^{4-}$ (Fig. 2-18 (III)) is postulated on the reasonable assumption that another similar six-membered ring is formed upon deuteration of the free thiolate group in $DZnL_2^{5-}$. The enantiomeric identity of *rac*-DMSA in the deuterated monomeric complexes is not clear, and it is likely that the complexes contain either (S,S-*rac*-DMSA) or (R,R-*rac*-DMSA) or both.

The protonation constant (log *K* value) of $Zn_2L_2^{4-}$ is 7.5, which implies that deuteration of $Zn_2L_2^{4-}$ only results in a simple deuteration of one of the bound thiolate groups in *rac*-DMSA without causing a significant change in conformation. Therefore, the conformation of $DZn_2L_2^{3-}$ of *rac*-DMSA should be very similar to that of $Zn_2L_2^{4-}$ of *rac*-DMSA. The proposed conformation of $DZn_2L_2^{3-}$, shown in Fig. 2-18 (V), is confirmed by the proton NMR results. It has been observed that the downfield shift of methine protons caused by deuteration of one adjacent thiolate group in DMSA was 0.14 ppm, but only a comparatively small downfield shift, 0.07 ppm, was observed as a result of deuteration of one thiolate group in $Zn_2L_2^{4-}$. Compared with the rigid conformation of $Zn_2L_2^{4-}$, in which all the methine protons of the ligand are in the deshielding plane of the C=O bonds, a small flexibility is expected in the conformation of $DZn_2L_2^{3-}$ because one S-Zn bond is disrupted. This induced flexibility lessens the

deshielding effect of C=O bonds on the methine protons in $DZn_2L_2^{3-}$ compared with the protons in $Zn_2L_2^{4-}$ and accounts for the observed small downfield shift. Deuteration of $DZn_2L_2^{3-}$ of *rac*-DMSA is assumed to take place at one bound thiolate group, because deuteration of one bound carboxylate group would be indicated by a protonation constant (log*K* value) much smaller than 4.0. Formation of $D_2Zn_2L_2^{2-}$ upon addition of one deuterium ion on $DZn_2L_2^{3-}$ causes a significant change in conformation, because the protonation constant (log*K* value) of $DZn_2L_2^{3-}$ is small, between 4.26 and 3.96, compared with the other zinc complexes of DMSA. The additional deshielding effect, which is present in the $Zn_2L_2^{4-}$ and $DZn_2L_2^{3-}$, of the C=O bonds on the methine protons is completely lost in the $D_2Zn_2L_2^{2-}$ since the complex completely loses the rigidity of the boat conformation present in $Zn_2L_2^{4-}$ as a result of the disruption of two S-Zn bonds. This accounts for the disappearance, rather than a further downfield shift, of the typical dimeric complex peak, when $DZn_2L_2^{4-}$ is further deuterated at pD around 5.0 (Fig. 2-17).

Zinc Chelates of *Rac*-DMSA Are More Stable Than the Corresponding Chelates of *Meso*-DMSA.

In an analysis of the conformations of various zinc complexes of DMSA proposed in Figs. 2-18 and 2-19, it is found that in all the zinc complexes of *rac*-DMSA in aqueous solution, the ligand adopts staggered anti-conformations with

respect to the carboxylate groups, whereas in all the zinc complexes of *meso*-DMSA, the ligand always adopts staggered gauche-conformations. The zinc complexes of *rac*-DMSA in aqueous solution are more stable than the corresponding complexes of its *meso* isomer because the electrostatic repulsion between two bulky carboxylate groups are minimized in the staggered anti-conformations. This accounts for the larger formation constants of zinc complexes of *rac*-DMSA than those of the corresponding complexes of its *meso* isomer and also explains, in part, why an increase in the excretion of endogenous zinc was observed with *rac*-DMSA.

CHAPTER THREE: STRUCTURES AND PROPERTIES OF LEAD CHELATES OF DMSA STEREOISOMERS IN AQUEOUS SOLUTION

Introduction

The deleterious effect of low-level lead on children has been reviewed in the introduction part of this dissertation. An inverse correlation of blood lead level with height, weight and chest circumference was unequivocally observed (*21*). The correlation of blood lead levels and the cognitive performance of preschool and school-age children indicated that a significant decrease in the cognitive and behavior score of children is associated with an elevation of average blood lead in the range 10-30 μg/dL.

Meso-DMSA has been increasingly used for the treatment of children with blood Pb ≥ 25 μg/dL, since its approval by the FDA in 1991 (*15*) for the treatment of children with blood Pb ≥ 45 μg/dL. Despite its increasing use for lead poisoning, the disadvantage in human use is its low solubility in aqueous solution. *Meso*-DMSA only removes lead from the extracellular fluid of plasma (*44*), and persistent efforts in searching for more effective intracellular chelators of lead ion are evident in the literature. The current direction and focus of the research is seemingly in the development of various alkyl esters of *meso*-DMSA (*109,110*). The use of monoalkyl esters of *meso*-DMSA invariably removes more lead from soft tissues such as kidney and brain than *meso*-DMSA

does (*110*). This potential advantage of using alkyl esters of *meso*-DMSA, however, is offset, at least in part, by the elevated acute toxicity of the esters. The unique characteristics of the hydrophilicity and lipophilicity of *rac*-DMSA indicate that it has the potential to be a more effective chelating agent than *meso*-DMSA as an intracellular chelator for lead poisoning. More importantly, the toxicity of *rac*-DMSA is almost as low as that of *meso*-DMSA, according to its LD_{50} value (*58*).

The relative efficacy of the two stereoisomers in mobilizing lead at physiological pH can be assessed by using the RPMI (*111*) from a prior knowledge of the lead chelates formed with the DMSA stereoisomers at physiological pH and the formation constants of these chelates. The formation constants of some lead chelates of *meso*-DMSA were determined by several groups (*77,78,93*). The formation constants of lead chelates of *rac*-DMSA, however, have never been determined. Therefore, one of the goals of this chapter is the determination of the formation constants of the lead chelates of *meso*- and *rac*-DMSA. The relative mobilizing ability of *rac*- and *meso*-DMSA for lead ions at physiological pH will be assessed later.

It was also reported (*112,113*) that ^{99m}Tc chelates of *rac*-DMSA did not show the osteotropic property which was observed for the corresponding ^{99m}Tc chelates of *meso*-DMSA. ^{99m}Tc-*rac*-DMSA was cleared from blood more rapidly

than ^{99m}Tc-*meso*-DMSA in 1-3 h after injection (*113*). The different *in vivo* behavior of the ^{99m}Tc chelates of DMSA diastereoisomers have been attributed to the difference in the steric arrangement of carboxylic groups of the isomeric ligands in the complexes (*113*). The experimental results obtained with ^{99m}Tc chelates of the two DMSA diastereoisomers clearly demonstrate that the *in vivo* behavior of metal chelates of DMSA diastereoisomers is closely related to the structures of the chelates, probably by altering the solubilities of the chelates, and by the possible interactions of these chelates with endogenous species. Therefore, a knowledge of the structures of these lead chelates formed in aqueous solution is crucial for an understanding of their transport through membranes, their redistribution among organs and the mechanism of excretion of lead chelates from the body. An additional goal of this chapter will be to provide experimental evidence for the binding sites of the DMSA stereoisomers in the chelates.

Formation constants of zinc chelates of DMSA stereoisomers have been determined by potentiometric titrations of the ligands at varying zinc:ligand ratios (*111*). The conformations of various zinc chelates of DMSA stereoisomers have been studied by NMR and IR spectroscopy. The experimental challenge in using the above methods to probe DMSA-lead chelates is the comparatively low solubilities of the chelates, which will cause precipitation in the course of the titrations. NMR is not a sufficiently sensitive technique at low concentrations.

Aqueous IR spectroscopy usually also requires a high concentration, because only samples that have a thickness of only a few dozen μm are suitable for IR measurements so that the intense absorption by solvent water may be minimized. To overcome the precipitation problem we used a competitive ligand in the titrations. To obtain experimental evidence of the binding sites of the ligands in lead chelates, IR experiments were performed under careful control of the experimental conditions and at low concentrations of the DMSA stereoisomers.

Experimental Section

Materials.

Deuterium oxide (99.9% deuterium) was purchased from Cambridge Isotope Laboratories (Woburn, MA); lead perchlorate hydrate (98%) was purchased from Aldrich Chemical Co. Inc. (Milwaukee, WI); *rac*-DMSA was synthesized as described previously (*55*); *meso*-2,3-dimercaptosuccinic acid was a gift from Johnson & Johnson Baby Products Co. (Skillman, NJ); buffer solutions were purchased from Fisher Scientific (Fair Lawn, NJ); siliconizing fluid was purchased from Princeton Applied Research (Princeton, NJ); all other inorganic compounds used were purchased from Mallinckrodt, Inc. (Paris, KY), and were of analytical reagent grade. ***Caution:*** *Gloves are necessary in the handling of all the above chemicals to avoid direct contact with skin.*

IR Titration of Na_4L of *Meso* and *Rac*-DMSA with $Pb(ClO_4)_2$.

The IR instrument and the sample ceil are the same as those described in Chapter Two. All experimental IR spectra were recorded at ambient temperature (20°C) after 64 scans against nitrogen background, and the resolution of the IR measurement was 2 cm^{-1} for all spectra. The processed IR spectra, plotted only in the frequency region between 1660 and 1300 cm^{-1} to show the asymmetric and symmetric stretching bands of the carboxylate groups in the DMSA isomers, were obtained after subtraction of the spectrum of D_2O from the experimental spectra

followed by a subtraction of the spectrum obtained with supporting NaCl solution, if additional NaCl was added, and a partial subtraction of the spectrum obtained with 1% H_2O in D_2O. The subtraction of H_2O-in-D_2O spectrum, which displayed a strong band at 3418 cm^{-1} and a weak band at 1462 cm^{-1} that interfered with the carboxylate stretching bands, was performed until the strong band at 3418 cm^{-1} in the resulting spectrum completely disappeared.

Stock solutions of 0.10 M tetrasodium DMSA of the two DMSA isomers were prepared by dissolving 0.40 mmol of the appropriate DMSA in 4.0 mL of D_2O containing 0.40 M NaOD. A stock solution of 0.1 M lead perchlorate was prepared by dissolving 0.11 mmol of lead perchlorate in 1.1 mL of D_2O, and its concentration was confirmed by EDTA titration to be 0.102 M. A stock solution of 4.8 M NaCl was prepared in a 10 mL volumetric flask by dissolving a weighed amount of NaCl crystals in D_2O.

Working solutions of 0.02 M of the two DMSA isomers were prepared by dilution of their 0.1 M stock solutions. Pb^{2+}:L^{4-} 1:1 working solutions of 0.02 M in the two isomeric DMSA ligands were prepared by mixing 240 μL 0.1 M lead perchlorate stock solution with 240 μL 0.1 M appropriate DMSA stock solution in 720 μL D_2O. The resulting 1:1 Pb:*rac*-DMSA is a clear solution, but the 1:1 Pb:*meso*-DMSA is an orange colloid. 200 μL of solution, used for IR measurement, at a desired lead:ligand ratio was made by (1) mixing the 0.02 M

DMSA working solution with the 0.02 M lead:ligand 1:1 working solution in different ratios, or (2) adding a calculated volume of D_2O in a polyethylene microcentrifuge tube, followed by addition of 40 μL of appropriate 0.1 M DMSA stock solution, a calculated volume of 4.8 M NaCl solution, (if necessary), and a calculated volume of 0.1 M lead perchlorate. All of the 0.02 M lead-*rac*-DMSA solutions used for IR measurement were clear and stable, if the Pb:ligand ratio did not exceed 1.0; if the Pb:ligand ratio exceeded 1.0, a yellowish precipitate formed. All IR "solutions" of *meso*-DMSA with varying Pb:ligand ratios were virtually colloids which were unstable and darkened in color within 30 min.

Potentiometric Determination of Formation Constants of Lead Chelates of DMSA Stereoisomers.

Standard KOH solutions of 0.1 M were prepared from 45% (w/w) KOH solution and CO_2-free double-deionized H_2O. The prepared base solutions were kept under a nitrogen atmosphere to prevent the absorption of CO_2. The carbonate content, determined as described by Martell et al.(*72*), was found to be 0.5% in the KOH solution; the exact molarity of KOH solution was determined with potassium acid phthalate with phenolphthalein as indicator. A stock HNO_3 solution of 0.1 M was prepared from concentrated HNO_3 and CO_2-free double-deionized H_2O and standardized by KOH titration. The standard EDTA solution of 0.1 M was prepared from disodium EDTA and CO_2-free double-deionized H_2O

and standardized by titration with a standard zinc solution, prepared from zinc oxide as described (*114*). A stock EDTA solution of 0.01 M was prepared from 0.1 M standard EDTA solution. A stock Pb^{2+} solution, 0.01 M, was prepared from $Pb(NO_3)_2$ and CO_2-free double-deionized H_2O and standardized by EDTA titration. The diastereoisomeric DMSA stock solutions of 0.01 M were prepared by weighing about 91.1 mg of the compound in a 50 mL volumetric flask, followed by addition of 20 mL of CO_2-free double-deionized H_2O and two equivalents of KOH. The solution was then diluted to 50 mL with CO_2-free double-deionized H_2O, transferred to a small plastic bottle, deaerated with argon for 1-2 min and finally kept in a freezer until use. The concentrations of the DMSA solutions were calculated from the initial weights of the ligands and then confirmed by KOH titration with methyl red as indicator.

The apparatus and procedures used for potentiometric measurement of hydrogen ion concentration have been described in Chapter One. The titration solutions were prepared according to the following procedures: 30 mL of CO_2-free deionized water was placed in a titration vessel into which 6 mL of the stock EDTA solution was transferred, followed by addition of 6 mL of the stock lead nitrate solution and 6 mL of the stock DMSA solution, when lead-DMSA complexes were titrated. Finally, a desired amount of KNO_3 was weighed and added to the titration vessel to maintain the ionic strength equal to 0.10±0.01

throughout the titration. The accuracy of volume transfer in the preparation of the stock solutions and the titration solutions was ensured by the exclusive use of volumetric pipets, which were previously siliconized with siliconizing liquid and calibrated with double-deionized water.

Results

IR Spectra of *Rac*-DMSA-Pb Solutions.

The correlation between the asymmetric stretching frequency (ν_a) and symmetric stretching frequency (ν_s) of a carboxyl group and their separation ($\Delta\nu$) with the nature of the coordination of a carboxylate group has been summarized by Deacon et al. (*99*). The unidentate coordination of a carboxylate group is generally associated with $\Delta\nu$ values $\geq$ 200 cm^{-1}; however, the bidentate coordination of a carboxylate group does not have a significant effect on $\Delta\nu$ values compared to that of a uncoordinated carboxylate group. In Chapter Two, the $\Delta\nu$ and intensity ratio of asymmetric and symmetric stretching bands of carboxylate groups in DMSA were used in the interpretation of the structures of zinc chelates of DMSA.

It was demonstrated in Chapter One that *rac*-DMSA ligands form ion-paired complexes with sodium ions, and the IR spectrum of the ligand alone in an aqueous solution changes with its concentration. Therefore, a high concentration of sodium ions (2.9 M) was maintained in the solutions containing less than 0.5 equivalents lead to minimize the effect of the change in the ligand that was not complexed with Pb^{2+} on the observed IR spectra. The IR spectra of 0.02 M tetrasodium *rac*-DMSA solutions at lead:ligand ratios ranging form 0 to

1.0 are plotted in Fig. 3-1. At a ligand concentration of 0.02 M and in the presence of 2.9 M sodium ions, the separation between the asymmetric band and the symmetric band of the carboxylate groups in the *rac*-DMSA alone was 159 cm^{-1} and their intensity ratio was 1.02 (Fig. 3-1), which agree with the values, 158 cm^{-1} and 1.08, reported in Chapter Two for the 0.1 M tetrasodium *rac*-DMSA solution. When the Pb:L ratio increases from 0 to 0.5, both bands gradually become narrowed and symmetrical, which indicates that both ion-paired and ligands that are not ion-paired are consumed to form PbL_2. The intensity ratio remains almost constant as the Pb:L ratio increases to 0.5. The asymmetric and symmetric stretching bands, however, shift to a higher frequency and a lower frequency, respectively, resulting in a band separation of 186 cm^{-1}. The net increase in the band separation is 28 cm^{-1}, which implies that one of the two carboxylate groups of the *rac*-DMSA in the PbL_2 complex is unidentately bound to a lead ion.

After more than 0.5 equivalents of lead is added, a new complex (PbL or Pb_2L_2) starts to form in the solution. At a Pb:L ratio between 0.5 to 0.7, the IR spectra of the solutions remain almost unchanged, indicating that the newly formed PbL complex still makes use of one of its two carboxylate groups to coordinate with the lead ion. When the Pb:L ratio becomes larger than 0.7, the symmetric stretching band starts to broaden and to split into two bands as a result

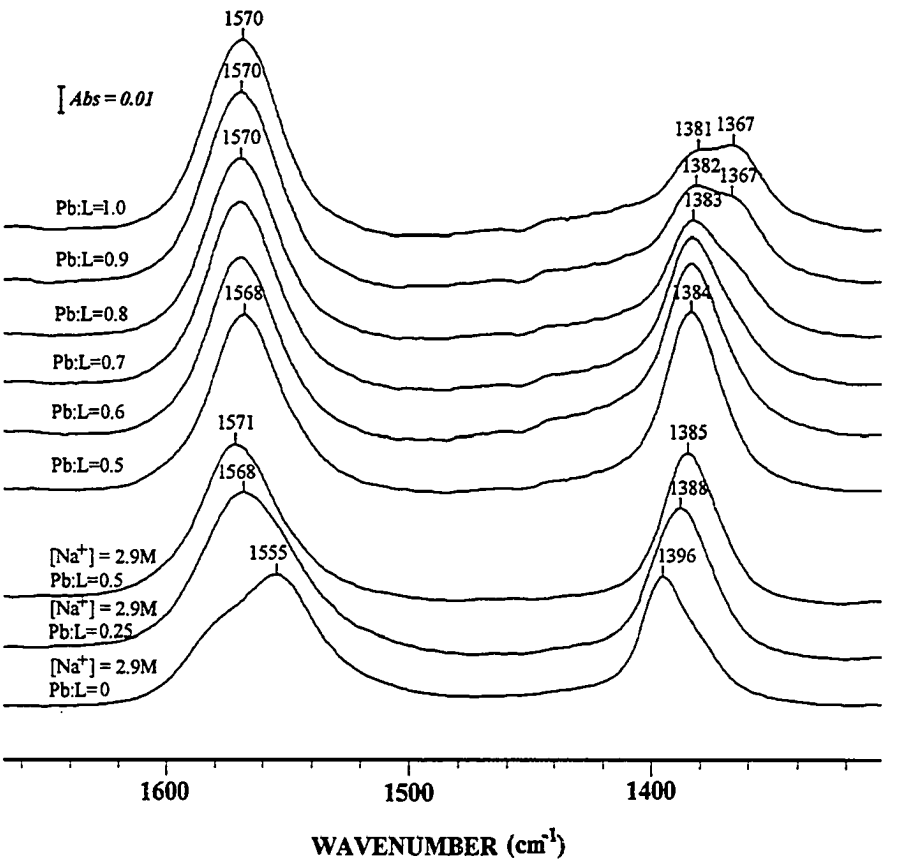

Figure 3-1. IR spectra of 0.02 M Na_4(*rac*-DMSA) solutions in the presence of Pb^{2+} at Pb:L ratios ranging from 0 to 1.0.

of the presence and the growth of a new peak at 1367 cm^{-1}, which is attributed to the formation of the dimeric complex, Pb_2L_2. The separation between the peak corresponding to the asymmetric stretch and the new peak is 203 cm^{-1}, and their intensity ratio is 2.09, which strongly indicates that both carboxylate groups of the *rac*-DMSA ligand in the Pb_2L_2 complex are involved in binding with lead ions.

IR Spectra of *Meso*-DMSA-Pb "Solutions".

The IR spectra of 0.02 M tetrasodium *meso*-DMSA solutions at lead:ligand ratios ranging from 0 to 1.0 are plotted in Fig. 3-2. There were no extra sodium ions added to any of the solutions used for IR measurements because the IR spectra were not affected by a change of ligand concentration below 0.02 M. At a ligand concentration of 0.02 M, the separation between the asymmetric band and the symmetric band of the carboxylate groups in the *meso*-DMSA alone was 169 cm^{-1} and their intensity ratio was 0.96 (Fig. 3-2). After 0.5 equivalents of lead was added, the band separation increased to 187 cm^{-1} and the intensity ratio of asymmetric stretching to symmetric stretching bands increased to 1.27. This indicates that the carboxylate groups of *meso*-DMSA ligands are involved in the formation of the complex PbL_2. It was reported in Chapter One that dilution of tetrasodium *meso*-DMSA solution from 0.1 to 0.02 M increases the band separation from 159 to 169 cm^{-1} due to a change in the solvation conditions of the carboxylate groups in the free ligands. Therefore, formation of PbL_2 in a

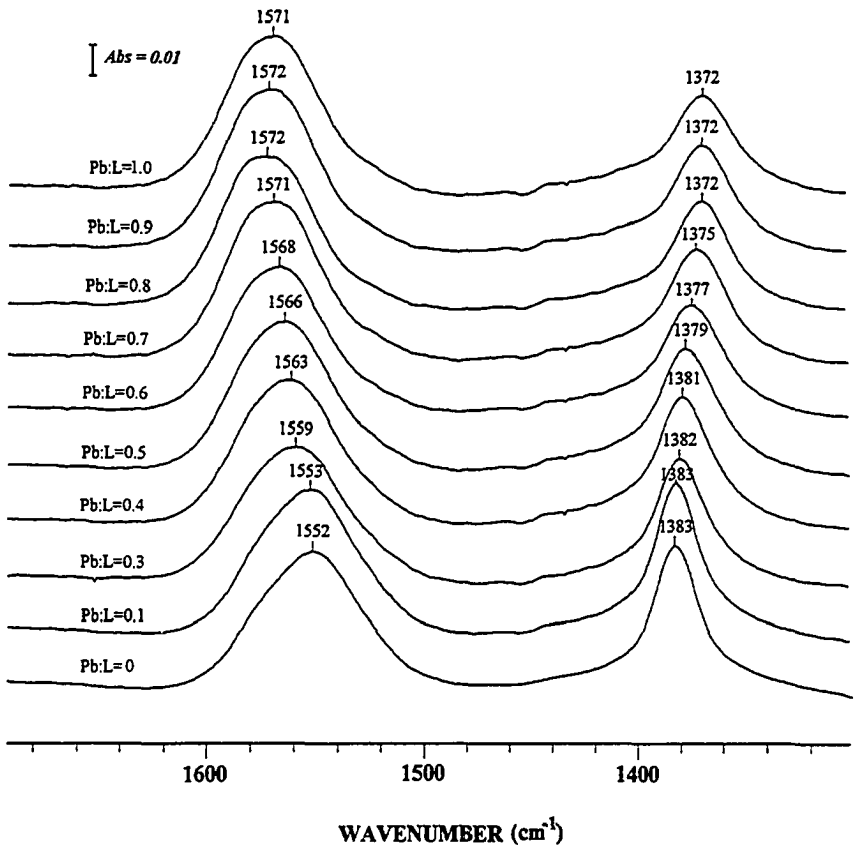

Figure 3-2. IR spectra of 0.02 M Na_4(*meso*-DMSA) solutions in the presence of Pb^{2+} at Pb:L ratios ranging from 0 to 1.0.

hypothetic 0.1 M ligand solution will increase the band separation from 159 to 187 cm^{-1}, assuming that the effect of dilution on a metal-bound carboxylate group is negligible in the IR; hence, a net increase of 28 cm^{-1} results. This value matches the value observed for the formation of PbL_2 of *rac*-DMSA, and denotes that like in PbL_2 of *rac*-DMSA, one of the two carboxylate groups of the *meso*-DMSA in the PbL_2 complex is also unidentately bound to a lead ion. After 1 equivalent of lead ion was added, both the band separation and the intensity ratio further increased to 199 cm^{-1} and 1.65, respectively, which may be an indication that both carboxylate groups of the *meso*-DMSA ligand are involved in the binding with a lead ion when PbL or Pb_2L_2 is formed. This interpretation, however, should be accepted with some caution because the samples used for the IR measurements were more colloidal than the samples at a Pb:L ratio less than 0.5, and the recorded IR spectra were severely complicated by the spectra of fine particles of the lead complexes.

Determination of Formation Constants.

The potentiometric titration data were used to calculate the formation constants of lead complexes of EDTA and DMSA with the aid of the BEST program (*72*). The BEST program calculates the formation constants of the species, which were assumed to be present in the titration solution, by minimizing the discrepancies between the calculated values of -log[H^+] and the experimental

values of -log[H^+] obtained in the potentiometric titration. Since the presence of the species which were included in the calculation by the BEST program cannot be proved by the potentiometric titration itself, the formation constants were determined only on the basis of statistics. It was noticed that several combinations of species appeared to fit the experimental titration data without a significant difference in the minimum value of $\sigma(pH)_{fit}$. Selection of the statistically most favorable model, which yields the smallest value of $\sigma(pH)_{fit}$ (*72*), as the true model to calculate the formation constants could, therefore, lead to chemically irrational conclusions. It is necessary, therefore, to report the manner in which the speciation model is generated when the formation constants are calculated on the basis of statistics.

Because of the low solubility of the lead chelates of DMSA stereoisomers, potentiometric titrations of lead-DMSA solutions were performed in the presence of a competing ligand, EDTA. In order to determine the formation constants of the lead chelates of DMSA stereoisomers, the formation constants of the lead complexes of EDTA have to be determined. Although the formation constants of various lead complexes of EDTA are available from the NIST database (*115*), they were verified independently in our laboratory to ensure the accuracy of the data as well as the validity of the potentiometric method.

Formation Constants of Lead Chelates of EDTA.

The five complexes PbEDTA, HPbEDTA, H_2PbEDTA, H_3PbEDTA and PbEDTAOH were initially assumed to be present in the Pb:EDTA 1:1 titration solutions, and therefore included in the calculation as a initial model to refine their formation constants. The log protonation constants of EDTA used in the refinement were chosen from the NIST Database (*115*). If any of the above five complexes were found to be less than 1% of the total lead concentration in the entire course of the titration, they were removed from the model and the remaining complexes were used to recalculate the formation constants. The procedures were iterated until no further complexes were excluded from the model, and the final resulting model was called the statistically favorable model. The formation constants of the complexes included in the statistically favorable model were simultaneously calculated by the BEST program.

The statistically favorable model for the titration of solutions containing a Pb:L ratio of 1:1, consists of PbEDTA, HPbEDTA and PbEDTAOH. The average formation constants calculated from two titrations are listed in Table 3-1. The formation constat of PbEDTAOH was not available for comparison. The reported formation constant of PbEDTA and its protonation constant are 18.1±0.1 and 2.8±0.1, respectively (*115*), which are in very good agreement with those determined in our laboratory, 18.18±0.01 and 2.65±0.02, respectively. This

Table 3-1. Formation Constants of Lead EDTA Chelates at μ = 0.10 and T = 25.0°C [a].

	species			log β_{pqr} [b]	
	p	q	r		
Pb:EDTA=1:1	1	1	0	18.18±0.01[c]	18.1±0.1(*115*)
	1	1	1	20.83±0.01[c]	20.9±0.2[d](*115*)
	1	1	-1	6.63±0.14[c]	

[a] L^{4-} represents the completely deprotonated EDTA in the titration of a 1:1 solution of Pb:EDTA.

[b] $\beta_{pqr} = [Pb_pL_qH_r^{-(4q-2p-r)}]/[Pb^{2+}]^p[L^{4-}]^q[H^+]^r$.

[c] The values were determined in our laboratory, and the estimated errors are calculated from the formation constants obtained by the BEST program from two individual sets of titration data with $\sigma(pH)_{fit}$ values being 0.0014 and 0.0036, respectively (*72*).

[d] The value was calculated from the reported protonation constant of PbL, 2.8±0.1.

verifies the validity of our potentiometric method for the determination of formation constants of metal chelates. PbEDTA, HPbEDTA and PbEDTAOH were always included later in the models for calculations of the formation constants of the lead complexes of DMSA. The potentiometric titration points of one trial at Pb:EDTA ratio 1:1 are plotted in Fig. 3-3, and the simulated titration curve by the BEST program is shown as a solid line.

Formation Constants of Lead Chelates of Rac-DMSA.

At first, a solution containing the species PbL, HPbL, H_2PbL, PbL_2, $HPbL_2$ and H_2PbL_2 of *rac*-DMSA was selected as a general model, assuming that there were no dimeric complexes and hydroxide complexes formed during the titrations. It is reasonable to exclude hydroxide species from our models because all titrations were stopped when all the protons initially associated with EDTA and *rac*-DMSA were completely consumed by addition of the strong base solution. A procedure similar to that used in obtaining the statistically favorable model for Pb-EDTA titrations was employed to generate a statistically favorable model of lead-*rac*-DMSA complexes for an individual set of competitive potentiometric titration data. The protonation constants of *rac*-DMSA have been determined previously (*111*). The presence of four lead complexes (PbL, HPbL, H_2PbL, and PbL_2) was deduced from the refinement by the BEST program, and their corresponding log formation constants, listed in Table 3-2, are 20.3, 26.2, 28.8

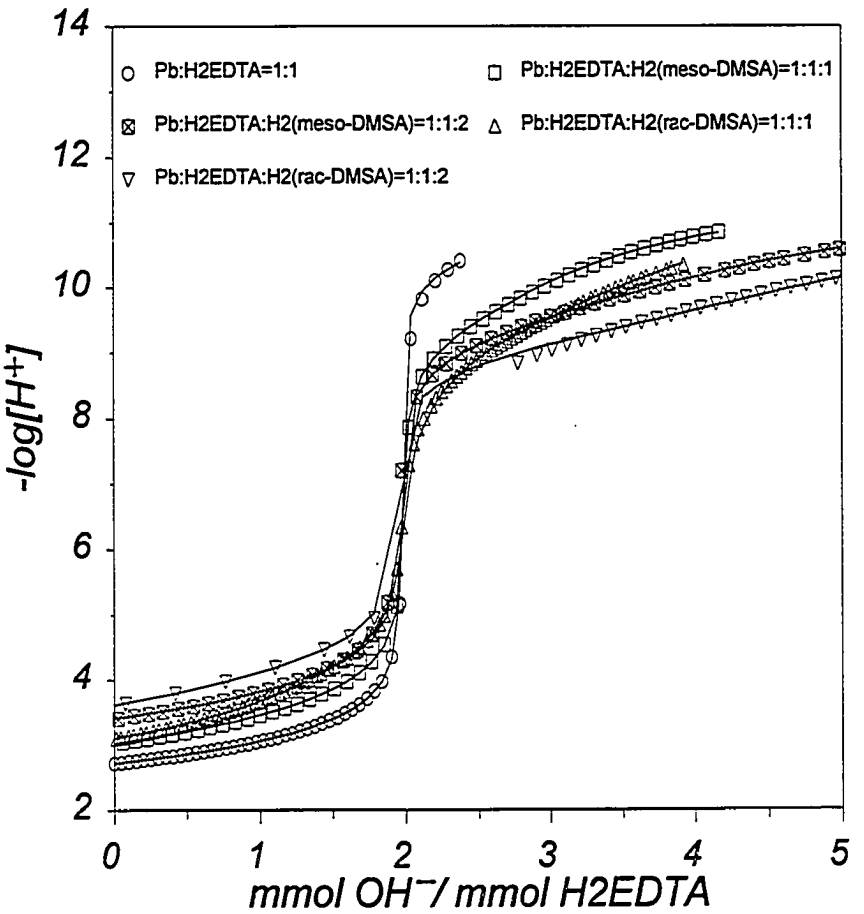

Figure 3-3. Potentiometric titration curves of the solutions containing ○ : 1.288 mM Na_2H_2EDTA and 1.268 mM Pb^{2+}, (i.e. Pb:H_2EDTA=1:1); △ : 1.255 mM Na_2H_2EDTA, 1.240 mM Pb^{2+} and 1.290 mM Na_2H_2(*rac*-DMSA), (i.e. Pb:H_2EDTA:H_2(*rac*-DMSA)=1:1:1); ▽ : 0.6276 mM Na_2H_2EDTA, 0.6202 mM Pb^{2+} and 1.241 mM Na_2H_2(*rac*-DMSA), (i.e. Pb:H_2EDTA:H_2(*rac*-DMSA)=1:1:2); □ : 1.338 mM Na_2H_2EDTA, 1.323 mM Pb^{2+} and 1.333 mM Na_2H_2(*meso*-DMSA), (i.e. Pb:H_2EDTA:H_2(*meso*-DMSA)=1:1:1); empty square with a cross inside : 0.6689 mM Na_2H_2EDTA, 0.6616 mM Pb^{2+} and 1.333 mM Na_2H_2(*meso*-DMSA), (i.e. Pb:H_2EDTA:H_2(*meso*-DMSA)=1:1:2).

Table 3-2. Formation Constants of Lead Chelates of DMSA Stereoisomers at μ = 0.10 and T = 25.0°C [a].

	species			log β_{pqr} [b]	
	p	q	r		
Pb:EDTA:*rac*-DMSA	1	1	0	20.3[c]	
=1:1:1	1	1	1	26.2[c]	
	1	1	2	28.8[c]	
	1	2	0	26.2[c]	
	2	2	0	42.5[c]	
Pb:EDTA:*rac*-DMSA	1	1	2	28.8[d]	
=1:1:2	1	2	0	26.0[d]	
Pb:EDTA:*meso*-DMSA	1	1	0	18.2[e]	17.46(*116*) 17.4(*93*)
=1:1:1	1	1	1	24.7[c]	24.82(*78*)
	1	1	2	27.5[e]	
Pb:EDTA:*meso*-DMSA	1	1	1	24.9[f]	
=1:1:2	1	2	1	32.3[f]	

[a] L^{4-} represents the completely deprotonated DMSA in the titration of Pb:EDTA:DMSA systems.

[b] $\beta_{pqr} = [Pb_pL_qH_r^{-(4q-2p-r)}]/[Pb^{2+}]^p[L^{4-}]^q[H^+]^r$.

[c] The values were determined in our laboratory with a minimum $\sigma(pH)_{fit}$ of 0.008 (*72*).

[d] The values were determined in our laboratory with a minimum $\sigma(pH)_{fit}$ of 0.02 (*72*).

[e] The values were determined in our laboratory with a minimum $\sigma(pH)_{fit}$ of 0.009 (*72*).

[f] The values were determined in our laboratory with a minimum $\sigma(pH)_{fit}$ of 0.009 (*72*).

and 26.2, respectively. Since it was demonstrated from the IR titration results obtained with *rac*-DMSA at 0.02 M that the dimeric complex, Pb_2L_2, coexists with monomeric complex, PbL, it is reasonable to believe that some dimeric complexes may be present in the titration solution at a mM level. Therefore, the two dimeric complexes Pb_2L_2 and HPb_2L_2 were included in the above speciation model at this point, and the revised model was refined again by the BEST program. The resulting new model contained Pb_2L_2 with a log formation constant of 42.5, listed in Table 3-1, but not HPb_2L_2. The validity of the formation constants determined from potentiometric titrations can be confirmed, but not proved, by titrating solutions containing the metal and the ligand at varying metal:ligand ratios. If a self-consistent set of complex formation constants is obtained for the complexes that are present in common in the different statistically favorable models, the potentiometric titration method is valid. Therefore, another titration at the Pb:L ratio of 1:2 was performed, and the titration data were used to refine a statistically favorable model for the solution. The starting model contained PbL, HPbL, H_2PbL, PbL_2, $HPbL_2$ and H_2PbL_2, and the two dimeric complexes, Pb_2L_2 and HPb_2L_2; the resulting statistically favorable model consisted of only two lead *rac*-DMSA chelates, H_2PbL and PbL_2. The log formation constants of these two chelates determined are 28.8 and 25.9, respectively, which are in fair agreement with the respective values, 28.8 and 26.2, determined from

a solution containing a 1:1 ratio of Pb:L. The potentiometric titration points of the solutions containing lead, EDTA and *rac*-DMSA at Pb:EDTA:DMSA ratio 1:1:1 and 1:1:2 are plotted in Fig. 3-3, and the simulated titration curves by the BEST program are shown as solid lines.

Formation Constants of Lead Chelates of Meso-DMSA.

The formation constants of various lead chelates of *meso*-DMSA were determined in the same manner as those of *rac*-DMSA. The species PbL, HPbL, H_2PbL, PbL_2, $HPbL_2$, H_2PbL_2, Pb_2L_2 and HPb_2L_2 of *rac*-DMSA were included in the initial model. The protonation constants of *meso*-DMSA have been determined previously (*111*). Three complexes, i.e. PbL, HPbL and H_2PbL, were contained in the statistically favorable model obtained from the titration data of a 1:1:1 solution of Pb:EDTA:*meso*-DMSA of approximately 1.3 mM. Two complexes, i.e. HPbL and $HPbL_2$, were contained in the statistically favorable model obtained from the titration data of a 1:1:2 solution of Pb:EDTA:*meso*-DMSA of approximately 1.3 mM *meso*-DMSA. The formation constants of the above complexes determined from the BEST program are listed in Table 3-2. The complex HPbL was found in both models. The formation constant of HPbL determined in both models is in fair agreement, and the average value of the log of the formation constant is 24.80±0.14, which is in good agreement with the value 24.82±0.06 reported by Willes et al. (*78*), despite the variation in

temperature and ionic strength employed in their potentiometric competition titration experiments. The temperature and ionic strength employed in Willes' study were 37 °C and 0.15. The potentiometric titration points of the solutions containing lead, EDTA and *meso*-DMSA at Pb:EDTA:DMSA ratios 1:1:1 and 1:1:2 are plotted in Fig. 3-3, and the simulated titration curves by the BEST program are shown as solid lines.

Discussion

Rac-DMSA Is More Effective In Mobilizing Lead Than *Meso*-DMSA at Physiological pH.

Although a tremendous increase in the use of *meso*-DMSA has been reported in the U.S. for the treatment of lead poisoning since its approval by the FDA (*15*) in 1991, there is still a lack of information about the reaction of lead with the ligand. There are only three publications which report the formation constants of several lead-*meso*-DMSA complexes because the low solubility of the lead complexes has precluded their study. Egorova (*116*) calculated the formation constants of Pb_2L and PbL on the basis of the pH dependance of the UV spectrum of the ligand solution at 10^{-5} M. Willes et al. (*78*) determined the formation constants of HPbL and PbLOH by performing a potentiometric competition titration of a mixture of lead and EDTA with an alkaline ligand solution. The lead species generated from their titration data are not exactly same as those found in our statistically favorable models. This difference can be attributed to the manner in which the potentiometric titration was performed (*78*). Instead of titrating a mixture of lead, EDTA and *meso*-DMSA with a strong base solution, Willes et al. titrated a mixture of lead and EDTA with an alkaline *meso*-DMSA solution. Nevertheless, the formation constants of the lead species, HPbL, determined in both studies are in good agreement. More recently, Harris et al.

determined the formation constant of PbL spectrophotometrically by using a competitive reaction between *meso*-DMSA and *N*-(2-hydroxyethyl)-ethylenediamine-*N,N',N'*-triacetic acid (HEDTA) for lead ions to prevent the precipitation of the lead-*meso*-DMSA complex. The formation constant of PbL determined in our laboratory is $10^{18.2}$, which is significantly larger than the value, $10^{17.4}$, determined by Harris et al. or the value, $10^{17.46}$, determined by Egorova et al. The difference between the reported values and the values determined by us, of the formation constant of PbL, are attributed to the inclusion of PbL_2 in our calculations. In both of the previous spectrophotometric studies, the presence and the contribution of PbL_2 in the mass balance equations, which were developed for calculation of the formation constant of PbL, were ignored. The assumption, by Harris, for the absence of PbL_2 even in the presence of excess of ligand was based on the observation that in a titration of lead ion with ligand, the absorbance of the solution did not increase significantly after 1 equivalent of ligand was added. There was no evidence, however, to show that the electronic spectrum of PbL_2, if it was indeed formed in the solution, was markedly different from that of PbL at the wavelength at which the measurements were performed. In contrast, in our titration of a solution of 1:1:2 Pb:EDTA:*meso*-DMSA, 14% of the lead was found to form $HPbL_2$ with *meso*-DMSA as the ligand.

There is no information about the formation constants of the lead chelates of *rac*-DMSA in the literature. Therefore, no literature comparison can be made with the formation constants of the lead chelates of *rac*-DMSA determined in our laboratory. The efficacy of *rac*- over *meso*-DMSA in mobilizing lead ions has been evaluated by calculation of lead distribution among various chelates as a function of pH in the presence of both DMSA stereoisomers with the aid of the computer program SPE (*72*). It was assumed in the calculation that only the lead chelates of *rac*- and *meso*-DMSA listed in Table 3-2 are present. The distributions of lead were calculated at various total concentrations of lead ranging from 45.5 μg/dL (2.2 μM) to 8.3 μg/dL (0.4 μM) and at various concentrations of ligand ranging up to 1.0 mM to mimic the conditions of lead poisoning and *in vivo* treatment with DMSA. The distribution curves, calculated for solutions containing 45.5 μg/dL lead, of various lead species which contribute more than 0.1% of the total lead in the pH region 4.5 to 9.0 are plotted in Fig. 3-4. It is shown in Fig. 3-4 (a) that lead is completely complexed, with 50% of the lead being complexed by *rac*-DMSA and the other 50% by its *meso* isomer, at pH 7.4, when one equivalent of the DMSA ligands is present. The lead chelates formed in this solution are PbL and HPbL of both stereoisomers of DMSA, and the contribution of HPbL complexes is relatively small. When the concentration of ligands is elevated, there are no new lead chelates formed at pH 7.4 but the lead distribution

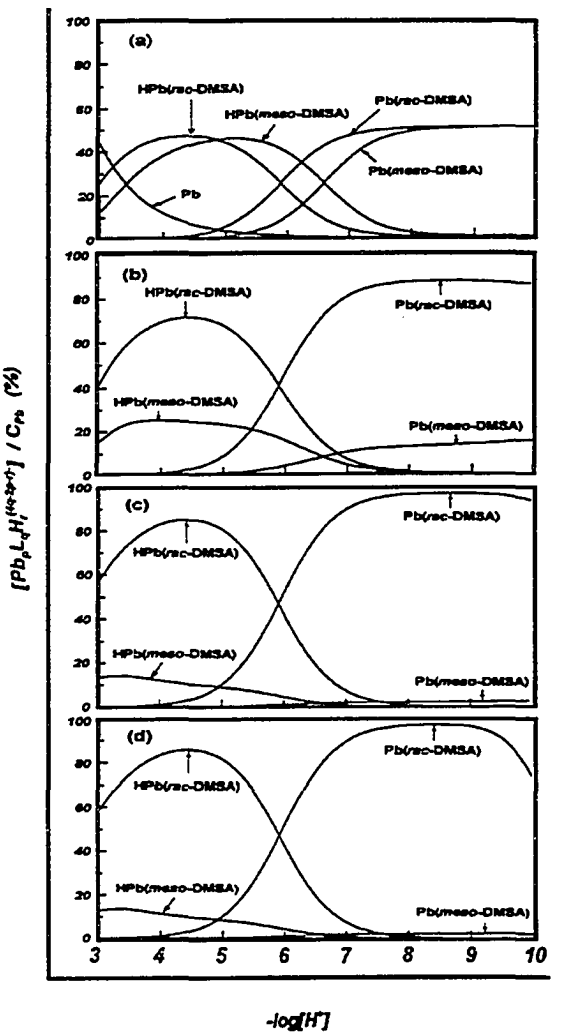

Figure 3-4. Distribution of lead chelates in solutions containing lead 2.2 μM and *rac*-DMSA and *meso*-DMSA (a) 1.1 μM each, (b) 2.2 μM each, (c) 25 μM each, (d) 250 μM each. The lead species plotted are only those which contribute to the total amount of lead by more than 0.001% in the vicinity of pH 7.4.

pattern undergoes a gradual change, shown in Fig. 3-4 (b)-(d), with the concentration of PbL of *meso*-DMSA being lowered while the concentration of PbL of *rac*-DMSA is increased.

The RPMI (*111*) values of *rac*-DMSA for lead ions over *meso*-DMSA at pH 7.4 were calculated for the solutions containing lead and both stereoisomers of DMSA by using the concentrations of the lead chelates obtained with the aid of the SPE program (*72*). The results are plotted in Fig. 3-5. The curves of RPMI vs log of the ratio of concentration of ligands to lead are superimposable on each other, indicating the independence of the value of RPMI on the absolute concentration of lead in solution. The RPMI value increases rapidly at the ratio of concentration of the ligands to lead below 10 and reaches a plateau at about 45. 40 to 45 times more lead will be complexed with *rac*- than with *meso*-DMSA under exactly the same conditions if the total molar concentration of the ligand surpasses the lead concentration, i.e. 2.2 μM, by a factor of 10 or more in solution, i.e. 22 μM. This level of ligand can be safely achieved in the blood in the treatment of lead poisoning. Therefore, on the basis of our calculation it is clear that *rac*-DMSA alone is superior to *meso*-DMSA in mobilizing lead ions if thermodynamic equilibrium has been attained.

There is another interesting feature in Fig. 3-4 (a) which is worthwhile discussing. It is reasonable to assume, from the experimental evidence provided,

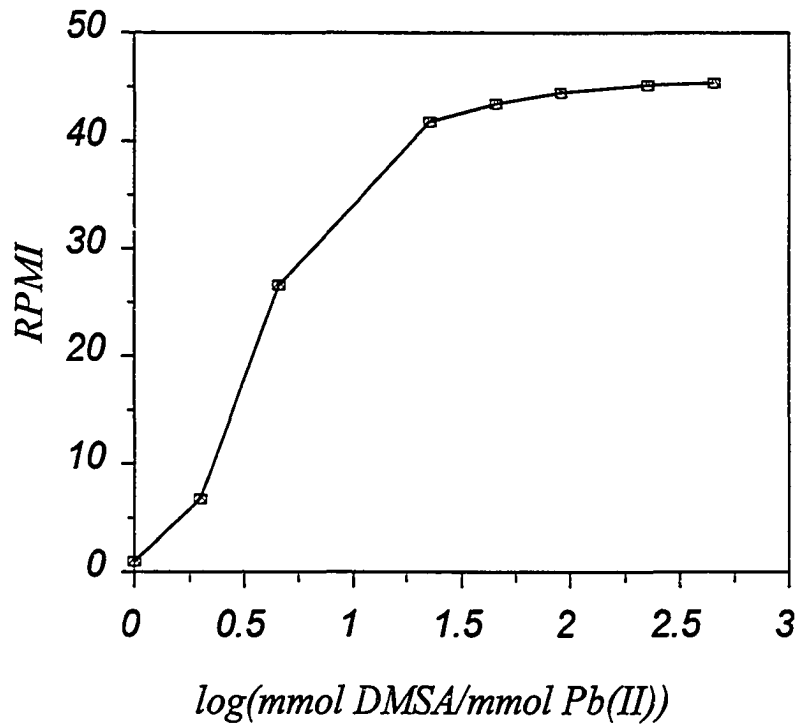

Figure 3-5. Relative plasma mobilizing index (RPMI) of *rac*-DMSA over *meso*-DMSA for lead(II) versus log of molar ratio of ligands to lead(II) at lead(II) concentrations of 2.2 μM (□), 1.2 μM (○), and 0.4 μM (△). Note: The total concentrations of *rac*-DMSA are always equal to the total concentration of *meso*-DMSA, being a half of the total concentration of the ligands used.

that lead is mobilized by DMSA *in vivo* in the form of PbL and HPbL. When these lead chelates are transported in the absence of excess ligand (this may happen shortly after a sudden cesation of chelation therapy with high dose administrations), they will reestablish equilibria with the surroundings; this situation can be reasonably described by Fig. 3-4 (a). At pH between 5 and 6, which corresponds to the pH range in urine, a few percent of the complexed lead will be released into solution in the form of lead ion, shown by the lead(II) distribution curve in Fig. 3-4 (a), which may accumulate in the kidney during the urinary excretion of lead and cause severe damage to the kidney. This demonstrates a possible mechanism that account for the adverse effects of chelation therapy which may result from the redistribution of toxic metals by chelating agents among various tissues and organs in which the pH is very different. This observation suggests that the use of an appropriate chelating agent under inappropriate solution conditions may also result in adverse effects. The dissociation of lead chelates in the kidney can be prevented, when DMSA is used therapeutically, if high dose treatments are followed by a very small dose of DMSA for a short period to ensure that the *in vivo* concentration of the lead chelate has been lowered to a negligible level.

The results of the analysis of lead chelate distributions are summarized below: (1) the stoichiometry of lead chelates formed at pH 7.4 is independent of

the stereoisomers of DMSA; (2) only two types of chelates, PbL and HPbL, are formed at pH 7.4, with the majority of lead being bound as PbL; (3) formation of PbL and HPbL at pH 7.4 is independent of the total concentrations of lead and ligand, and so is the concentration ratio of PbL and HPbL; (4) lead is completely chelated at pH 7.4 when the total concentration of ligand is equal to or greater than the total concentration of lead present; (5) lead tends to bind to a greater extent with *rac*-DMSA than with *meso*-DMSA, and the relative extent increases with an increase in the ratio of concentration of ligand to lead and finally reaches a constant of 45.

ZnL_2 of *Rac*-DMSA Is a Better Lead Chelator for Therapeutical Use.

Increased urinary excretion, approximately by 2-fold, of zinc by *rac*-DMSA was reported (*57,62*) when identical doses of *meso*- and *rac*-DMSA were administered to rats. Analysis of the distribution model of zinc indicates that much more than a 2-fold amount of zinc will be mobilized by *rac*-DMSA than by its *meso* isomer (*111*). To overcome the loss of endogenous zinc in chelation therapy, ZnL_2 of *rac*-DMSA can be used in the treatment of lead poisoning instead of *rac*-DMSA alone. The suggestion was made by Fang et al. (*111*) on the basis of the analysis of a hypothetical solution containing equimolar (0.25 mM) amounts of *rac*-DMSA, *meso*-DMSA, zinc ion and lead ion. The analysis was performed by assuming that only the PbL complexes of the DMSA stereoisomers

were formed in the solution. There are some concerns about the validity of extending the conclusion made in our previous study (*111*) to an *in vivo* system, because (1) 0.25 mM (5.2 mg/dL) of lead is too high in comparison with the lead burden in the human blood; (2) the species, HPbL, of DMSA is not included in the previous analysis; (3) zinc will react with *meso*-DMSA also, and therefore, the results obtained from the previous study are more appropriate for a comparison of the zinc chelates of two DMSA stereoisomers rather than a comparison of the species, ZnL_2, of *rac*- and *meso*-DMSA, for their efficacy in mobilizing lead. Therefore, the capability of ZnL_2 of *rac*-DMSA in mobilizing lead ion was reassessed with all the concerns raised above. The capability of a chelating agent in mobilizing lead ion is represented by the absolute concentration of lead present in solution after the same number of moles of chelating agent, (i.e. either ZnL_2 of *rac*- or *meso*-DMSA alone), is added. The total concentration of lead used in the calculations was kept constant at 2.2 μM; the total concentrations of ligand were 2.2, 10, 100 and 500 μM, respectively, if ZnL_2 of rac-DMSA was added, or 4.4, 20, 200 and 1000 μM, respectively, if *meso*-DMSA was added. The calculations were performed with the aid of the SPE program (*72*). The calculated results are listed in Table 3-3. It is clearly shown in Table 3-3 that a small amount, μg/dL to sub-μg/dL, of free zinc ion is always maintained in the solution by the chelating agent itself if ZnL_2 of *rac*-DMSA is used, and this low level of

Table 3-3. Equilibrium Concentrations of Lead(II) and Zinc(II) in Solutions Containing 2.2 μM Lead(II) and ZnL_2 of *Rac*- or *Meso*-DMSA at pH 7.4, Ionic Strength 0.10 and T = 25.0 °C.

Total Concentration(μM)				
ZnL_2	*meso*-DMSA	$[Pb^{2+}](x10^{-14}M)$		$[Zn^{2+}](\mu g/dL)$
2.2	4.4	180[a]	306[b]	2.5
10	20	12[a]	38[b]	0.3
100	200	1.7[a]	3.4[b]	0.07
500	1000	0.5[a]	0.7[b]	0.03

a. The values were determined from solutions containing ZnL_2 of *rac*-DMSA.

b. The values were determined from solutions containing *meso*-DMSA alone.

free zinc ions will depress the competition of *rac*-DMSA for endogenous zinc with zinc-integrated proteins, and therefore, presumably overcome the problem associated with an increase in the loss of endogenous zinc. It is predictable that the endogenous zinc will be depleted by ZnL_2 of *rac*-DMSA to a lower extent than by *meso*-DMSA alone.

ZnL_2 of *rac*-DMSA is also superior to *meso*-DMSA in reducing the concentration of free lead ion in solution at all the ligand concentration levels chosen, but as shown in Table 3-3 the superiority of ZnL_2 of *rac*-DMSA is marginal. In addition to the concern about the depletion of endogenous zinc, the main advantage of the proposed use of ZnL_2 of *rac*-DMSA over the current use of *meso*-DMSA in clinical practice does not rely on the consideration of its lead mobilizing capability but on its high solubility, which facilitates gastrointestinal absorption of the drug after oral administration. At pH 2 to 3, which corresponds to the pH range in the stomach, ZnL_2 of *rac*-DMSA at a concentration of 0.1 M remains in solution, forming mainly $H_2Zn_2L_2^{2-}$, H_3L^- and H_4L (*117*). About 20-25% of the ligand exists in the form of neutral H_4L which is highly lipophilic, and therefore will enhance transportation of the ligand through a biomembrane. In conclusion, we predict that ZnL_2 of *rac*-DMSA is a safe and more effective chelator than *meso*-DMSA for the clinical treatment of lead poisoning.

The Lead Chelates of *Rac*-DMSA Are More Stable Than the Corresponding Chelates of *Meso*-DMSA in Aqueous Solution

The structures of PbL of the stereoisomers of DMSA in the solid state have been studied by Rivera et al. (*50*). Two forms of PbL of *rac*-DMSA were identified by IR spectroscopy. In one of them the ligand was found to bind to a lead ion via one sulfur atom and one oxygen atom, whereas in the other form the ligand uses two sulfur atoms to bind to a lead ion. Only one form of PbL of *meso*-DMSA, in which the ligand was bound to lead via one sulfur atom and one oxygen atom, was found by Rivera et al. There is no report on the structures of lead chelates of DMSA formed in solution. We postulate in this chapter that in PbL and PbL_2 of *rac*-DMSA the ligand uses two thiolate groups and one carboxylate group to bind with lead ions. The absence of free thiolate groups in both chelates is deduced from the log values of their protonation constants, 5.9 for PbL and 2.8 for PbL_2; the participation of one carboxylate group in the coordination of Pb^{2+} is deduced from our IR evidence obtained with solutions containing the ligand and lead ion at varying ratios. In PbL_2 of *meso*-DMSA the ligand uses one carboxylate group to bind to lead ion, but the manner in which the thiolate groups of the ligand are involved in the coordination is still not clear because of the lack of knowledge of the protonation constant of PbL_2 of *meso*-DMSA. The log protonation constant of PbL of *meso*-DMSA is 6.6, which

implies that both thiolate groups in the chelate are bound to lead ion. The IR evidence suggests that at least one of the two carboxylate groups of the ligand has to bind to lead ion. It is unclear on the basis of our IR evidence if the second carboxylate group of the ligand participates in coordination or not. It is energetically unfavorable, however, to have both carboxylate groups as well as both thiolate groups of the *meso*-DMSA bind with a lead ion in the PbL complex. The energetically favorable structures proposed for PbL and PbL_2 of the stereoisomers of DMSA in solution are illustrated in (Fig. 3-6). With the aid of a molecular model, it is found that in both of the lead chelates of *rac*-DMSA in aqueous solution, the ligand adopts staggered anti-conformations (Fig. 3-6 (I) and (II)) with respect to the carboxylate groups, whereas in the lead chelates of *meso*-DMSA, the ligand adopts a staggered gauche-conformation (Fig. 3-6 (III)). The lead chelates of *rac*-DMSA in aqueous solution are more stable than the corresponding chelates of its *meso* isomer because the electrostatic repulsion between two bulky carboxylate groups are minimized in the staggered anti-conformations. This accounts for the larger formation constants of lead chelates of *rac*-DMSA than those of the corresponding chelates of its *meso* isomer.

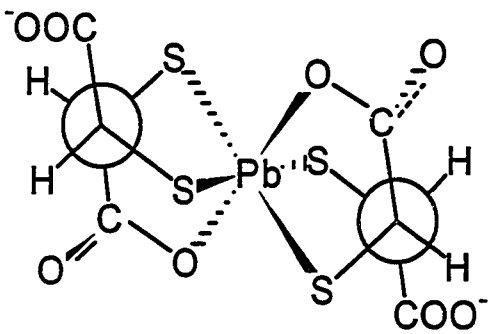

(I)

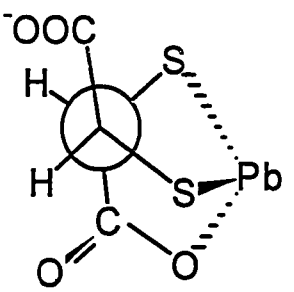

(II)

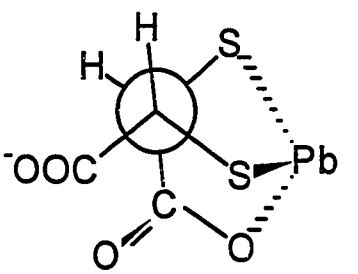

(III)

Figure 3-6. Energetically favorable structures of the lead chelates of: PbL_2 of *rac*-DMSA (I), PbL of *rac*-DMSA (II), and PbL of *meso*-DMSA (III).

CONCLUSIONS AND FUTURE RESEARCH

There is a rapid increase in the use of *meso*-DMSA in the U.S. for the treatment of childhood lead poisoning over traditional chelation therapy with chelating agents such as EDTA. The ultimate limitation is the low solubility of *meso*-DMSA which retards its absorption after oral administration. In addition, *meso*-DMSA was found to remove lead only from the extracellular fluid of plasma. Alkyl esters of *meso*-DMSA were invariably found in animal studies to remove more lead from soft tissues such as kidney and brain than *meso*-DMSA. This potential advantage, however, of using the alkyl esters of *meso*-DMSA is offset by their increase in toxicity.

Rac-DMSA was found in our studies to exhibit high solubilities in both aqueous solution and non-aqueous solvents such as ethyl ether. On the basis of the unique properties of *rac*-DMSA, its hydrophilicity and lipophilicity, we have proposed that *rac*-DMSA will be absorbed more readily than its *meso* isomer after oral administration, and it can be potentially a more effective intracellular chelator than *meso*-DMSA for the treatment of lead poisoning. In vitro studies with lead and the stereoisomers of DMSA support our proposal, from a thermodynamic perspective. *Rac*-DMSA exhibits a higher lead-mobilizing capability than *meso*-DMSA at physiological pH. The difference in the mobilization of lead by the two stereoisomers of DMSA arises, at molecular level, exclusively from the

differences in the structures of their lead chelates in solution. In all the lead chelates of the stereoisomers of DMSA formed in solution, *rac*-DMSA was found to exist in a staggered anti-conformation, with respect to the two carboxylate groups. The electrostatic repulsion and the steric hindrance between the two bulky carboxylate groups of the ligand are minimized in the staggered anti-conformation. On the other hand, *meso*-DMSA adopts staggered gauche-conformations in its lead chelates.

The potential shortcoming in the use of *rac*-DMSA as a clinical chelator is that it caused an elevated loss of endogenous zinc in animal studies. The increase in excretion of zinc by *rac*-DMSA was rationalized in our studies by comparing the zinc-mobilizing capabilities of both stereoisomers of DMSA at pH 7.4. The higher zinc-mobilizing ability of *rac*-DMSA was attributed, at a molecular level, to the differences in the structures of the zinc chelates formed in solution by both stereoisomers. *Rac*-DMSA adopts a staggered anti-conformation, with respect to the two carboxylate groups of the ligand, in its zinc chelates, whereas *meso*-DMSA adopts a staggered gauche-conformation in its zinc chelates.

The use of the ZnL_2 chelate of *rac*-DMSA, instead of the ligand alone, in clinical practice has been proposed to prevent the potential enhancement of zinc excretion by *rac*-DMSA. It was concluded on the basis of our studies that ZnL_2 of *rac*-DMSA is a safe and more effective chelator than *meso*-DMSA in the

clinical treatment of lead poisoning. ZnL_2 of *rac*-DMSA is found to mobilize lead ions to a greater extent than *meso*-DMSA alone at pH 7.4. In addition, a small amount of free zinc ions, which depresses the uptake of endogenous zinc from the zinc-integrated proteins by *rac*-DMSA, is always maintained by the presence of the zinc chelate in solution.

The investigation of *rac*-DMSA is still in its infancy compared with *meso*-DMSA; it has never been studied with either human subjects or animals for its efficacy in the treatment of lead poisoning. A comparison of the efficacy in the excretion of lead by both stereoisomers of DMSA in animals is of very high priority in future studies. As a result of our studies, it was deduced that *rac*-DMSA is an effective intracellular chelator under certain conditions. The removal of lead from critical organs and tissues, such as the brain, after administration of *rac*-DMSA is also important to investigate.

The *in vivo* studies with *rac*-DMSA which indicated its superiority in enhancing excretion of metals in urine were conducted after mercury and cadmium administration in acute doses. There is no report, however, on the formation constants, distribution as a function of pH and structures of the chelates of mercury and cadmium formed in aqueous solution with *rac*-DMSA. Cadmium, unlike other toxic metals, is excreted very slowly from the body because the cadmium which accumulates in animals and in humans is bound intracellularly,

to metallothionein (*118*). *Meso*-DMSA is ineffective in mobilizing cadmium from metallothionein-bound intracellular sites of sequestration. At the present time there is no acceptable chelating agent for the treatment of cadmium poisoning. The chelating agent which can deplete cadmium from cells must be able to cross the cell membrane and compete with metallothionein for cadmium. *Rac*-DMSA may function as an extracellular as well as an intracellular chelator for cadmium. Therefore, studies of the interaction of both DMSA stereoisomers with mercury and cadmium in solution are also of great importance.

Attempts have been made to increase the lipophilicity of *meso*-DMSA by esterification of the carboxylic acid groups in the ligands. The resulting esterified chelating agents have been shown to remove intracellular deposits of lead. A similar strategy may by applied with *rac*-DMSA. The syntheses of the esters of *rac*-DMSA and their complexing properties with metals, such as zinc, lead, cadmium and mercury, are also important to undertake.

APPENDIX A.

Crystal parameters, experimental details and structure solution and refinement (Table I) for *rac*-BATSA, crystal parameters, experimental details and structure solution and refinement (Table II) for *rac*-DMSA, final positional and isotropic thermal parameters (Table III) for *rac*-BATSA, final positional and isotropic thermal parameters (Table IV) for *rac*-DMSA, and a stereoview of the monoclinic unit cell of *rac*-BATSA (Fig. I).

Table I. Experimental Details of X-Ray structure of *rac*-BATSA.

A. Crystal Data

Formula	$S_2O_6C_8H_{10}$
F.W. 266.29	F(000) = 552
crystal dimensions	0.33x 0.25x 0.37 mm
peak width at half-height:	0.25°
Mo Kα radiation	λ = 0.70930 Å
temperature	23 ± 1°
monoclinic space group	$P2_1/n$

a = 11.404 (3) Å b = 7.531 (2) Å c = 13.335 (3) Å
β = 93.37 (2)°
V = 1143.3 Å^3
Z = 4 ρ = 1.55 g/cm^3
μ = 4.5 cm^{-1}

B. Intensity Measurements

Instrument:	Enraf-Nonius CAD4 diffractometer
Monochromator:	Graphite crystal, incident beam
Scan type:	ω-θ
Scan rate:	3-20°/min
Scan width, deg:	scan width = 0.6 + 0.340 tanθ
Maximum 2θ:	50.0°
No. of refl. measured:	2313 total, 1999 unique
Corrections:	Lorentz-polarization
	Reflection averaging
	(agreement on I = 1.3%)

C. Structure Solution and Refinement

Solution:	Direct methods
Hydrogen atoms:	Refined with Biso = 5.0Å^2
Refinement:	Full-matrix least-squares
Minimization function:	$\Sigma w(\|Fo\|-\|Fc\|)^2$
Least-squares weights:	$4Fo^2/\Sigma^2(Fo^2)$
Anomalous dispersion:	All non-hydrogen atoms
Reflections included:	1786 with $Fo^2>3.0\sigma(Fo^2)$
Parameters refined:	175
Unweighted agreement factor:	0.028
Weighted agreement factor:	0.046
Esd of obs. of unit weight:	1.90
Convergence, largest shift:	0.05σ
High peak in final diff. map:	0.34 (4) e$^-$/Å^3
Low peak in final diff. map:	-0.21 (0) e$^-$/Å^3
Computer hardware:	VAX
Computer software:	SDP/VAX (Enraf-Nonius)

Table II. Experimental Details of X-ray structure of *rac*-DMSA.

A. Crystal Data

Formula:	$S_2O_4C_4H_6$
F.W. : 182.22	F(000) = 752
crystal dimensions:	0.60x 0.30x 0.13 mm
peak width at half-height:	0.36°
Mo Kα radiation:	λ = 0.71073 Å
temperature:	20 ± 1°
monoclinic space group	C2/c

a = 23.906 (4) Å b = 6.262 (1) Å c = 10.162 (2) Å

β = 103.21 (24)°

V = 1481.0 Å^3

Z = 8 ρ = 1.63 g/cm^3

μ = 6.4 cm^{-1}

B. Intensity Measurements

Instrument:	Syntex-Nicolet $P2_1$ diffractometer, with Crystal Logics control system
Monochromator:	Graphite crystal, incident beam
Scan type:	θ-2θ
Scan rate:	3°/min
Scan width, deg:	$(2\theta K\alpha_2+1.6)-(2\theta K\alpha_1+1.3)$
Maximum 2θ:	50.0°
No. of refl. measured:	1470 total, 1297 unique
Corrections:	Lorentz-polarization Reflection averaging (agreement on I = 1.0%)

C. Structure Solution and Refinement

Solution:	Direct methods
Hydrogen atoms:	Refined with Biso = 5.0Å^2
Refinement:	Full-matrix least-squares
Minimization function:	$\Sigma w(\|Fo\|-\|Fc\|)^2$
Least-squares weights:	$4Fo^2/\Sigma^2(Fo^2)$
Anomalous dispersion:	All non-hydrogen atoms
Reflections included:	937 with $Fo^2>3.0\sigma(Fo^2)$
Parameters refined:	109
Unweighted agreement factor:	0.043
Weighted agreement factor:	0.059
Esd of obs. of unit weight:	1.56
Convergence, largest shift:	0.14σ
High peak in final diff. map:	0.13 (3) e$^-$/Å^3
Low peak in final diff. map:	-0.12 (3) e$^-$/Å^3
Computer hardware:	VAX
Computer software:	SDP/VAX (Enraf-Nonius)

Table III. Positional Parameters and Their Estimated Standard Deviations of X-Ray Structure of *Rac*-BATSA.

Atom	x	y	z	B(A2)
S1	0.97787(4)	0.13373(6)	0.75053(3)	2.721(8)
S2	0.69725(4)	0.07343(6)	0.68127(3)	2.897(8)
O1A	0.9940(1)	0.4485(2)	0.6161(1)	3.35(3)
O1B	0.8092(1)	0.4063(2)	0.5596(1)	3.44(2)
O4A	0.7503(1)	-0.2502(2)	0.5611(1)	3.57(3)
O4B	0.9420(1)	-0.2083(1)	0.59495(9)	3.01(2)
O5	1.1655(1)	0.0756(2)	0.6487(1)	5.00(3)
O6	0.5909(1)	0.1571(2)	0.5064(1)	4.11(3)
C1	0.9006(1)	0.3501(2)	0.5962(1)	2.41(3)
C2	0.9209(1)	0.1554(2)	0.6209(1)	2.20(3)
C3	0.8126(1)	0.0434(2)	0.5950(1)	2.25(3)
C4	0.8422(1)	-0.1524(2)	0.5843(1)	2.44(3)
C5	1.1285(2)	0.0927(3)	0.7307(2)	3.35(4)
C6	1.2033(2)	0.0835(3)	0.8268(2)	4.95(5)
C7	0.5786(2)	0.1373(2)	0.5946(1)	3.01(3)
C8	0.4657(2)	0.1568(3)	0.6453(2)	4.39(4)

Anisotropically refined atoms are given in the form of the isotropic equivalent displacement parameter defined as: (4/3) * [a2*B(1,1) + b2*B(2,2) + c2*B(3,3) + ab(cos gamma)*B(1,2) + ac(cos beta)*B(1,3) + bc(cos alpha)*B(2,3)].

Table IV. Positional Parameters and Their Estimated Standard Deviations of X-RAY Structure of *Rac*-DMSA.

Atom	x	y	z	B(A2)
----	-	-	-	-----
S1	0.44108(4)	0.0753(2)	0.5923(1)	5.70(3)
S2	0.43695(4)	0.4480(2)	0.3410(1)	6.55(3)
O1A	0.31613(9)	0.1409(4)	0.6467(2)	3.54(5)
O1B	0.29602(9)	0.0170(4)	0.4342(2)	3.56(5)
O4B	0.29284(9)	0.4832(4)	0.3537(2)	3.45(5)
O4A	0.30970(9)	0.3491(4)	0.1624(2)	3.49(5)
C1	0.3257(1)	0.1170(5)	0.5247(3)	2.61(6)
C2	0.3797(1)	0.2330(6)	0.5117(3)	3.09(7)
C3	0.3781(1)	0.2784(6)	0.3621(3)	3.23(7)
C4	0.3222(1)	0.3821(5)	0.2927(3)	2.67(6)

Anisotropically refined atoms are given in the form of the isotropic equivalent displacement parameter defined as:(4/3) * [a2*B(1,1) + b2*B(2,2) + c2*B(3,3) + ab(cos gamma)*B(1,2) + ac(cos beta)*B(1,3) + bc(cos alpha)*B(2,3)].

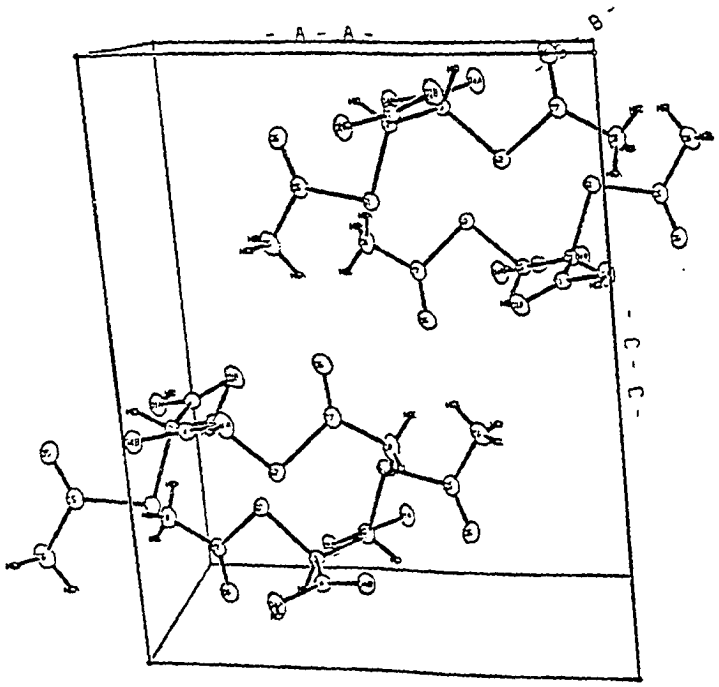

Figure I. Molecular packing in the unit cell of *rac*-2,3-bis-(acetylthio)succinic acid (*rac*-BATSA).

REFERENCES

1. Stockton L. A. and Thompson, R. H. S. (1946) British Anti-Lewisite. 2. Dithiol compounds as antidotes for arsenic. ***Biochem. J.*** **40**:535-548

2. Longcope, W. T., Luetscher, J. A., Wintrobe, M. M. and Juger, V. (1946) The treatment of arsenical dermatitis with preparations of BAL. ***J. Clin. Invest.*** **25**:528-533

3. Woody, N. C. and Kometani, J. T. (1948) BAL in the treatment of arsenic ingestion of children. ***Pediatrics*** **1**:372-378

4. Longcope, W. T. and Luetscher, J. A. (1949) The use of BAL (British Anti-Lewisite) in the treatment of the injurious effects of arsenic, mercury, and other metallic poisons. ***Ann. Intern. Med.*** **31**:545-553

5. Germuch, F. G. and Eagle, H (1948) The efficacy of BAL (2,3-dimercaptopropanol) in the treatment of experimental lead poisoning in rabbits. ***J. Pharm. Exp. Ther.*** **92**:397-410

6. Glotzer, D. E., Bauchner, H. (1992) Management of childhood lead poisoning. A survey. ***Pediatrics*** **89**:614-18

7. Hammond, P. B. (1971) The effects of chelating agents on the tissue distribution and excretion of lead. ***Toxicol. Appl. Pharmacol.*** **18**:296-310

8. Hammond, P. B., Aronson, A. L. and Olson, W. C. (1967) The mechanism of mobilization of lead by ethylendiaminetetraacetate. ***J. Pharmacol. Exp. Ther.*** **157**:196-206

9. Cory-Slechta, D. A., Weiss, B. and Cox, C. (1987) Mobilization and redistribution of lead over the course of calcium disodium ethylenediaminetetraacetate chelation therapy. ***J. Pharmacol. Exp. Ther.*** **243**:804-13

10. Araki, S., Aono, H. and Murata, K. (1986) Mobilization of heavy metals into the urine by $CaNa_2EDTA$: relation to erythrocyte and plasma concentrations and exposure indicators. ***Br. J. Ind. Med.*** **43**:636-41

11. Araki, S., Aono, H., Fukahori, M. and Tabuki, K. (1984) Behavior of lead and zinc in plasma erythrocytes, and urine and ALAD in erythrocytes following intravenous infusion of CaEDTA in lead workers. ***Arch. Environ. Health*** **39**:363-7

12. Chisolm, J. J. (1971) Treatment of lead poisoning. ***Med. Treat.*** **8**:593-611

13. Thomas, D. J. and Chisolm, J. J. (1986) Lead, zinc and copper decorporation during calcium disodium ethylenediaminetetraacetate treatment of lead poisoned children. ***J. Pharmacol. Exp. Ther.*** **239**:829-35

14. Chisolm, J. J. Jr. (1968) The use of chelating agents in the treatment of acute and chronic lead intoxication in childhood. ***J. Pediatr.*** **73**:1-38

15. FDA Medical Bulletin: Succimer Approved for Severe Lead Poisoning. Vol 21, Part 1, p. 5, March, 1991

16. Shannon, M., Graef, J. and Lovejoy, F. H. (1988) Efficacy and toxicity of D-penicillamine in low-level lead poisoning. ***J. Pediatr.*** **112**:799-804

17. Shannon, M., Grace, A. and Graef, J. W. (1989) Use of D-penicillamine in children with small lead burdens. (Letter). ***N. Engl. J. Med.*** **321**:979-80

18. Chisolm, J. J. (1992) BAL, EDTA, DMSA and DMPS in the treatment of lead poisoning in children. ***Clin. Toxicol.*** **30**:493-504

19. Aaseth, J. (1983) Recent advances in the therapy of metal poisonings with chelating agents. ***Hum. Toxicol.*** **2**:257-72

20. Cory-Sletchta D. A. (1988) Mobilization of lead over the course of DMSA chelation therapy and long-term efficacy. ***J. Pharmacol. Exp. Ther.*** **246**:84-91

21. Schwaetz, J., Angel, C., Pitcher, H. (1986) Relationship between childhood blood levels and stature. ***Pediatrics*** **77**: 281-88

22. Fulton, M., Raab, G., Thomson, G., Laxen, D., Hunter, R., and Hepburn, W. (1987) The influence of Blood Lead on the Ability and Attainment of Children in Edinburgh. ***Lancet*** **1**:1221-25

23. Hatsakis, A., Kokkevi, A., Katsouvanni, K., Maravelias, K., Salaminios, F. et al. (1987) Lead exposure and children's cognitive functions and behavior. In **Int. Conf. Heavy Metals in the Environment**, ed. S. E. Lindberg, T. C. Hutchinson, 1:204-9, Edinburgh, UK: CEP Consultants

24. Bergomi, M., Borella, P., Fantuzzi, G., Vivoli, G., Sturloni, N., et al. (1989) Relationship between lead exposure indicators and neuropsychological performance in children. ***Dev. Med. Child Neurol.*** **31**:181-90

25. Landsdown, R., Urbanowicz, M. A., Hunter, J. (1986) The relationship between blood-level concentrations, intelligence, attainment and behavior in a school populations: the second study. ***Int. Arch. Occup. Environ. Health*** **57**:225-35

26. Davis, J. M. and Svendsgaard, D. J. (1987) Lead and Child Development. ***Nature,*** **329:** 297-300.

27. Angle, C. R. (1993) Childhood Lead Poisoning and Its Treatment. ***Annu. Rev. Pharmacol. Toxicol.*** *32:* 409-434.

28. Agency for Toxic Substances and Diseases Registry, Public Health Service, US DHHS (1988) ***The Nature and Extent of Lead Poisoning in Children in the United States: A Report to Congress.*** Atlanta, GA.

29. USCDC. (1985) Preventing Lead Poisoning in Young Children (No. 99-2230) US DHHS Atlanta.

30. Center for Disease Control. 1991. Preventing Lead Poisoning in Young Children. A Statement by the Centers for Disease Control, October 1991. US Department of Health Human Service, Atlanta

31. Shannon, M. W. and Graef, J. W. (1992) Lead intoxication in infancy. ***Pediatrics*** **89**:87-90

32. Kostygov, N. M. (1958) The antidotal action of mercaptosuccinic acid and Unithiol against mercury. ***Farmakologiia i Toksikologiia*** **21**:64-69

33. Ting, K. S., Liang, Y. I., Shi, J., Chen, W. and Gu, T. et al. (1965) Chelate stability of sodium dimercaptosuccinate on the intoxication from many metals. ***Chinese Medical Journal*** **51**:304-7

34. Wang, S. C., Ting, K. S. and Wu, C. C. (1965) Chelating therapy with Na-DMS in occupational lead and mercury intoxications. ***Chinese Medical Journal*** **84**:437-39

35. Friedheim, E., Graziano, J. H., Popovac, D., Dragovic, D. and Kaul, B. (1978) Treatment of lead poisoning by 2,3-dimercaptosuccinic acid (DMSA). ***Lancet*** **2**:1234-36

36. Graziano, J. H., Lolacono, N. J. and Meyer, P. (1988) Dose-response study of oral 2,3-dimercaptosuccinic acid in children with elevated blood lead concentrations ***J. Pediatr.*** **113**:751-7

37. Bentur, Y., Brook, J. G., Behar, R. and Taitelman, U. (1987) Meso-2,3-dimercaptosuccinic acid (DMSA) in the diagnosis and treatment of lead poisoning. ***Clin. Toxicol.*** **25**:39-51

38. Fournier, L., Thomas, G., Garnier, R., Buisine, A., Houze, P., Pradier, S. and Dally, S. (1988) 2,3-Dimercaptosuccinic acid treatment of heavy metal poisoning in humans. ***Med. Toxicol.*** **3**:499-504

39. Kuntzelman, D. R., England, K. E. and Angle, C. R. (1990) Urine lead (UPb) in outpatient treatment of lead poisoning with dimercaptosuccinic acid (DMSA). ***Vet. Hum. Toxicol.*** **4**:364 (Abstr.)

40. Montalvan, J., Okose, P. and Marcus, S. (1990) Outpatient chelation therapy of 24 patients with lead intoxication by dimercaptosuccinic acid. ***Vet. Hum. Toxicol.*** **4**:343 (Abstr.)

41. Grandjean, P., Jacobsen, I. A. and Jorgensen, P. J. (1991) Chronic lead poisoning treated with dimercaptosuccinic acid. ***Pharmacol. Toxicol.*** **68**:266-69

42. Mann, K. V. and Travers, J. D. (1991) Succimer, an oral lead chelator. ***Clin. Pharm.*** **10**:914-22

43. Deborah, E. G. (1993) The current role of 2,3-dimercaptosuccinic acid (DMSA) in the management of childhood lead poisoning. ***Drug Safety*** **9**:85-92

44. Aposhian, H. V., and Aposhian, M. M. (1990) Meso-2,3-dimercaptosuccinic acid: chemical, pharmacological and toxicological properties of an orally effective metal chelating agent. ***Annu. Rev. Pharmacol. Toxicol.*** **30**:279-306

45. Ding, G.-S. and Liang, Y.-Y. (1991) Antidotal effects of dimercaptosuccinic acid. ***J. Appl. Toxicol.*** **11**:7-14

46. Jones, M. M. (1991) New developments in therapeutic chelating agents as antidotes for metal poisoning. ***Crit. Res. Toxicol.*** **21**:209-233

47. Angle, C. R. (1993) Childhood lead poisoning and its treatment. ***Annu. Rev. Pharmacol. Toxicol.*** **32**:409-434

48. Matsuda, Y., (1968) Experimental study on sodium dimercaptosuccinic acid. ***Gifu. Daigacu. Igakubu. Kiyo.*** **1**:869-88

49. Harris, W. R., Chen, Y., Stenback, J. and Shah, B. (1991) Stability constants for dimercaptosuccinic acid with bismuth(III), zinc(II), and lead(II). ***J. Coord. Chem.*** **23**:173-86

50. Rivera. M, Aposhian, H. V. and Fernando, Q. (1989) Lead chelates of meso- and racemic-dimercaptosuccinic acid. ***J. Inorg. Biochem.*** **37**:283-93

51. Rivera-Laos, M. (1991) Complexing properties of 2,3-dimercaptosuccinic acid and its monomethyl and dimethyl esters. Ph.D. Dissertation, The University of Arizona

52. Maiorino, R. M., Akins, J. M., Blaha, K., Castes, D. E. and Aposhian, H. V. (1990) Determination and metabolism of dithiol-chelating agents: X. In humans, meso-2,3-dimercaptosuccinic acid is bound to plasma protein via mixed disulfide formation. ***J. Pharmacol. Exp. Ther.*** **254**:570-577

53. Aposhian, H. V, Maiorino, R. M., Dart, R. C. and Perry, D. F. (1989) Urinary excretion of meso-2,3-dimercaptosuccinic acid in human subjects. ***Clin. Pharmacol. Ther.*** **45**:520-526

54. Dart, R. C., Hurlbut, K. M., Maiorino, R. M., Mayersohn, M. Aposhian, H. V. and Hassen, L. V. B. (1994) Pharmacokinetics of meso-2,3-dimercaptosuccinic acid in patient with lead poisoning and in healthy adults. ***J. Pediatr.*** **125**:309-316

55. Fang, X. and Fernando, Q. (1994) Synthesis, structure, and properties of *rac*-2,3-dimercaptosuccinic acid, a potentially useful chelating agent for toxic metals. ***Chem. Res. Toxicol.*** **7**:148-56

56. Okonishnikova, I. E. (1970) The comparative antidote potency of stereoisomeric dimercaptosuccinic acids in mercury poisoning. ***Gig. Tr. Prof. Zabol.*** **14**:18-22

57. Okonishnikova, I. E. (1971) The effect of steric isomers of dimercaptosuccinic acid on the elimination of some heavy metals from body. ***Gig. Tr. Prof. Zabol.*** **15**:50-52

58. Aposhian, H. V., Hsu, C.-A. and Hoover, T. D. (1983) DL- and meso-dimercaptosuccinic acid: *in vitro* and *in vivo* studies with sodium arsenite. ***Toxicol. Appl. Pharmacol.*** **69**:206-13

59. Egorova, L. G. and Nirenburg, V. L. (1980) The study of complexing properties of dimercaptocarboxylic acids IV. Complexing of cadmium ions with dl- and meso-dimercaptosuccinic, dl-dimercaptoglutaric and meso-dimercaptoadipic acids. ***Zh. Obsch. Khim.*** **50(2)**:426-30

60. Egorova, L. G., Nirenburg, V. L. (1973) Complexing properties of dimercaptocarboxylic acids. III. Complexing of lead(II) with d,l-dimercaptosuccinic acid and d,l-dimercaptoglutaric acid", ***Zh. Obsch. Khim.*** **43**:1548-52.

61. Egorova, L. G., Okonishnikova, I. E., Nirenburg, V. L. and Postovskii, I. Y. (1971) Comparative study of the interaction of spatial isomers of dimercaptosuccinic acid with some metals. ***Khim. Farmat. Zhur.*** **5**:26-30

62. Egorova, L. G., Okonishnikova, I. E., Nirenburg, V. L. and Postovskii, I. Y. (1972) Complex formation of certain metals with dimercaptosuccinic acid stereoisomer. ***Khim. Farmat. Zhur.*** **6**:14-16

63. Gerecke, M., Friedheim, E. A. H., and Brossi, A. (1961) Zur Kenntnis der 2,3-Dimercapto Dernsteinsäuren. ***Helv. Chim. Acta.*** **44**:955-960.

64. CAD4 Operations Manual, Enraf-Nonius, Delft, Holland, 1977.

65. Cromer, D. T., and Waber, J. T. (1974) ***International Tables for X-Ray Crystallography***, **Vol. IV,** Table 2.2B, The Kynoch Press, Birmingham, England.

66. Ibers, J. A., and Hamilton, W. C. (1964) Dispersion Corrections and Crystal Structure Refinements. ***Acta Crystallogr.*** **17:**781.

67. Cromer, D. T. (1974) ***International Tables for X-Ray Crystallography"***, **Vol. IV,** Table 2.3.1, The Kynoch, Press, Birmingham, England.

68. Frenz, B. A. (1978) The Enraf-Nonius CAD 4 SDP - A Real-time System for Concurrent X-Ray Data Collection and Crystal Structure Determination. In ***Computing in Crystallography*** (Schenk, H., Olthof-Hazelkamp, R., Vankonigsveld, H., and Bassi, G. C., Eds.)pp 64-71, Delft University Press. Delft, Holland.

69. Hardware: Crystal Logical automation system.
Software: UCLA Crystallographic Computing Package (C. Strouse)

70. Gran, G. (1952) Determination of the equivalence point in potentiometric titrations. part II. ***Analyst,*** **77,** 661-671.

71. Meites, L. ed. ***Handbook of Analytical Chemistry,*** **1-6----1-7,** McGraw-Hill Book Company, Inc., New York, NY, 1963

72. Martell, A. E., and Motekaitis, R. J. (1988) ***Determination and Use of Stability Constants.*** VCH Publishers Inc., New York, NY.

73. Sudmeier, J. L., and Reilley, C. N. (1964) Nuclear Magnetic Resonance Studies of Protonation of Polyamine and Aminocarboxylate Compounds in Aqueous Solution. ***Anal. Chem.*** **36:**1698-1706

74. Grim, W. M. III; Fateley, W. G.; Grasselli, J. G. (1984) ***Fourier Transform Infrared Spectroscopy.*** Theophanides, T. ed, D. Reidel Publishing Company, Dordrecht, 25-42.

75. Lenz, G. R. and Martell, A. E. (1965) Metal chelates of mercapto-succinic acid and α,α'-dimercaptosuccinic acid. ***Inorg. Chem.*** **4:**378-84

76. Anderegg, G., and Malik, S. (1970) Die Komplexbildungetendenz des Dreiwertigen Antimons in Waserriger Losung. ***Helv. Chim. Acta*** **53:**577

77. Egorova, L. G., Nirenburg, V. L. (1973) Complexing properties of dimercaptocarboxylic acids. III-Complexing of Lead(II) with d,l-dimercaptosuccinic acid and d,l-dimercaptoglutaric acid. ***Zh. Obsch. Khim.*** **43**:1548-52

78. Willes, M. J. and Williams, D. R. (1985) The selectivity of *meso*-dimercaptosuccinic acid for lead(II) in blood plasma. ***Inorg. Chim. Acta*** **106**:L21-L22

79. Letkeman, P., and Martell, A. E. (1979) Nuclear Magnetic Resonance and Potentiometric Protonation Study of Polyaminopolyacetic Acids Containing from Two to Six Nitrogen Atoms. ***Inorg. Chem.*** **18**:1284-1288

80. Letkeman, P., and Westmore, J. B.(1971) Metal-amionopolycarboxylic acid complexes. II. Studies of triethylenetetraaminehexaacetic acid and its lead(II) complexes in aqueous solution by proton magnetic resonance spectroscopy. ***Can. J. Chem.*** **49**:2086

81. Fried, A. R. Jr., and Martell, A. E. (1971) Structure and conformation of Th(IV)-complexes of triethylenetetraaminehexaacetic acid in aqueous solution. ***J. Coord. Chem.*** **1**:47

82. Silverstein, R. M., Bassler, C. G., and Morrill, T. C. (1991) ***Spectrometric Identification of Organic Compounds***, 5th Ed, pp 175, John Wiley & Sons Inc., New York, NY.

83. Jackman, L. M., and Sternhell, S. (1969) ***Applications of Nuclear Magnetic Resonance Spectroscopy in Organic Chemistry***, 2nd ed, Pergamon Press, New York.

84. G. Capozzi and G. Modena (1974) Oxidation of Thiols.In ***The Chemistry of the Thiol Group***, (Saul Patai, Ed.) pp 785-840, John Wiley & Sons, New York.

85. Pyrka, G. J., Scott, N., and Fernando, Q. (1992) Structure of the 1:2 Adduct of *meso*-2,3-Dimercaptosuccinic Acid and *N,N*-Dimethylformamide. ***Acta Cryst.*** **C48**:2007-9

86. Rivera, M., Bruck M. A., Aposhian. H. V. and Fernando, Q. (1991) The dimethyl ester of *meso*-2,3-dimercaptosuccinic acid and its interactions with Cd^{2+} and rabbit liver metallothionein I. ***Chem. Res. Toxicol.*** **4:472-80**

87. Subcommittee on zinc, National Research Council (1979) ***Zinc*** chapter 6, University Park Press, Baltimore, MD.

88. Oldendorf, W. H. (1971) Brain uptake of radiolabeled amino acids, amines, and hexoses after arterial injection. ***Amer. J. Physiol.*** **221**:1629-1639

89. Chvapil, M. (1973) New aspects in the biological role of zinc: A stabilizer of macromolecules and biological membranes. ***Life Sci.*** **13**:1041-1049

90. Dorsey, N. E. (1940) ***Properties of Ordinary Water Substance.*** Reinhold Publishing Corp., New York, 341.

91. Gore, R. C.; Barnes, R. B.; Petersen, E. (1949) Infrared absorption of aqueous solutions of organic acids and their salts. ***Anal. Chem.*** **21**:382-386

92. Jones, D. C., Smith, G. L., May, P. M. and Williams, D. R. (1984) Assessment of pharmaceutical agents for removing cadmium from humans using chemical speciation models. ***Inorg. Chim. Acta*** **93**:93-100

93. Harris, W. R. and Chen, Y. (1991) Stability constants for dimercaptosuccinic acid with bismuth(III), zinc(II), and lead(II). ***J. Coord. Chem.*** **23**:173-186

94. Motekaitis, R. J., and Martell, A. E. (1982) BEST-a new program for rigorous calculation of equilibrium parameters of complex multicomponent systems. ***Can. J. Chem.*** **60**:2403-2409

95. Pople, J. A.; Schneider, W. G.; Bernstein, H. J. (1959) ***High-resolution Nuclear Magnetic Resonance***, McGraw-Hill, New York, chap. 10.

96. Caldin, E. F. (1964) ***Fast Reactions in Solution***, John Wiley & Sons, New York, chap. 11.

97. Sandström, J. (1982) ***Dynamic NMR Spectroscopy.*** Academic Press, New York.

98. Rivera, M and Fernando, Q. (1992) Synthesis, structure, and stability of the zinc complex of the dimethyl ester of *meso*-2,3-dimercaptosuccinic acid. ***Chem. Res. Toxicol.*** **5**:142-147

99. Deacon, G. B. and Phillips, R. J. (1980) Relationships between the carbon-oxygen stretching frequencies of carboxylate complexes and the type of carboxylate coordination. ***Coord. Chem. Rev.*** **33:**227-50

100. Nakamoto, K.; Morimoto, Y; Martell, A. (1961) Infrared spectra of aqueous solutions. I. Metal chelate compounds of amino acids. ***J. Am. Chem. Soc.*** **83:**4528-32

101. Nakamoto, K. (1978) ***Infrared and Raman Spectra of Inorganic and Coordination Compounds.*** John Wiley & Sons, Inc., New York, part III.

102. Ramsay, D. A. (1952) Intensities and shapes of infrared absorption bands of substances in the liquid phase. ***J. Am. Chem. Soc.*** **74:**72-80

103. Jones, R. N.; Ramsay, D. A.; Kier, D. S.; Dorbriner, K. (1952) The intensities of carbonyl bands in the infrared spectra of steroids. ***ibid.*** **74:** 80-88.

104. Ito, K.; Bernstein, H. J. (1956) The vibrational spectra of the formate, acetate, and oxalate ions ***Can. J. Chem.*** **34:**170-8

105. Hadzi, D.; Sheppard, N. (1953) The infrared absorption bands associated with the COOH and COOD groups in dimeric carboxylic acids. ***Proc. Roy. Soc. (London)*** **A216:**247-66

106. Perrin, D. D., and Sayce, I. G. (1967) Stability constants of polynuclear mercaptoacetate complexes of nickel and zinc. ***J. Chem. Soc.*** **A:** 82-88

107. Sabatini, A., Vacca, A. and Gans, P. (1974) MINIQUAD-A general computer program for the computation of formation constants from potentiometric data. ***Talanta*** **21:**53-77

108. May, P. M. and Williams , D. R. (1977) Computer simulation of chelation therapy. Plasma mobilizing index as a replacement for effective stability constant. ***FEBS Lett.*** **78:**134

109. Jones, M. M., Singh, P. K., Gale, G. R., Smith, A. B. and Atkins, L. M. (1992) Cadmium mobilization in vivo by intraperitoneal or oral administration of monoalkyl esters of *meso*-2,3-dimercaptosuccinic acid. ***Pharmacol. Toxicol.*** **70:**336

110. Walker, E. M. Jr., Stone, A., Milligan, L. B., Gale, G. R., Atkins, L. M., Smith, A. B., Jones, M. M., Singh, P. K. and Basinger, M. A. (1992) Mobilization of lead in mice by administration of monoalkyl esters of *meso*-2,3-dimercaptosuccinic acid. ***Toxicol.*** **76:**79-87

111. Fang, X. and Fernando, Q. (1994) A comparative study of meso- and rac-2,3-dimercaptosuccinic acids and their zinc complexes in aqueous solution. ***Chem. Res. Toxicol.*** 7:770-78

112. Johannsen, B., Spies, H. and Syhre, R. (1978) *Meso* and *racemic*-2,3-dimercaptosuccinatotechnetate(V). ***Radiochem. Radioanal. Lett.*** **36:**111-16

113. Awh, O. D., Kim, J. R. and Shim, S. C. (1989) $^{99}Tc^{m}$-diastereoisomeric dimercaptosuccinic acid complexes: comparison of their biodistribution. ***Nucl. Med. Commun.*** **10:**449-54

114. Meites, L. ed. ***Handbook of Analytical Chemistry***, Section 3, 3-95. McGraw-Hill Book Company, Inc., New York, NY, 1963

115. ***NIST Critical Stability Constants of Metal Complexes Database*** **version 1.0,** NIST Standards Reference Database 46, Gaithersburg, MD.

116. Egorova, L. G. (1972) Complex-forming properties of 2,3-dimercaptosuccinic acid. Complex formation of lead with *meso*-2,3-dimercaptosuccinic acid. ***Zh. Obsch. Khim.*** **42(10)**:2240-5

117. Fang, X. and Fernando, Q. (1994) Conformations of zinc chelates of *meso*- and *rac*-2,3-dimercaptosuccinic acid in aqueous solution. ***Chem. Res. Toxicol.*** 7:882-90

118. Klaassen, C. D. (1990) Heavy metals and heavy-metal antagonists. ***The Pharmacological Basis of Therapeutics, 8th edn.***, Gilman, A. G., Rall, T. W., Nies, A. S. and Taylor, P. (Eds.), p1592, Pergamon Press, New York.